DNS for RANS combustion modelling in multiple injection configurations

Eleftherios Gorgoraptis

université PARIS-SACLAY

CentraleSupélec

NNT : 2018SACLC111

Thèse de doctorat

Simulation numérique directe pour la modélisation de la combustion Diesel dans des configurations d'injections multiples

Thèse de doctorat de l'Université Paris-Saclay
préparée à CentraleSupélec

Ecole doctorale n°579 Sciences mécaniques et énergétiques, matériaux et géosciences (SMEMAG)
Spécialité de doctorat : Énergétique

Thèse présentée et soutenue à Rueil-Malmaison, le 19 décembre 2018, par

ELEFTHERIOS GORGORAPTIS

Composition du Jury :

Nasser Darabiha Professeur, CentraleSupélec	Président
Pascale Domingo Directeur de Recherche, CORIA	Rapporteur
Fabrice Foucher Professeur, Université d'Orléans	Rapporteur
Iyad Balloul Group Manager, Volvo Group Trucks Technology	Examinateur
Antonio Pires da Cruz Program Manager, IFP Énergies nouvelles	Directeur de thèse
Jean-Baptiste Michel Project Manager, IFP Énergies nouvelles	Co-directeur de thèse
Stéphane Chevillard Ingénieur de Recherche, IFP Énergies nouvelles	Invité

Nomenclature

Roman letters

Symbol	Significance
c	Normalised progress variable
$\overline{c''^2}$	Normalised progress variable variance
C_k	The mole concentration of the k^{th} species
C_p	Heat capacity at constant pressure
D_c	Coefficient de diffusion pour la variable d'avancement
$\mathcal{D}_t$	Turbulent diffusivity
Da	Damköhler number
E	Total non-chemical energy
$h_{s,k}$	Sensible enthalpy of the k^{th} species
k	Turbulence kinetic energy
K	Wavenumber
l_t	Integral length scale
m_j	Atomic mass of atom j
$n_{j,k}$	Number of atoms j contained in the molecule of k^{th} species
p	Static pressure
R	Ideal gas constant
P	Probability density function
$\mathcal{Q}_r$	Mole progress rate of the r^{th} reaction
Re_t	Turbulent Reynolds number
$\overline{S_c}$	Normalised progress variable segregation factor
Sc_t	Turbulent Schmidt number
$\widetilde{S_Z}$	Mixture fraction unmixedness
t	Time
T	Temperature
u	Local flow velocity
W_k	Molecular weight of the k^{th} species
X_k	Mole fraction of the k^{th} species
Y_k	Mass fraction of the k^{th} species
Y_c	Progress variable
Z	Mixture fraction
$\widetilde{Z''^2}$	Mixture fraction variance

Greek symbols

Symbol	Significance
$\delta_{i,j}$	Kronecker symbol
Δx	Mesh size
ε	Turbulence kinetic energy dissipation rate
η_k	Kolmogorov length scale
λ	Thermal diffusion coefficient
μ_t	Turbulent viscosity
ν	Kinematic viscosity
ρ	Density
$\tau_{i,j}$	Viscous stress tensor
τ_c	Chemical time scale
τ_t	Turbulent time scale
ϕ	Fuel-air equivalence ratio
χ	Scalar dissipation rate of the mixture fraction Z
$\dot{\omega}$	Reaction rate

Indexes and Superscripts

Symbol	Significance
$Q_{i,j}$	Direction of a vector component
$\overline{Q}$	Reynolds average of quantity Q
$\widetilde{Q}$	Favre average of quantity Q
Q'	Fluctuation component of quantity Q when applying Reynolds decomposition
Q''	Fluctuation component of quantity Q when applying Favre decomposition
Q^{eq}	Quantity Q associated to thermodynamic equilibrium state
Q^{HR}	Quantity Q related to homogeneous reactor conditions
Q_{st}	Quantity Q at stoichiometric ratio

Abbreviations

Symbol	Significance
ADF	Approximated Diffusion Flame
AI	Autoignition
BMF	Burnt Mass Fraction
CAD	Crank Angle Degree
CFM	Coherent Flame Model
CMC	Conditional Moment Closure
DI	Direct Injection
DNS	Direct Numerical Simulation
ECFM3Z	3-zones Extended Coherent Flame Model
FGM	Flamelet Generated Manifolds
FPI	Flame Prolongation of ILDM
FPV	Flamelet Progress Variable
S2FT	Self-Similar Flame Tabulation
THR	Tabulated Homogeneous Reactor
TKI	Tabulated Kinetics of Ignition
HCCI	Homogeneous Charge Compression-Ignition
ILDM	Intrinsic Low Dimensional Manifold
ISAT	In Situ Adaptive Tabulation
LES	Large Eddy Simulation
ODE	Ordinary differential equation
PCM	Presumed Conditional Moment
RANS	Reynolds-Averaged Navier-Stokes
RIF	Representative Interactive Flamelets

Contents

Chapter 1

Introduction

1.1 The research problem

Diesel engines are widely used, mainly due to their high thermal efficiency and consequent low carbon dioxide (CO_2) emissions [1]. Stringent demand for reduced fuel consumption and pollutant emissions has urged a concerted effort to make further advances in automotive Diesel technology. This urgent need for innovation calls upon a deeper understanding of the physical phenomena implied and the simultaneous development and evaluation of promising concepts by means of experimental and numerical studies.

The conventional working cycle of a direct injection (DI) Diesel engine is presented in Figure 1.1. During the intake stroke, the piston moves downwards and the intake valves open letting air inside the combustion chamber. The intake pipe and port are designed to generate a large-scale swirl motion of the air entering the cylinder in order to improve fuel-air mixing. In naturally aspirated engines, the air is drawn into the cylinder by the under-pressure created as the piston moves towards the bottom dead center (BDC). Currently, most Diesel engines are equipped with a supercharger which delivers pre-compressed air to increase the engine power output and efficiency. The absolute intake charge pressure may reach up to 3 bar [2].

The compression stroke begins after the piston passes the BDC. Charge pressure at the end of this phase is in the range of 30-100 bar, with temperatures above 700 K. The combustion phase is initiated by a high-pressure fuel injection (typically 500-1500 bar, and up to 3000 bar [4]) into the combustion chamber at the end of the compression stroke. The temperature and pressure in the chamber are sufficient to cause the spontaneous autoignition of the air-fuel mixture without an external source of ignition, such as a hot spot or a spark. This is a brutal

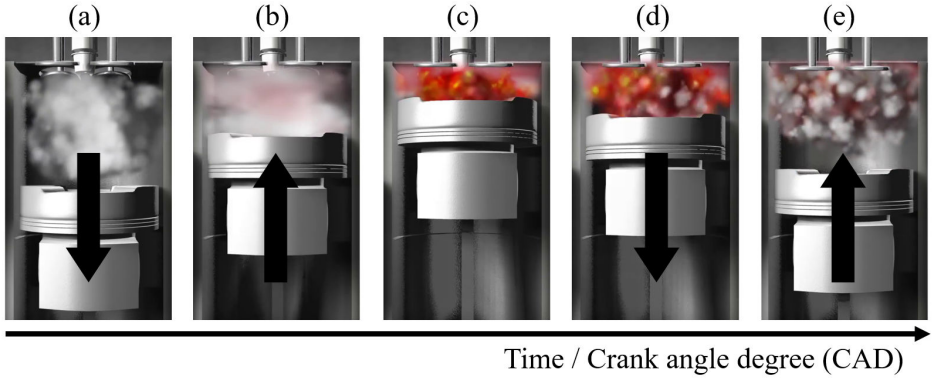

Figure 1.1: Four-stroke Diesel engine cycle : a) intake stroke, b) compression stroke, c) fuel injection, d) power stroke, e) exhaust stroke [3].

phenomenon that involves many different physical mechanisms, such as molecular diffusion, turbulent mixing, flame-generated vorticity, viscous effects and stretching of flow structures. After the piston passes the top dead center (TDC), the power stroke begins. Expanding burnt gases act on the piston pushing it towards the BDC and the energy of the gases is converted into mechanical work (see Figure 1.1(d)). At the end of the power stroke, the exhaust valve opens and lets the burnt gases out. During the exhaust stroke the piston is moving towards the TDC expelling the burnt gases out of the cylinder.

When compared to gasoline engines, the main disadvantage of the Diesel engines at their most basic form is that they favour the emissions of nitrogen oxides (NO_x) and particulate matter (soot), two of the major pollutants regulated by international emission standards. As it can be seen in Figure 1.2, the burnt gases temperature curve corresponding to the conditions inside the Diesel combustion chamber crosses NO_x and soot formation zones in terms of mixture equivalence ratio and temperature. Furthermore, NO_x and soot formation zones are almost complementary : decreasing soot emissions usually results in an increase of NO_x, and *vice versa*.

1.2 Multiple Diesel injection strategies

One of the great challenges in meeting future emission regulations affecting Diesel engines is the simultaneous reduction of NO_x and soot emissions, without increasing fuel consumption [6, 7]. For a given fuel injection system, this trade-off between NO_x and soot can be optimised by adjusting the beginning of the injection [8]. Developing this concept even further,

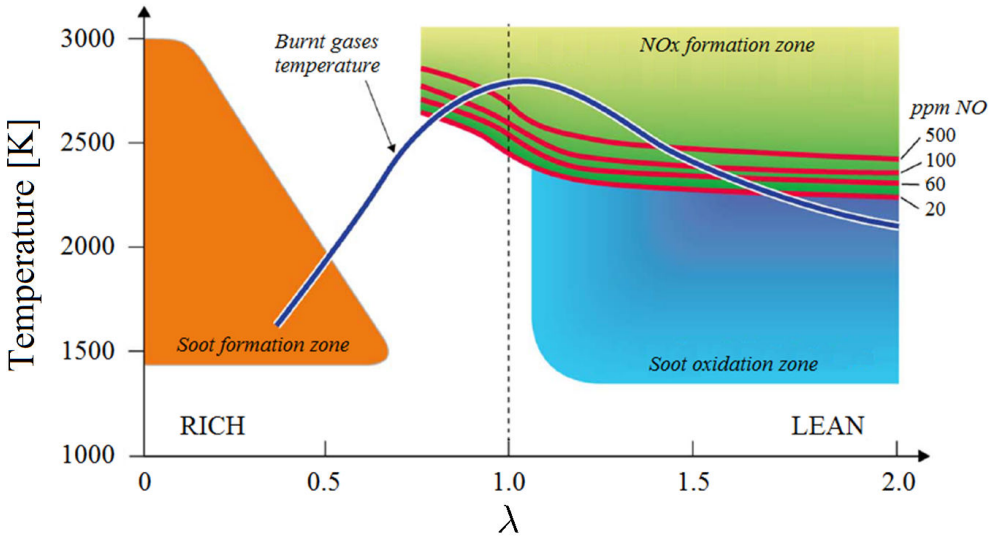

Figure 1.2: Pischinger diagram [5], temperature versus air-fuel equivalence ratio λ, that is the actual air-to-fuel ratio of the mixture over the stoichiometric air-to-fuel ratio. Burnt gases temperature curve corresponding to the conditions inside the Diesel combustion chamber and zones of NO_x and soot formation and soot oxidation.

the injection can be split in several pulses (see Figure 1.3) using early injections called "pilot injections" and late injections during the expansion stroke, named "post injections". Additionally to the pollutant emissions reduction, multiple injections permit an improved control over the heat release rate, thus decreasing the level of combustion noise [9].

In order to accomplish such a complex manipulation of the fuel injection into the cylinder, elaborate technological means are necessary. High pressure common rail (CR) injection systems combined with electronic control have made flexible and precise fuel injection a reality. Thanks to this technology, various injection parameters, such as timing and pressure, can be adjusted very accurately [10, 11]. Modern common rail injection systems, equipped with piezoelectric injectors, allow a very high degree of flexibility in the timing and quantity control of multiple injections and are capable of up to eight injection events per cycle.

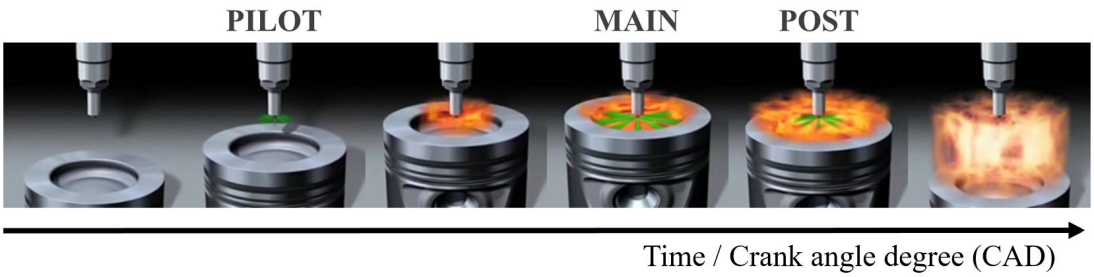

Figure 1.3: The multiple injections concept [12].

Multiple injections strategies become more and more popular due to their advantages over conventional single injection cycles. The physical phenomena involved in such configurations, however, are complex and remain challenging. There is significant interaction between the mixture fields of the consecutive injections [13] and this interaction strongly depends on the injection timing [14]. The progress of multiple injection technology depends to a great extent on the more profound understanding of these mechanisms.

Multiple injections have been the subject of numerous experimental studies. Tow and Reitz [15] studied various injection strategies ; they observed that at high loads two consecutive injections separated by a relatively large time interval can effectively reduce soot with no increase in NO_x. At 25% load, a smaller interval between the injections can lower NO_x emissions. They also pointed out that triple injections, with a significantly delayed third injection, can decrease soot by up to 50% and NO_x by up to 30%. A post injection in both double and triple injections strategies could effectively accelerate soot oxidation rate, thus reducing soot emissions, possibly thanks to the enhanced fuel-air mixing process.

Nehmer and Reitz [16] proposed a pilot fuel mass increase up to 75% of total fuel mass on a single cylinder heavy duty DI Diesel engine. They observed that the split injection exploited better the intake air compared to a single injection and enabled combustion to last into the expansion stroke, without increasing soot emissions. Ishikawa [17] suggested that soot emissions can be reduced by applying an early pilot injection for a better mixing. The two main mechanisms proposed by Beatrice *et al.* [18] to minimise emissions are splitting the main injection to improve air utilisation and using post injection to promote soot oxidation. Dronniou *et al.* [19] observed the best emission results when the pilot injection is carried out sufficiently early.

Ikemoto *et al.* [20], Desantes *et al.* [21] and O'Connor *et al.* [22] demonstrated that post injection reduces smoke emissions, basically consisting of soot and unburned fuel. The smoke reduction effect of post injection against the post injection timing seems to depend on the operating conditions and specifications of the engine. When applying early post injection, the post spray is able to entrain sufficient oxygen before the main spray flame reaches the path, as shown in Figure 1.4(a). As a result, soot from the main spray decreases because a portion of the main injection fuel is moved to the post injection, where it evaporates and burns producing less soot thanks to the more favourable conditions. Therefore, close post injection leads to low smoke emission. On the other hand, retarded post injection entrains a high-temperature and low-oxygen mixture from the main spray flame, which rolls up to interrupt the post spray (Figure 1.4(b)), creating soot.

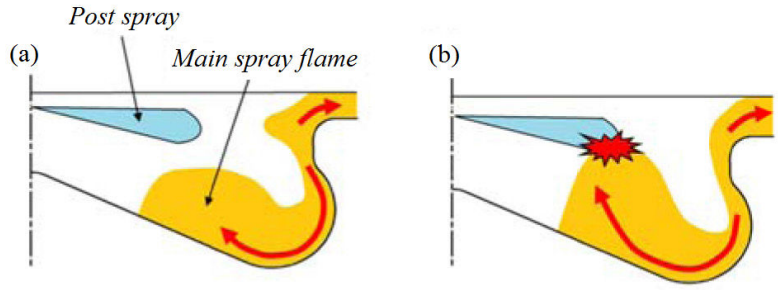

Figure 1.4: Interaction of main spray flame and post spray : (a) advanced post injection and (b) retarded post injection [23].

1.3 Simulation and modelling

Although the experimental research has led to key advancements in internal combustion engine technology, observation of the in-cylinder processes remains limited even with optical diagnostics. Recent developments rely more and more on Computational Fluid Dynamics (CFD), which, accompanied by experiments, helps evaluating the most promising technologies at a preliminary stage of the engine design, at costs that are much lower than those associated with experiments [24]. Numerical simulation studies can not only provide closer observations on the combustion, but also have the potential to develop various methods to facilitate analysis.

The physical phenomena encountered inside the combustion chamber of an internal combustion engine could be grouped under the general heading of turbulent combustion. A full description of such phenomena is entangled in the combination of the Navier-Stokes equations, which describe the motion of viscous fluid substances, with chemical kinetics, dealing with the determination of chemical reaction rates. The great challenge of simulating such systems resides in the fact that they involve a large range of time and length scales. Some chemical phenomena controlling combustion take place in very short times over thin layers and are associated with large mass fractions, temperature and density gradients [25]. Additionally, turbulence involves a wide range of structure sizes and its complete description remains an open question.

Fluid dynamics simulation

The numerical resolution of the Navier-Stokes equations can be approached from different angles. In Direct Numerical Simulation (DNS), the turbulent flow is resolved using sufficient resolution both in time and space to capture scales over the whole turbulence spectrum, from the largest to the smallest. This approach is, for the moment, limited to simple configurations due to the very high spatial and temporal discretisation demanded. The assessment of the minimum discretisation is discussed in Section 4.2.

Reynolds-Averaged Navier-Stokes (RANS) equations describe mean flow fields and are adapted to practical industrial applications. Unlike the DNS formalism, all temporal and spatial scales of the turbulent flow are modelled under the RANS formalism ; only mean quantities are directly computed. The RANS method is computationally affordable and can be useful to obtain averaged flow and combustion parameters, but requires an important modelling effort. Large Eddy Simulation (LES) lies between DNS and RANS, both with respect to form and computational cost [26]. In LES, the largest turbulence scales are explicitly resolved whereas the effects of smaller ones, below a certain cut-off length, are modelled. In the limit of an infinitesimal cut-off length, LES converges to DNS.

Chemical kinetics

Combustion chemistry involves, at its most basic form, one single global reaction between a combustible and an oxidiser to form combustion products. In reality, the reaction proceeds in multiple steps through complex chemical mechanisms. Chemical kinetics is the study of chemical reactions with respect to reaction rates, formation of intermediates *etc.*, and is of great importance for the proper simulation of reactive flows. The introduction of detailed chemical kinetics involving many species and chemical reactions is required to correctly represent ignition delay, pollutant emissions *etc.*, over a broad range of engine operating conditions (pressure, temperature, composition). Implementation of detailed chemistry in DNS is feasible but leads to an extremely high CPU cost [27]. Simpler semi-detailed mechanisms that are adapted to the thermodynamic conditions of interest can be used instead (see Section 4.4). The stiffness associated with the determination of rates of chemical reactions in DNS is often more restrictive in terms of discretisation than that associated with the resolution of the smallest scales in turbulent flows.

Combustion modelling and chemistry tabulation

Combustion modelling calls upon the proper selection and implementation of a model suitable to faithfully represent the complex physical and chemical mechanisms associated with any combustion process. A combustion model is necessary to represent unclosed terms in the transport flow equations (see Section 3.1) or to simplify terms that are computationally expensive to solve directly (see Section 3.3). The model is coupled with the general transport equations for fluid flow and heat transfer as well as the additional equations of combustion chemistry

and chemical kinetics incorporated into that as per the simulating environment desired [28]. It delivers information related to the species concentration, their volumetric rate of production/consumption and changes in the parameters of the system like enthalpy, temperature and mixture density.

A promising modelling approach consists in the off-line generation of chemistry look-up tables based on simple computations (*e.g.* 0-D homogeneous reactors or 1-D laminar diffusion flames) using complex chemical schemes ; the tabulations are then used in the CFD simulation, combined with turbulent combustion models, integrating the effects of detailed chemistry at a minimal CPU cost. Until present, Reynolds-averaged Navier-Stokes (RANS) simulation of Diesel engines is performed with satisfactory results, using a variety of such combustion models [29, 30]. In the case of multiple Diesel injection configurations, however, the validity of the existing tabulated combustion models remains to be demonstrated. Mean in-cylinder pressure evolution over a part of a Diesel combustion cycle (fuel injection and autoignition) is presented in Figure 1.5 ; experimental data in dashed lines and RANS simulation results in solid lines are compared for different loads and injection strategies. As it can be seen in this representative example, contrary to the single injection case, where the simulation results match perfectly the experimental data (cyan curves), the combustion model used in the multiple injections RANS simulations fails to correctly predict the timing of the second pressure rise or the level of the pressure peak inside the chamber.

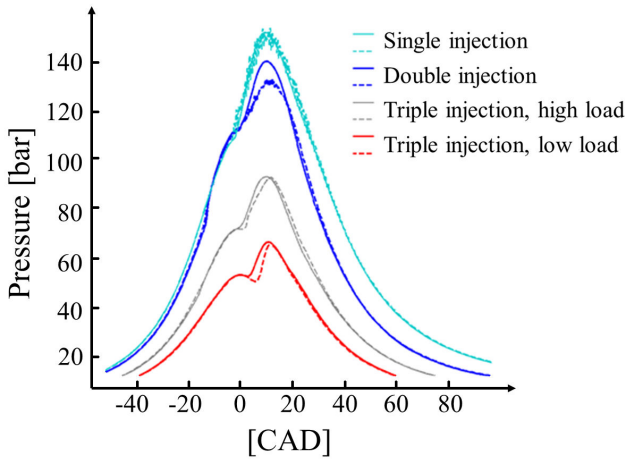

Figure 1.5: Mean in-cylinder pressure evolution, comparison between experimental data (dashed lines) and RANS simulation results (solid lines) [31]. Time evolution in crank angle degrees (CAD), 0° for TDC.

Numerical studies of multiple Diesel injection strategies

The predictive capabilities of the existing combustion modelling approaches are limited when it comes to multiple injections Diesel cycles. Nevertheless, some general trends can be discerned by means of numerical simulation. The studies listed below used RANS simulation to investigate the pollutant formation and the interaction between separate injections in multi-injection configurations. Main conclusions are resumed without further description of the numerical set-up of each work ; the studies are referenced in Subsection 3.3.2 along with the description of the corresponding modelling approach.

Han *et al.* [14] investigated different strategies for simultaneous reduction of soot and NO_x. They proposed that with multiple injections, the excess of fuel at the jet tip is reduced ; instead, the fuel in the second pulse is injected into a relatively fuel-lean, high temperature region and is consequently burned before a rich soot-producing region is formed. They noted that the dwell time between injections should be carefully adjusted to obtain an improved fuel distribution in the combustion chamber and to create a favourable environment for the second injection, prompting fast combustion and reducing soot. Hessel *et al.* [32] used CFD tools to provide local identification and quantification of the soot formation and oxidation on a heavy-duty Diesel engine. It was concluded that short post-injections reduce the amount of fuel-vapour available for soot formation, while long post-injections significantly increase the presence of fuel-vapour, in agreement with the experimental studies cited above.

Ra *et al.* [33] showed that operation of light-duty DI engines under full-load conditions is significantly extended to higher loads by using a triple-injection strategy. They also pointed out that increasing injection pressure reduces soot emissions significantly. Mobasheri *et al.* [34] indicated that the pilot injection reduces the ignition delay and therefore the premixed combustion period, leading to lower temperatures and NO_x emissions. They also demonstrated the effectiveness of multiple injections at controlling soot emission under exhaust gas recirculation (EGR) conditions. The influence of EGR in a heavy-duty Diesel engine on the interaction between post and main injection was also extensively investigated by Pandurangi *et al.* [35]. They proposed that an elevation of the soot oxidation rate occurs at the immediate vicinity of the jet, caused by the additional momentum imparted by it and the consequent entrainment of oxygen. This phenomenon can counterbalance the soot formation resulting from the small further enrichment of the already fuel-rich regions at the head of the post-jet, present from the main injection.

DNS for RANS combustion modelling

Prior to full scale simulations, turbulent combustion models can be evaluated and ameliorated to contribute more decisively to the engine design. Several studies investigated the validity of tabulated combustion models, either in academic geometries [36, 37, 38, 39, 40] or in the industrial context [41, 42], relying on the comparison of numerical simulation results with experimental data. These computations are strongly dependent on the choice of the detailed chemistry mechanism. Drawing conclusions on the reliability of the tested models based on comparisons with experimental data can therefore be unsafe, since it is impossible to determine whether the observed differences are due to modelling hypotheses or to chemical kinetics approximations. Pires da Cruz [43] and Chevillard *et al.* [29, 44] followed a methodology for an *a priori* evaluation of turbulent combustion models ; reactive DNS was used to retrieve the input data of the combustion model as well as precise results that were compared with the model output. The DNS was conducted using the same skeletal reaction mechanism implemented for RANS and LES tabulated chemistry models. Therefore, the focus was exclusively put on the modelling assumptions, excluding any misleading influence of the chemical scheme. This methodology is applied in the present study for the evaluation and the extension of various tabulated combustion models on multi-injection Diesel engine-relevant conditions.

DNS of autoigniting stratified turbulent mixtures

Aside from the evaluation of the hypotheses of different modelling approaches according to the above methodology, DNS can also provide a detailed insight into turbulent non-premixed combustion from a phenomenological point of view. Previous DNS works have investigated autoignition phenomena in mixing layers under decaying turbulence. Mastorakos *et al.* [45] demonstrated that first ignition spots are localised in regions of the flow with low scalar dissipation rate χ, that is in regions with low species diffusion, and around a specific, "most reactive" value of mixture fraction, that is around a specific mixture richness. These results, obtained with 2-D DNS with simplified methane chemistry at non-Diesel-relevant conditions, were later confirmed by DNS works in high-pressure Diesel and Homogeneous Charge Compression Ignition (HCCI) engine-relevant configurations [46], including 3-D [47], and complex chemistry [48] studies.

Recent numerical works investigated two-stage ignition and negative temperature coefficient (NTC) regime, characteristic of many Diesel engine operating points. Mukhopadhyay and Abraham observed the impact of scalar dissipation rate χ on each of the two stages of the ignition process in laminar [49] and turbulent [50] mixing layers at Diesel-relevant conditions. Bansal *et al.* [51] and Luong *et al.* [52] conducted a parametric investigation of key variables such as temperature and composition stratification magnitude, turbulence intensity, *etc.* and identified their impact on the ignition delay and heat release. Krisman *et al.* [53, 54] identified a diffusively-supported front of low-temperature chemistry (LTC) as a distinct combustion feature that affects the second stage of the ignition.

Useful insights have been obtained from the aforementioned DNS studies. However, analyses of the interaction of partially burnt gases with fresh fuel, corresponding respectively to separate injection phases in a multi-injection Diesel engine, remain limited. Given the prominence of this interaction, observed in Diesel injection-relevant experiments [13], further investigation of ignition and progress of combustion at these conditions is merited.

1.4 Objective of the thesis

In the framework of this Ph.D. thesis, self-ignited combustion in turbulent heterogeneous reactors will be studied through DNS coupled with semi-detailed chemistry. A configuration representative of the physical problem addressed will be proposed. A 2-D DNS database will be generated and analysed, covering a range of single and split Diesel injection-relevant conditions. These simulations will serve as numerical experiments providing a model-free insight into the interaction between turbulent mixing and combustion chemistry when using multiple injections strategies.

The specific goal of this work is to evaluate turbulent combustion models based on tabulated chemistry and to elaborate a strategy to adapt them to the needs of modern multi-injection Diesel engine simulations. The different modelling approaches tested are related to works undertaken over the past few years within IFPEN, focusing on the development of turbulent combustion models for rigorous and affordable RANS simulation of internal combustion engines, gas turbines and furnaces. The evaluation of the models will be based on an *a priori* comparison with the DNS results of the generated database.

First, the studied models will be evaluated under single and split injection conditions, without any modifications. Then, a new modelling approach adapted to multiple injections configurations will be elaborated. Finally, a strategy for the application of the new modelling approach in 3D RANS will be proposed for prospective multi-injection Diesel engine simulations with an improved accuracy.

1.5 Organisation of the manuscript

This Ph.D. manuscript is divided into seven chapters :

- In the first chapter, the general context of the study is presented.
- The second chapter is devoted to the description of the conservation equations governing multi-species reactive gaseous flows and their resolution in DNS.
- RANS combustion modelling is discussed in the third chapter. Some useful tools for non-premixed combustion modelling are summarised next. The studied combustion models are presented along with the methodology used for their evaluation.
- The DNS configuration is then presented in the fourth chapter.
- The fifth chapter is dedicated to the analysis of DNS results corresponding to single Diesel injection conditions and the *a priori* evaluation of the studied combustion models against these DNS results.
- The sixth chapter presents the analysis of results corresponding to multiple Diesel injections conditions. A split injection DNS database is studied. Combustion models are then evaluated against the DNS results.
- An extended modelling approach, using the adapted chemical kinetics tabulations, is proposed as perspective work in the seventh chapter.
- Finally, the last chapter regroups the key findings of the present work and discusses the perspectives arising from it.

Chapter 2

Governing equations and their resolution

2.1 Conservation equations

The methodology and equations that follow are presented with respect to the numerical simulation of combustion in the CFD code AVBP [55], co-developed by CERFACS and IFPEN, and used in the present work to perform DNS.

2.1.1 Multi-species compressible reactive flow equations

Note : in this Section, the Einstein summation notation is used.

The considered variables used to describe the conservation laws of multi-species compressible reactive flows are the density ρ, the mass fraction Y_k of the k^{th} species, the velocity vector u_i, the total non-chemical energy E and the static pressure p :

$$\frac{\partial \rho}{\partial t} + \frac{\partial \left(\rho u_i\right)}{\partial x_i} = 0 \tag{2.1}$$

$$\frac{\partial \rho Y_k}{\partial t} + \frac{\partial \rho \left((u_i + V_{k,i}) Y_k\right)}{\partial x_i} = \rho \dot{\omega}_{Y_k} \tag{2.2}$$

$$\frac{\partial \rho u_i}{\partial t} + \frac{\partial \rho u_i u_j}{\partial x_j} = -\frac{\partial p}{\partial x_i} + \frac{\partial \tau_{i,j}}{\partial x_j} \tag{2.3}$$

$$\frac{\partial \rho E}{\partial t} + \frac{\partial \rho E u_i}{\partial x_i} = -\frac{\partial q_i}{\partial x_i} + \frac{\partial \tau_{i,j} u_i}{\partial x_j} - \frac{\partial p u_i}{\partial x_i} + \dot{\omega}_T \tag{2.4}$$

Eqs. (2.1)-(2.4) correspond to the conservation of mass, species, momentum, total non-chemical energy, generally known under the name of Navier-Stokes equations. Eq. (2.5) is the ideal gas law, an equation of state of a hypothetical ideal gas approximating the behaviour of a real gas :

$$\frac{p}{\rho} = rT \tag{2.5}$$

The energy conservation can be described in terms of several different variables [25]. In the present dissertation, the total non-chemical energy is expressed as follows :

$$E = \sum_{k\in\Omega} h_{s,k}Y_k - (p/\rho) + \frac{1}{2}u_i u_j \tag{2.6}$$

$h_{s,k}$ is the sensible enthalpy of the k^{th} species and is related to the mass heat capacity at constant pressure $C_{p,k}$ according to the following expression :

$$h_{s,k} = \int_{T_0}^{T} C_{p,k}dT \tag{2.7}$$

where $\Omega = [\![1, N]\!]$, N referring to the total number of species in the mixture. In Eqs. (2.1)-(2.5), $V_{k,i}$ is the i^{th} component of the diffusion velocity of the k^{th} species. It characterises the molecular transport properties of the mixture. $\rho\dot{\omega}_{Y_k}$ stands for the rate of production/consumption of the k^{th} species by chemical reactions, while $\dot{\omega}_T$ refers to the heat release due to chemical reactions. The ideal gas law is used to close the system of, where T refers to temperature and r refers to the mixture constant defined as :

$$r = \frac{R}{W} \tag{2.8}$$

where $R = 8.314J\cdot mol^{-1}\cdot K^{-1}$ stands for the ideal gas constant, and W is the mean molecular weight of the mixture :

$$W = \sum_{k\in\Omega} X_k W_k = \left(\sum_{k\in\Omega} Y_k/W_k\right)^{-1} \tag{2.9}$$

X_k and W_k respectively refer to the mole fraction and the molecular weight of the k^{th} species.

The viscous stress tensor $\tau_{i,j}$ is given by the following relation :

$$\tau_{i,j} = \left(-\frac{2}{3}\,\mu\right)\frac{\partial u_l}{\partial x_l}\delta_{i,j} + \left(\frac{\partial u_j}{\partial x_i} + \frac{\partial u_i}{\partial x_j}\right) \tag{2.10}$$

where $\delta_{i,j}$ is the Kronecker symbol ($\delta_{i,j} = 1$ if $i = j$, else $\delta_{i,j} = 0$), μ is the dynamic viscosity (related to the kinematic viscosity using $\nu = \mu/\rho$). Dynamic viscosity in this study is assumed to be independent of the gas composition and only depends on temperature according to the power law :

$$\mu = \mu_{ref}\left(\frac{T}{T_{ref}}\right)^b \tag{2.11}$$

where b is an empirical coefficient and μ_{ref}, T_{ref} are dynamic viscosity and temperature reference values, in K and $kg/(s.m)$ respectively. The heat flux q_i involved in the total non-chemical energy equation E, is given by :

$$q_i = -\lambda\frac{\partial T}{\partial x_i} + \rho\sum_{k\in\Omega} h_{s,k}Y_k V_{k,i} \tag{2.12}$$

The first term of the Eq. (2.12) corresponds to the Fourier flux, which is the temperature diffusion by molecular effect ; λ stands for the thermal diffusion coefficient. The second term is related to heat diffusion due to molecular multi-species transport, that characterizes the species sensible enthalpy transport by its diffusion velocity $V_{k,i}$.

2.1.2 Modelling of multi-species transport terms

Note : in this Section, a vector notation is used.

The conservation of mass, momentum, energy and heat during the numerical resolution of the Eqs. (2.1)-(2.5) has to be ensured according to the following constraints :

$$\sum_{k\in\Omega} Y_k = \sum_{k\in\Omega} X_k = 1 \tag{2.13}$$

$$\sum_{k\in\Omega} \dot{\omega}_{Y_k} = 0 \tag{2.14}$$

$$\sum_{k\in\Omega} Y_k V_{k,i} = 0 \tag{2.15}$$

An accurate approach to determine the diffusion velocity $V_{k,i}$ of Eq. (2.2) would be the inversion of the system of Williams [56]. However, this is a very costly task as the system has to be solved in every dimension, each time step. The simpler Hirschfelder and Curtiss [57] approximation is thereby preferred.

$$\vec{V_k} X_k = -\mathcal{D}_k \vec{\nabla} X_k \quad \text{with} \quad \mathcal{D}_k = \frac{1 - Y_k}{\sum_{j \neq k} X_k / \mathcal{D}_{jk}} \tag{2.16}$$

where $\mathcal{D}_{jk}$ is the binary mass diffusion coefficient of species j into species k and $\mathcal{D}_k$ is an equivalent diffusion coefficient for each species. Using the expression of Eq. (2.9), Eq. (2.16) can be expressed in terms of mass fraction :

$$\vec{V_k} Y_k = -\mathcal{D}_k \frac{W_k}{W} \vec{\nabla} X_k \tag{2.17}$$

The Hirschfelder and Curtiss approximation does not necessarily satisfy mass conservation. To overcome this issue, a correction velocity is introduced in the expression of the diffusion velocity (Eq. (2.17)) so that the compatibility of species and mass conservation equation is ensured :

$$\vec{V_k} = -\mathcal{D}_k \frac{\vec{\nabla} X_k}{X_k} + \vec{V}^{cor} \tag{2.18}$$

The expression of the correction velocity $\vec{V}^{cor}$ is obtained by introducing the expression of Eq. (2.18) in the species conservation equation, (Eq. (2.2)) and summing up all species :

$$\vec{V}^{cor} = \sum_{k \in \Omega} \mathcal{D}_k \frac{W_k}{W} \vec{\nabla} X_k \tag{2.19}$$

The relation between the mole fraction gradients and their mass fraction counterparts reads :

$$\vec{\nabla} X_k = \frac{W}{W_k} \vec{\nabla} Y_k - \frac{W^2}{W_k} Y_k \sum_{l \in \Omega} \frac{1}{W_l} \vec{\nabla} Y_l \tag{2.20}$$

Knowing the expression of the correction velocity and the mole fraction gradient expressions given by Eqs. (2.19)-(2.20), the diffusive mass flux $\vec{J_k}$ reads :

$$\vec{J_k} = \rho \vec{V_k} Y_k = -\rho \left(-\mathcal{D}_k \frac{W_k}{W} \vec{\nabla} X_k - Y_k \vec{V}^{cor} \right) \tag{2.21}$$

$\mathcal{D}_k$ is here determined according to Eq. (2.22), considering a Schmidt number [1] Sc_k per species, constant in time and space.

$$\mathcal{D}_k = \frac{\mu}{Sc_k} \tag{2.22}$$

2.1.3 Chemical kinetics equations

A chemical system of N species reacting through R reactions is considered as follows :

$$\sum_{k\in\Omega} \nu^f_{k,r}\mathcal{M}_k \rightleftharpoons \sum_{k\in\Omega} \nu^b_{k,r}\mathcal{M}_k \quad \text{for} \quad r = 1, R \tag{2.23}$$

where $\mathcal{M}_k$ is the chemical symbol of the k^{th} species, $\nu^f_{k,r}$ and $\nu^b_{k,r}$ stand for the stoichiometric coefficients of the k^{th} species in the r^{th} reaction, respectively. Mass rate of production/consumption of the k^{th} species $\rho\dot{\omega}_{Y_k}$ is then given by :

$$\rho\dot{\omega}_{Y_k} = W_k \sum_{r=1}^{R} (\nu^b_{k,r} - \nu^f_{k,r})\mathcal{Q}_r \tag{2.24}$$

where $\mathcal{Q}_r$ is the mole progress rate of the r^{th} reaction given by :

$$\mathcal{Q}_r = C_M \left(k^f_r \prod_{k\in\Omega} (C_k)^{\nu^f_{k,r}} - k^b_r \prod_{k\in\Omega} (C_k)^{\nu^b_{k,r}} \right) \tag{2.25}$$

where $C_k = \rho Y_k / W_k$ is the mole concentration of the k^{th} species. k^f_r and k^b_r respectively denote for the forward and backward rate constants of the r^{th} reaction.

Some chemical kinetics mechanisms contain chemical reactions whose rate depends on the surrounding species in the mixture. These are called third-body reactions. A third-body M is involved in both sides of such a reaction, *i.e.* in the reactants and the products. M has a kinetic impact but is not chemically involved. C_M, given in Eq. (2.26) is the equivalent mole concentration of the third-body M.

$$C_M = \sum_{k\in\Omega} \alpha_{k,r} C_k \tag{2.26}$$

$\alpha_{k,r}$ is defined as the efficiency of the k^{th} species in the r^{th} reaction. C_M is equal to 1 for reactions that do not involve a third body.

[1] Schmidt number Sc compares momentum and molecular diffusion.

The forward rate constant of the r^{th} reaction is calculated using the Arrhenius law :

$$k_r^f = A_r T^{\beta_r} exp\left(\frac{-Ea_r}{RT}\right) \tag{2.27}$$

where A_r is the pre-exponential constant, β_r is the temperature exponent and Ea_r is the activation energy of the r^{th} reaction. The equilibrium constant K_r^{eq} is determined using [58] :

$$K_r^{eq} = \left(\frac{p_0}{RT}\right)^{\sum_{k\in\Omega}(\nu_{k,r}^b - \nu_{k,f}^f)} exp\left(\frac{\Delta S_0^r}{R} - \frac{\Delta H_0^r}{RT}\right) \tag{2.28}$$

where p_0 is a reference pressure, here chosen equal to the atmospheric pressure. ΔS_0^r and ΔH_0^r are the entropy and enthalpy of the r^{th} reaction at a reference thermodynamic state. The backward constant is then computed as :

$$k_r^b = k_r^f / K_r^{eq} \tag{2.29}$$

Finally, the heat release rate due to chemical reactions reads :

$$\dot{\omega}_T = -\sum_{k\in\Omega} \triangle h_{f,k}^o \rho \dot{\omega}_{Y_k} \tag{2.30}$$

where $\triangle h_{f,k}^o$ is the enthalpy of formation of the k^{th} species.

2.2 Resolution of transport and chemical kinetics equations

2.2.1 General features of the AVBP code

The CFD code AVBP [55] solves the time-dependent compressible Navier-Stokes equations for multi-species reactive flows in two and three space dimensions. It is based on an unstructured and hybrid grid approach and uses a cell-vertex finite-volume (FV) method for the numerical discretisation. In cell-vertex methods, variables are stored at the grid nodes (else called "cell vertices") whereas the control volume is delimited by the centres of the adjacent cells, as illustrated in Figure 2.1. This approach enables a flexible use of both finite-volume (FV) and finite-element (FE) numerical schemes.

Different numerical schemes are available in the AVBP code. In the present thesis, the finite element numerical scheme used is a two-step Taylor-Galerkin (TTGC) scheme [59], a third-order scheme in space and time, barely dissipative and dispersive, therefore suitable for DNS [60, 61].

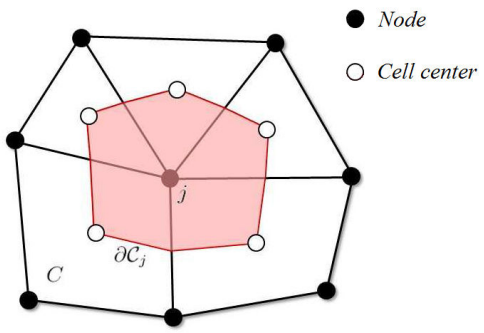

Figure 2.1: Control volume associated with node j [55].

In the present work, the AVBP code is coupled with the chemical kinetics solver CLOE (CLosed hOmogeneous rEactor) from the IFP-Kinetics package [62], developed and owned by IFPEN. The implementation of CLOE into the current version of AVBP (Version 7) was performed in the framework of this Ph.D. The numerical resolution of gas-phase chemistry along with diffusive and convective transport processes is described in the following subsection.

2.2.2 Numerical resolution methodology

Gas-phase chemistry is represented by the source term $\rho\dot{\omega}_{Y_k}$ in the R.H.S of Eq. (2.2). The latter can be either integrated directly, at the same time and with the same method as the transport terms, or solved independently of the diffusive and convective terms according to an operator-splitting technique. The heat release due to reactions is always taken into account explicitly, *i.e.* no splitting is performed concerning energy. $\dot{\omega}_T$ is calculated as shown in Eq. (2.30) once $\rho\dot{\omega}_{Y_k}$ is obtained.

Explicit resolution

In this case, the source term $\rho\dot{\omega}_{Y_k}$ in the R.H.S of Eq. (2.2) is first calculated as in Eq. (2.24). The temporal integration is performed including transport processes as follows :

$$\rho Y_k^{n+1} = \rho Y_k^n + dt \left[R_k^{\text{conv}} + R_k^{\text{diff}} + R_k^{\text{chem}} \right] \tag{2.31}$$

where dt is the time step of the integration, R_k^{conv} and R_k^{diff} are respectively the operators expressing the rates of change of Y_k due to convective and diffusive transport. R_k^{chem} is the operator giving the rate of change due to chemical reactions. It implies that the inclusion of the source

term $\rho\dot{\omega}_{Y_k}$ is performed at the same time as the diffusive and convective terms. No assumptions are made regarding the differences between the chemical, diffusive and convective time scales. If the chemical kinetics are stiff [63], the explicit integration might undergo numerical instabilities if the time step is not sufficiently small. The numerical time step can be decreased but this is likely to yield impractical CPU times.

Operator-splitting technique

The alternative to the explicit resolution is to isolate the chemistry resolution. In this case, chemistry is separated from the diffusive and convective transport terms. Hence, the transport equation for species mass fractions (Eq. (2.2)) can be expressed in the following form :

$$\forall\ k \in \Omega : \frac{\partial \rho Y_k}{\partial t} = R_k^{\text{chem}}(t) + R_k^{\text{conv}}(t) + R_k^{\text{diff}}(t) \tag{2.32}$$

This is the general idea used for the coupling of AVBP and CLOE. In order to solve Eq. (2.32), the integration of chemistry is performed with respect to the following steps :

- Step 1 : the vector $\vec{\psi}$ that includes the species and temperature is defined as shown in Eq. (2.33). Superscript HR indicates that the variable only undergoes chemical reactions independently of transport, as in a homogeneous reactor.

$$\psi_i = \begin{pmatrix} \psi_1 \\ . \\ . \\ . \\ \psi_N \\ \psi_{N+1} \end{pmatrix} = \begin{pmatrix} \rho Y_1^{\text{HR}} \\ . \\ . \\ . \\ \rho Y_N^{\text{HR}} \\ T^{\text{HR}} \end{pmatrix} \tag{2.33}$$

- Step 2 : each time step and at every node of the mesh, the i^{th} component of $\psi_i(t)$ is communicated to CLOE, that solves the system of Eq. (2.34), where R_i^{chem} is the i^{th} component of the chemical operator that includes the chemical source terms :

$$\begin{cases} \vec{\psi} = \left(\rho Y_1^{\text{HR}}, ..., \rho Y_k^{\text{HR}}, ..., \rho Y_N^{\text{HR}}, T^{\text{HR}}\right) \\ \dfrac{\partial \psi_i}{\partial t} = R_i^{\text{chem}}(t) \quad \forall,\ i \in [\![1, N+1]\!] \end{cases} \tag{2.34}$$

- Step 3 : Once the integration over a time step dt is completed, the solution $\psi_i(t+dt)$ is returned to the AVBP code.

- Step 4 : $Y_k^{\mathrm{HR}}(t+dt)$ is used to estimate the chemical source term $\rho\dot{\omega}_{Y_k}$ of Eq. (2.2) in the following way :

$$\rho\dot{\omega}_{Y_k} = \frac{\rho\left(Y_k^{\mathrm{HR}}(t+dt) - Y_k(t)\right)}{dt} \tag{2.35}$$

- Step 5 : finally, R_k^{chem} is replaced in Eq. (2.32) using the expression of Eq. (2.35). The time integration over a time step dt expressed in Eq. (2.31) becomes :

$$\rho Y_k(t+dt) = \rho Y_k^{\mathrm{HR}}(t+dt) + dt\left(R_k^{\mathrm{conv}} + R_k^{\mathrm{diff}}\right) \tag{2.36}$$

It should be noted that the chemical operator R_k^{chem} is not expressed in spatial dimensions, contrary to the convective and diffusive operators. In other words, chemistry is considered a local process for each grid node. As a result, Eq. (2.34) corresponds to an N_n independent ODE system, comprising $N+1$ unknowns, where N_n is the number of grid nodes.

As explained, each computational node of the mesh can be seen as an independent homogeneous reactor governed by the ODE system of Eq. (2.34), resolved by a dedicated solver in the CLOE code. The chemical kinetics used in this study are quite stiff, especially under the studied conditions (see Section 4.4). To achieve fast and robust time integration, implicit methods, involving both the current state of the system and the later one, can be used. Implicit methods don not have inherent limits on the size of the required time step. The time step used here is limited by the Courant-Friedrichs-Lewy (CFL) [64] condition for the resolution of the convective transport terms.

Implicit methods require a series of sub-iterations to establish equilibrium within a certain tolerance ; the Jacobian matrix is inverted several times over the course of a time step, which is an expensive operation. The implicit ODE solver DVODE [65], available in the CLOE code, is used in the present work. This solver includes aspects such as step and order resetting and Jacobian matrix saving, permitting an efficient resolution of stiff chemical kinetic ODEs.

In the case of implicit solvers, such as DVODE, the homogeneous reactor ODE includes the temperature equation in order to update the temperature value at every sub-iteration. A proper resolution is thereby ensured. This results in a system having a size of $N+1$:

$$\begin{cases} \vec{\psi} = \left(\rho Y_1^{\text{HR}}, ..., \rho Y_k^{\text{HR}}, ..., \rho Y_N^{\text{HR}}, T^{\text{HR}}\right) \\ \dfrac{\partial \rho Y_k^{\text{HR}}}{\partial t} = R_k^{\text{chem}}(t) = \rho \dot{\omega}_{Y_k} \quad \forall\, k \in \Omega \\ \dfrac{\partial T^{\text{HR}}}{\partial t} = R_{N+1}^{\text{chem}}(t) = -\dfrac{\sum\limits_k h_k \rho \dot{\omega}_{Y_k}^{\text{HR}}}{\rho c_p} \quad \forall\, k \in \Omega \end{cases} \tag{2.37}$$

where $\dot{\omega}_{Y_k}^{\text{HR}}$ is the chemical source term determined by the kinetic solver. In the present work, the energy equation is enthalpy based, assuming that pressure remains constant over the computational time step. If a constant volume equation was considered, an internal energy based equation should be used. These assumptions are made in order to decouple chemical reactions and convection. A more accurate approach would consist in a generic formulation accounting for both pressure and volume variations.

2.2.3 Validation case

In order to validate the proper functioning of the coupling of the AVBP code and the kinetic solver CLOE, a homogeneous reactor (HR) simulation is conducted. The 0-D HR configuration is composed of 3^3 hexahedral computational cells. Its boundaries are all set to be adiabatic and free-slip, resulting in a simple closed volume reactor exclusively exhibiting chemical reactions and no molecular or convective transport. The chemical kinetics mechanism used in this validation case is a skeletal mechanism [66], hereafter called "ERC mechanism", proposed for n-heptane/air combustion. The numerical solver used for the present computation is the implicit solver DVODE [65]. The chosen initial conditions correspond to a stoichiometric n-C_7H_{16} / air mixture (see Table 2.1). The numerical results are compared with the ones obtained using the chemical kinetics solver CLOE alone. Other conditions were tested showing equivalent accuracy.

Mixture	ϕ	Initial conditions	Reaction mechanism	Integration method
n-C_7H_{16} / air	1	35 bar, 1000 K	ERC mechanism [66]	DVODE [65]

Table 2.1: Homogeneous reactor validation case initial conditions.

Figure 2.2 shows the resulting time evolution of temperature and species mass fractions. As 29 species are involved, only two major species (C_7H_{16}, CO_2) and the hydroxyl radical OH are shown. The coupling results match the results given by the kinetics solver alone.

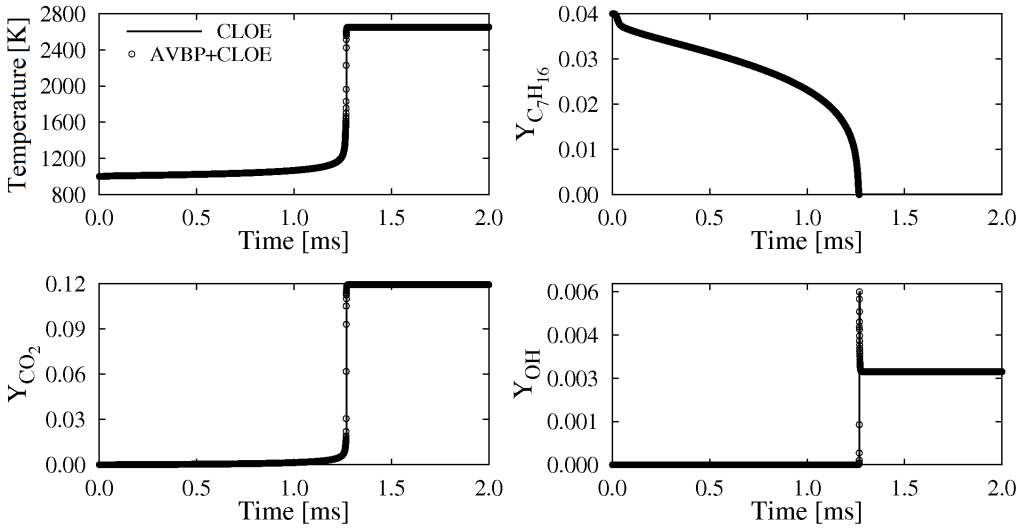

Figure 2.2: Validation case ; time evolution of temperature and species in the HR configuration, comparison between CLOE (lines) and AVBP/CLOE coupling results (circles).

Chapter 3

Turbulent combustion modelling in RANS simulation

3.1 Reynolds-Averaged Navier-Stokes equations

The following equations are presented with respect to the RANS simulation of multi-species compressible reactive flows. In this context, the resolved variables correspond to statistical averages. Each flow variable is decomposed into a mean $\overline{Q}$ and a fluctuating part Q' :

$$Q = \overline{Q} + Q' \quad \text{with} \quad \overline{Q'} = 0 \tag{3.1}$$

In compressible flows, density variations induce some extra terms that need to be modelled. This additional complexity can be avoided using a density weighted average, called Favre average :

$$\widetilde{Q} = \frac{\overline{\rho Q}}{\overline{\rho}} \tag{3.2}$$

The decomposition into mean and fluctuating part can then be expressed as :

$$Q = \widetilde{Q} + Q'' \quad \text{with} \quad \widetilde{Q''} = 0 \tag{3.3}$$

Using this formalism, the compressible reactive flow transport equations become :

$$\frac{\partial \overline{\rho}}{\partial t} + \frac{\partial \overline{\rho} \widetilde{u_i}}{\partial x_i} = 0 \tag{3.4}$$

$$\frac{\partial \overline{\rho}\widetilde{Y_k}}{\partial t} + \frac{\partial}{\partial x_i}\left(\overline{\rho}\widetilde{u_i}\widetilde{Y_k}\right) = -\frac{\partial}{\partial x_i}\left(\overline{V_{k,i}Y_k} + \overline{\rho}\widetilde{u_i''Y_k''}\right) + \overline{\rho}\widetilde{\dot{\omega}}_{Y_k} \tag{3.5}$$

$$\frac{\partial \overline{\rho}\widetilde{u_i}}{\partial t} + \frac{\partial \overline{\rho}\widetilde{u_i}\widetilde{u_j}}{\partial x_j} = -\frac{\partial \overline{p}}{\partial x_i} + \frac{\partial}{\partial x_j}\left(\overline{\tau_{i,j}} - \overline{\rho}\widetilde{u_i''u_j''}\right) \tag{3.6}$$

$$\frac{\partial \overline{\rho}\widetilde{h_s}}{\partial t} + \frac{\partial \overline{\rho}\widetilde{u_i}\widetilde{h_s}}{\partial x_i} = \overline{\dot{\omega}_T} + \overline{\frac{Dp}{Dt}} + \frac{\partial}{\partial x_i}\left(\overline{\lambda\frac{\partial T}{\partial x_i}} - \overline{\rho}\widetilde{u_i''h_s''}\right) + \overline{\tau_{i,j}\frac{\partial u_i}{\partial x_j}} - \frac{\partial}{\partial x_i}\left(\overline{\rho\sum_{k\in\Omega} V_{k,i}Y_k h_{s,k}}\right) \tag{3.7}$$

where

$$\overline{\frac{Dp}{Dt}} = \frac{\partial \overline{p}}{\partial t} + \overline{u_i\frac{\partial p}{\partial x_i}} = \frac{\partial \overline{p}}{\partial t} + \widetilde{u_i}\frac{\partial \overline{p}}{\partial x_i} + \overline{u_i''\frac{\partial p}{\partial x_i}} \tag{3.8}$$

In these averaged balance equations only the mean flow is solved and the ensemble of the turbulent scales is modelled based on statistical means. This system of equations contains more unknowns than equations ; the term $\overline{\rho}\widetilde{u_i''u_j''}$, called "Reynolds stress", the pressure-velocity correlation $\overline{u_i''\partial p/\partial x_i}$, the species and enthalpy turbulent fluxes $\overline{\rho}\widetilde{u_i''Y_k''}$, $\overline{\rho}\widetilde{u_i''h_s''}$ are unknown and have to be modelled. This is known as the turbulence closure problem.

Turbulent combustion modelling focuses on the closure of the species chemical reaction rates $\widetilde{\dot{\omega}}_{Y_k}$. Coming back to Eq. (3.5), a possible closure for the turbulent fluxes $\overline{\rho}\widetilde{u_i''Y_k''}$ is obtained by introducing turbulent viscosity μ_t, modelled by a turbulence model, and a turbulent Schmidt number Sc_t :

$$\overline{\rho}\widetilde{u_i''Y_k''} = -\mathcal{D}_t\frac{\partial \widetilde{Y_k}}{\partial x_i} \quad \text{where} \quad \mathcal{D}_t = \frac{\mu_t}{Sc_t} \tag{3.9}$$

The diffusive flux $\overline{V_{k,i}Y_k}$ is often modelled using Fick's law :

$$\overline{V_{k,i}Y_k} = -\overline{\rho}\overline{\mathcal{D}}_k\frac{\partial \widetilde{Y_k}}{\partial x_i} \tag{3.10}$$

where $\overline{\mathcal{D}}_k$ is the mass diffusion coefficient of species k. Under the assumption that diffusivities of all the involved species $\overline{\mathcal{D}}_k$ are equal to $\mathcal{D}$, Eq. (3.5) becomes :

$$\frac{\partial \overline{\rho}\widetilde{Y_k}}{\partial t} + \frac{\partial}{\partial x_i}\left(\overline{\rho}\widetilde{u_i}\widetilde{Y_k}\right) = \frac{\partial}{\partial x_i}\left(\overline{\rho}(\mathcal{D}+\mathcal{D}_t)\frac{\partial \widetilde{Y_k}}{\partial x_i}\right) + \overline{\rho}\widetilde{\dot{\omega}}_{Y_k} \tag{3.11}$$

3.2 Tools for non-premixed modelling

In Diesel engines, fuel and oxidiser enter separately into the combustion chamber ; hot compressed air is entrained into the fuel spray, leading to liquid fuel breakup, evaporation, and finally autoignition. At first, the premixed fraction of the mixture is rapidly consumed. Then, combustion takes place under non-premixed conditions, *i.e.* fuel and oxidiser mix and burn during continuous interdiffusion, while fresh fuel is being introduced inside the combustion chamber. To ensure understanding, key elements of the modelling of this process are summarised below.

Mixture fraction and progress variable

A quantity widely used for the description of non-premixed combustion is the mixture fraction variable Z, a passive scalar indicating the local fuel-oxidiser ratio. Out of the various definitions of Z [67] for a fuel consisting entirely of carbon and hydrogen, the carbon and hydrogen atom conservation is retained here :

$$Z = \sum_{k\in\Omega} \frac{Y_k \; n_{C,k} \; m_C}{W_k} + \sum_{k\in\Omega} \frac{Y_k \; n_{H,k} \; m_H}{W_k} \quad , \quad 0 \leq Z \leq 1 \tag{3.12}$$

where $n_{C,k}$, $n_{H,k}$ are the number of carbon and hydrogen atoms contained in the k^{th} species molecule and m_C, m_H are the respective atomic masses. A mixture is called stoichiometric if the fuel-oxidiser ratio is such that both fuel and oxidiser are entirely consumed after combustion is completed.

The progress of combustion with respect to the equilibrium state, *i.e.* the transition between fresh reactants and fully burnt products, is represented by a progress variable Y_c. The definition of the progress variable used in the present work is based on CO and CO_2 mass fractions [68] :

$$Y_c = Y_{\text{CO}} + Y_{\text{CO}_2} \tag{3.13}$$

with the corresponding reaction rate :

$$\dot{\omega}_{Y_c} = \dot{\omega}_{Y_{\text{CO}}} + \dot{\omega}_{Y_{\text{CO}_2}} \tag{3.14}$$

Y_c^{eq} is the value of Y_c when the equilibrium state is reached (fully burnt gases), depending on equivalence ratio and initial temperature. In the present work, initial temperature directly

depends on Z, therefore, Y_c^{eq} exclusively depends on the mixture fraction Z. The initial value of progress variable Y_c^{init} also depends exclusively on Z, since initial species mass fraction are chosen to be linearly correlated with Z. A normalised progress variable can be defined as :

$$c = \frac{Y_c - Y_c^{\text{init}}}{Y_c^{\text{eq}} - Y_c^{\text{init}}} \quad , \quad c \in [0, 1] \tag{3.15}$$

From a statistical analysis viewpoint, the above parameters Z and c can be treated using either Reynolds-averaging ($\overline{Q}$) or Favre-averaging (mass weighted averaging $\widetilde{Q}$). Mixture fraction Z can thus be decomposed into a density weighted mean $\widetilde{Z}$ and a fluctuation Z''. Unmixedness, denoted $\widetilde{S_Z}$, can then be defined as following :

$$\widetilde{S_Z} = \frac{\widetilde{Z''^2}}{(\widetilde{Z} - Z_{\text{min}})(Z_{\text{max}} - \widetilde{Z})} \tag{3.16}$$

where Z_{min} and Z_{max} are the minimum and maximum values of mixture fraction. $\widetilde{S_Z}$ is equal to zero for a perfectly homogeneous mixture. Similarly, a segregation factor can be defined for c :

$$\overline{S_c} = \frac{\overline{c'^2}}{\overline{c}\,(1 - \overline{c})} \tag{3.17}$$

Probability density functions

A popular approach to describe and model turbulent combustion is through probability density functions (PDFs), accounting for the flame structure below the size of the computational cell. The involved variables, for example Z, are expressed in terms of statistical means and variances and are integrated over PDFs, according to the following properties :

$$\int \widetilde{P}(Z)\,\mathrm{d}Z = 1 \tag{3.18}$$

$$\int Z\widetilde{P}(Z)\,\mathrm{d}Z = \widetilde{Z} \tag{3.19}$$

$$\int (Z - \widetilde{Z})^2\,\widetilde{P}(Z)\,\mathrm{d}Z = \widetilde{Z^2} - \widetilde{Z}^2 = \widetilde{Z''^2} \tag{3.20}$$

Laminar diffusion flame

The counterflow diffusion flame is a common configuration used to represent a laminar diffusion flame. Its geometry consists of opposed and axi-symmetric fuel and oxidizer jets (see Figure 3.1), mixing along a stagnation plane. In this configuration there is no flame propagation; fuel and oxidiser are on each side of the reaction zone where heat is released. Combustion occurs around stoichiometry, closer to the oxidiser side with respect to the stagnation plane. The burning rate is controlled by the molecular diffusion of the reactants towards a reaction zone.

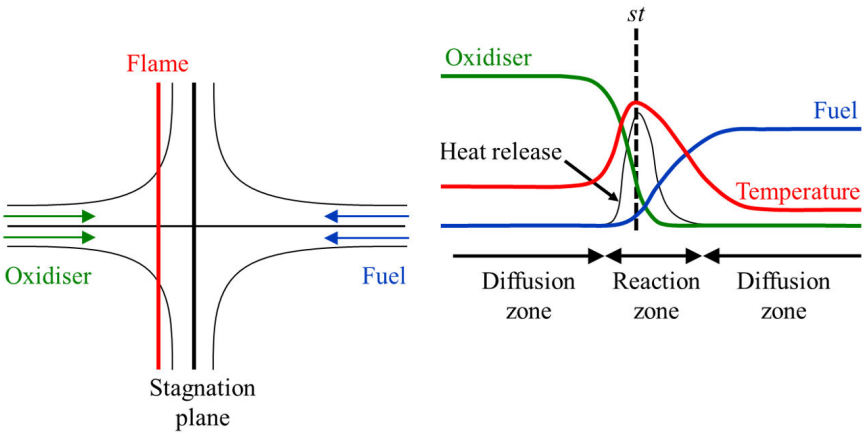

Figure 3.1: Sketch of a counter-flowing fuel and oxidiser diffusion flame (left) and generic structure of a laminar diffusion flame (right).

The balance equation for every chemical species k involved in the combustion process can be written as follows :

$$\frac{\partial \rho Y_k}{\partial t} + \frac{\partial \rho Y_k u_i}{\partial x_i} = \frac{\partial}{\partial x_i}\left(\rho \mathcal{D} \frac{\partial Y_k}{\partial x_i}\right) + \rho \dot{\omega}_{Y_k} \tag{3.21}$$

considering a diffusion coefficient $\mathcal{D}$, common for all species. Diffusion flames are often described in terms of mixture fraction Z (see Eq.(3.12)) evolving through the diffusive layer from zero (pure oxidiser) to unity (pure fuel). Under the assumption that temperature and mass fractions of all species involved in the combustion process can be expressed as functions of mixture fraction Z and time t [69], Eq. (3.21) becomes :

$$\frac{\partial Y_k}{\partial t} = \dot{\omega}_{Y_k} + \chi \frac{\partial^2 Y_k}{\partial Z^2} \tag{3.22}$$

In the above equation, $\chi\,\partial^2 Y_k/\partial Z^2$ is the diffusion term and $\dot{\omega}_{Y_k}$ is the reaction term. The scalar dissipation rate of the mixture fraction χ is defined as follows :

$$\chi = \mathcal{D}\left(\frac{\partial Z}{\partial x_i}\frac{\partial Z}{\partial x_i}\right) \tag{3.23}$$

χ has the dimension of an inverse time and therefore represents the inverse of a diffusive time τ_χ. It can also be seen as a diffusivity in mixture fraction space. χ can be modelled as follows :

$$\chi(Z,a) = a\;\mathcal{F}(Z) \tag{3.24}$$

where a is the strain rate of the laminar diffusion flame, and $\mathcal{F}(Z)$ is derived from the classical expression [69] adapted for counterflow diffusion flames where the fuel stream is at Z_{max}, not necessarily equal to unity, and the oxidiser stream is at Z_{min}, not necessarily equal to zero :

$$\mathcal{F}(Z) = \frac{(Z_{\text{max}} - Z_{\text{min}})^2}{2\pi}\text{exp}(-2[\text{erfc}^{-1}\left(2\,\frac{Z - Z_{\text{min}}}{Z_{\text{max}} - Z_{\text{min}}}\right)]^2) \tag{3.25}$$

The strain rate a has a strong influence on the behaviour of the diffusion flame. The inverse of a is the characteristic time scale of the problem. In an unstrained counterflow diffusion flame, the amount of heat transported away from the reaction zone is exactly balanced by the heat released by combustion [70]. As the distance between the jets is decreased and/or the velocity of the jets is increased, the flame departs from its chemical equilibrium ; then, quenching starts occurring since the heat fluxes leaving the reaction zone become greater than the chemical heat production, until an eventual extinction.

Non-premixed turbulent combustion regimes

Turbulent combustion involves a variety of length and time scales characterising the flow field and the chemical reactions taking place. A physical analysis can be based on the comparison between these scales. The Damköhler number Da compares a turbulent (τ_t) with a chemical (τ_c) time scales.

$$Da = \frac{\tau_t}{\tau_c} \tag{3.26}$$

Two limit cases are important for non-premixed turbulent combustion modelling : In the perfectly stirred reactor limit ($Da << 1$), reactants and products are mixed by turbulent structures before reacting. This situation corresponds to slow chemical kinetics. In the infinitely

fast chemistry limit ($Da >> 1$), the chemical time is short compared to the turbulent one, corresponding to a thin reaction zone distorted and convected by the flow field. The internal structure of the flame is not strongly affected by turbulence and may be described as a laminar flame element called a 'flamelet' [70]. In practical situations, a wide range of Damköhler number values may be encountered ; fuel oxidation generally corresponds to short chemical time scales ($Da >> 1$), whereas pollutant production and destruction, such as NO_x formation or CO oxidation, are generally slower.

It is intrinsically difficult to identify characteristic length and time scales in non-premixed turbulent combustion. This difficulty arises from the fact that the thickness of the flame depends on the aerodynamics controlling local mixing and from the absence of flame propagation imposing a characteristic speed. A rough classification of combustion regimes can be based on a Damköhler number Da characterising the reacting zones of the flow, and a turbulent Reynolds number Re_t representing the ratio of inertial forces to viscous forces within the fluid. The different non-premixed combustion regimes are schematically presented in Figure 3.2, related to these two dimensionless numbers.

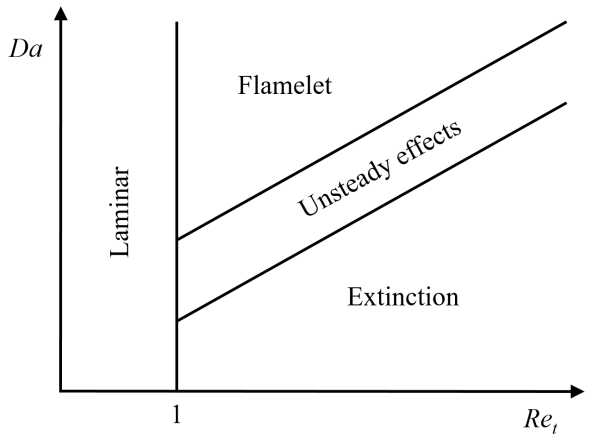

Figure 3.2: Regimes for turbulent non-premixed combustion as a function of the Damköhler number Da (based on the turbulence integral time scale τ_t and the chemical time τ_c) and the turbulent Reynolds number Re_t [25].

When the Damköhler number is assumed to be large (a common assumption in combustion modelling), the reaction rate is limited by turbulent mixing described in terms of scalar dissipation rates [71]. The burning rate can then be quantified in terms of turbulent mixing. A version of this approach is to consider the turbulent flame as an aggregate of thin, laminar 1-D flamelet structures present within the turbulent flow field. This assumption is only valid for combustion regimes where the inner structure of the flame is not impacted by turbulent mixing. In geometrical terms, this would mean that flame thickness is small compared to turbulent length scales, whereas in terms of temporal scales, that chemical time scales are shorter than the turbulent time scales.

The flamelet concept is the basis of many different turbulent combustion models such as RIF [72], FPV [73] or ADF [74], presented latter on. In the present work, the studied thermodynamic conditions of high pressure and temperature, and the presence of free radicals in the partially burnt gases of pilot and pre-injections result into a high reactivity of the mixture, highlighting this concept as an interesting candidate amongst the existing approaches.

3.3 Non-premixed combustion modelling approaches

This section is dedicated to an overview of non-premixed combustion modelling approaches based on complex or semi-detailed chemistry. Combustion models developed for simplified chemistry or assuming infinitely fast chemistry are not reviewed, since their predictivity is insufficient for engine simulations with fuel surrogates, especially in terms of pollutant emissions. The presented models can be classified according to two basic criteria : (i) the method applied for the treatment of chemical kinetics, and (ii) the way the interaction of turbulence with chemistry and the resulting heterogeneities of the mixture are accounted for.

Many industrial CFD codes used for combustion simulation include turbulence models developed for non-reacting flows, such as k-ε [75], simply rewritten in terms of Favre averaging. This approach necessitates the transport of as many additional variables as species contained in the chemical kinetics mechanism and the parallel resolution of chemistry. These demands can result in high CPU cost, especially when detailed chemical kinetics mechanisms are involved.

The need to take into account the effects of detailed chemistry at a minimal computational cost has led to the development of several methods for an *a priori* tabulation of chemistry, ready for use before launching CFD simulations. The basic idea is to generate look-up tables based on simple computations (*e.g.* homogeneous reactors or laminar diffusion flames) using complex reaction mechanisms. The combustion quantities of interest, such as temperature, heat release

rate, mass fractions, reaction rates, *etc.*, are related to a number of parameters. During the CFD simulation, values are extracted from the tables by means of interpolation and are exploited by a turbulent combustion model. Under this method, a small number of transport equations can be preserved, one for each of the model input parameters. Nevertheless, CPU costs are proportional to the number of parameters included in the model used.

3.3.1 Tabulation models

ILDM

Numerous methods exist for the treatment of the chemistry tabulation. The Intrinsic Low Dimension Manifold (ILDM) [76] is a mathematical method based on the analysis of characteristic time scales of a reactive flow. Quantities of interest are tabulated as functions of a limited number of species that evolve slowly. Hence, a subspace called Manifold is created, containing the minimum number of species required for the representation of chemical kinetics. This method gives satisfactory results in Diesel engine simulation [77]. However, it is not suitable for the simulation of low-temperature regimes, since under these conditions chemical time scales become very long.

FPI and FGM

In order to address this problem, the Flame Prolongation of ILDM (FPI) [78] was introduced. Initially based on laminar premixed flames, the approach was extended to non-premixed flames and homogeneous reactors and incorporated in premixed [79] and non-premixed [80] combustion modelling. The Flamelet Generated Manifolds (FGM) [81] is a similar approach also using 1-D laminar flames that has been applied to premixed [82], partially premixed [83] and non-premixed [84] combustion simulations. In these approaches, the slowly evolving chemical species can be replaced by mixture fraction Z, representing local fuel concentration, and progress variable c, describing the evolution of combustion. The number of transported variables can be thus drastically limited. Enthalpy can also be added as a parameter of the tabulation [68], to account for the enthalpy losses. As will be discussed in the following chapters, more dimensions can potentially be added to the chemistry tabulation, so to take into account the effect of multiple injections' interaction.

S2FT

The application of such tabulation models in more and more complex configurations [85] gradually leads to an increased number of input parameters. To tackle this issue, Self-Similar Flame Tabulation (S2FT) [86] allows a significant reduction of the number of chemistry tables' dimensions using the self-similarity of reaction rates and mass fractions of chemical species in certain reaction mechanisms. Indeed, in certain cases, the reaction rates of each chemical species at different thermodynamic conditions can be superposed, leading to a significant decrease of the size of the tabulations. This method has been applied in RANS simulation of a methane flame [87] and adapted for cases with enthalpy losses and gas recirculation [88], as well as for cool flame simulation [89].

ISAT

Instead of generating the chemistry tabulation beforehand, In Situ Adaptative Tabulation (ISAT) proposed by Pope [90], permits the generation of needed tables during CFD simulation. Species reaction rates are at first obtained by the direct resolution of a reaction mechanism. These values are stored in a chemistry data base evolving along with the CFD simulation. When local conditions met along the simulation happen to be similar to conditions previously obtained, tabulated values are used via interpolation. In a sense, ISAT can be considered as a tabulation model or as a model of chemical kinetics implementation, via an algorithm for the approximation of non-linear relationships. This methodology, however efficient it may be when used with reduced chemical kinetics mechanisms, remains infeasible for detailed reaction mechanisms, since the composition space becomes enormous due to the number of chemical species involved. This limitation was lifted by Yang and Pope and their In Situ Adaptive Tabulation in Principal Directions (ISATPD) model [91], using a decomposition of the tabulation in principal directions that are the only ones to be stored.

3.3.2 Turbulent combustion models

Direct integration of chemical kinetics

There exist a variety of different assumptions to model the effect of the turbulence on the combustion process. The strongest among them is to ignore any interaction of the flow with chemistry below the grid level ; combustion is supposed homogeneous at the level of the computational cell (RANS) or of the spatial filter (LES). Average local composition and thermodynamic conditions obtained by the conservation equations in every computational cell and at every time-step are provided to a chemical kinetics solver that returns the corresponding reaction rates $\dot{\omega}_{Y_k}$. Hence, a chemical kinetics mechanism is implemented in the CFD computation without any additional bias [92]. Alternatively, chemical kinetics can be used in the generation of tabulations that are then used in the CFD simulation. Although encouraging results were obtained on Diesel engines [32, 93], the effects of mixture fraction and temperature fluctuations on combustion are completely neglected and thus, the reliability of this method is questionable. The limits of this approach in RANS are discussed in Section 6.2.

Transported PDFs approach

In order to overcome the assumption of local homogeneity and to take into account the impact of turbulent movement, a statistical approach can be coupled with the resolution of a chemical kinetics mechanism. PDF modeling [94] implies the resolution of the following system of equations :

$$\widetilde{f} = \int_{\Psi_1,\Psi_2,...,\Psi_N} f(\Psi_1, \Psi_2, ..., \Psi_N)\widetilde{P}(\Psi_1, \Psi_2, ..., \Psi_N)\,\mathrm{d}\Psi_1\,\mathrm{d}\Psi_2, ..., \mathrm{d}\Psi_N \tag{3.27}$$

for some variable f (*e.g.* reaction rate) depending on $\Psi_1, \Psi_2, ..., \Psi_N$ other variables (*e.g.* temperature, species mass fractions). Values of f are directly obtained by the resolution of chemistry, using $\Psi_1, \Psi_2, ..., \Psi_N$ variables as inputs. Then, these values are integrated over PDFs, here denoted by $\widetilde{P}$, obtained via the parallel resolution of transport equations. The number of these PDFs is a limiting factor from a CPU cost perspective. In practice, stochastic particles are often introduced, using Monte-Carlo methods, to describe the local composition of the mixture [95]. This approach, costly as it may be, has been coupled with the ISAT method for the simulation of a lifted methane flame [96] and has also been applied in Diesel engine RANS simulations [97, 98].

CMC

The Conditionnal Moment Closure (CMC) model, independently proposed by Klimenko [99] and Bilger [100], considers the impact of turbulence on the combustion process by introducing averages of species mass fractions $\left(\overline{Y_k|_{Z^*}}\right)$ conditioned on discretised mixture fraction values Z^*. These conditional moments are obtained by resolution of transport equations. The number of transport equations is thus equal to the number of species included in the reaction mechanism, multiplied by the number of mixture fraction sections, demands that can be very costly in terms of CPU. Mean mass fractions $\widetilde{Y_k}$ are then computed by integrating the conditional moments over a PDF of the mixture fraction $\widetilde{P}(Z)$, as in Eq. (3.28). This model has been applied in Diesel engine simulations using RANS [35, 101, 102] and LES [103] formalisms.

$$\widetilde{Y_k} = \int \left(\overline{Y_k|_{Z^*}}\right) \widetilde{P}(Z^*)\,\mathrm{d}Z^* \tag{3.28}$$

RIF

The Representative Interactive Flamelets (RIF) model was developed by Pitsch *et al.* [72, 104] based on the works of Peters [105] and describes the local structure of the flame through the flamelet approach. For this purpose, a 1-D flamelet code is coupled to the CFD code. Equations for the flow, the turbulence, the mean enthalpy and the mixture fraction mean and variance are solved in the CFD code. Strain rate and mean pressure values are passed on to the flamelet code, which solves the unsteady flamelet equations and provides the species mean mass fractions. A β distribution of mixture fraction depending on its mean and variance is then applied, so to represent the fluctuations due to turbulent movement. The mean temperature is then calculated through the mean enthalpy, depending on the species mixture fractions, and is finally passed to the CFD code.

The Eulerian Particule Flamelet Model (EPFM) [106, 107] was derived from the RIF model, introducing transported particles each of which represents one flamelet. Thus, a value of local strain rate is attributed to each of these particles, allowing to take better account of the species heterogeneities in the flow. CPU time related to the resolution of the flamelet equations (one for every particle) is important, even though in practice a small number of particles is introduced. Diesel engine RANS simulations have been carried out [108, 109] using this approach.

RIF model was also extended to applications involving split [110] and multiple Diesel injections [111] with interesting results that come, however, at a high computational cost. Two-dimensional laminar flamelet equations were derived based on the original Peters' flamelet equation [105], to describe the transfer of heat and mass between two interacting mixture fields. This modelling strategy was then generalised for multiple injection events, identifying different phases of combustion in the interaction between the mixture fields resulting from different injections.

ECFM3Z and TKI

Colin *et al.* [112] proposed the Extended Coherent Flame Model (ECFM) that is based on a conditioning averaging technique which allows precise reconstruction of local properties in fresh and burned gases, and a flame surface density equation which takes into account the wrinkling of the flame front surface by turbulent eddies. Initially developed to model combustion in perfectly or partially mixed mixtures, the ECFM formalism was adapted to also account for unmixed combustion. In the 3-zones Extended Coherent Flame Model (ECFM3Z) [113], the mixing state is represented by three mixing zones : a pure fuel zone, a pure air plus possible residual gases zone and a mixed zone, in which the ECFM combustion model is applied. ECFM3Z can be seen as a simplified CMC type model where the mixture fraction space would be discretised by only three points, or as a simplified PDF consisted of three Dirac functions, one for each zone. The conditioning technique is applied to the three mixing zones and allows to reconstruct the gas properties in the fresh and burned gases of the mixed zone.

The premixed turbulent flame description is given directly by ECFM. The diffusion flame is accounted for thanks to the three zones mixing structure which represents phenomenologically the diffusion of fuel and air towards the reactive layer, that is the mixed zone. The interchange between these zones is described introducing a characteristic turbulent time scale. In order to take into account the autoignition mechanisms, ECFM3Z is often coupled with the Tabulated Kinetics of Ignition (TKI) approach [114, 115]. In its initial version, an autoignition precursor is traced in the flow, helping to quantify the autoignition delay, and the autoignition chemistry is accounted for using constant pressure homogeneous reactor tabulations. ECFM3Z is able to reproduce the relative importance of auto-ignition and diffusion flame on the total heat release, depending on the engine operating conditions considered. The model was first presented [116] in a comparative work with Diesel experiments covering different engine operating conditions. Mobasheri *et. al.* [34] used it in multi-injection Diesel studies (see Section 1.3).

FPV

The Flamelet Progress Variable (FPV) model [73] is based on 1-D stationary laminar diffusion flames' tabulations using three parameters : the mixture fraction Z, a normalised progress variable c and a parameter λ allowing to identify the strain rate of every flame unequivocally. This approach takes into consideration the heterogeity due to turbulent mixing through a β distribution approximating the local distribution of Z. Ihme *et al.* [117] used an additional β distribution to approximate the fluctuations of parameter λ. The extended Unsteady Flamelet Progress Variable (UFPV) model [118] was then proposed, using unsteady strained 1-D laminar diffusion flame tabulations. A variant of this approach [119] uses enthalpy-based progress variable. It should be noted that the duration of generation of such tabulations can be particularly long, limiting the application of this model to reduced chemical kinetic mechanisms.

3.4 Description of the studied turbulent combustion models

This dissertation is a continuation of works undertaken over the past few years at IFPEN focusing on the development of turbulent combustion models for rigorous and affordable RANS simulation of internal combustion engines, gas turbines and furnaces in the context of industrial applications. The turbulent combustion models based on tabulated chemistry that are chosen to be evaluated and expanded offer a good compromise between precision and CPU costs and are subject of long time and extensive studies within IFPEN, namely those of Vervisch [120], Michel [121], Tillou [122], Galpin [123] and Aubagnac-Karkar [124].

The chemistry tabulations used in this study relate the combustion quantities of interest to the mixture fraction Z and the normalised progress variable c, as in FPI [78] tabulation approach. The studied models are based on the assumption that the statistical behaviour of heterogeneous reacting turbulent mixtures can be described through probability density functions (PDFs) for Z and c. In its most basic form, the idea consists in considering a joint PDF of Z and c, denoted $\widetilde{P}(Z,c)$. All combustion quantities of interest are directly related to the respective tabulated values, denoted by the TAB superscript, as shown below for the mean progress variable reaction rate $\widetilde{\dot{\omega}}_{Y_c}$:

$$\widetilde{\dot{\omega}}_{Y_c} = \int_{Z_{\min}}^{Z_{\max}} \int_0^1 \dot{\omega}_{Y_c}^{\mathrm{TAB}}(Z,c)\widetilde{P}(Z,c)\,\mathrm{d}Z\,\mathrm{d}c \tag{3.29}$$

This approach does not, in itself, constitute a feasible modelling approach, since the local $\widetilde{P}(Z,c)$ is not available in the context of RANS simulation. It defines, nonetheless, the maximum precision to be expected by models built on the assumption of a direct relation of all quantities to a mixture fraction Z and a normalised progress variable c. The inputs and the assumptions of the studied models are described below.

3.4.1 THR

The Tabulated Homogeneous Reactor (THR) approach directly uses tabulated values without any additional modelling to describe the influence of heterogeneities of the mixture. All combustion quantities are therefore directly related to the respective tabulated values that correspond to the mean mixture fraction $\widetilde{Z}$ and the mean normalised progress variable $\overline{c}$, as shown below for $\widetilde{\dot{\omega}}_{Y_c}$:

$$\widetilde{\dot{\omega}}_{Y_c} = \dot{\omega}_{Y_c}^{\mathrm{TAB}}(\widetilde{Z},\overline{c}) \tag{3.30}$$

This approach can be seen as the equivalent of a direct integration of the chemical kinetics combined with chemistry tabulation. The interaction of the flow with chemistry below the grid level is ignored and combustion is supposed locally homogeneous. From a turbulent combustion modelling perspective, the THR approach is equivalent to the direct integration of chemical kinetics presented in Subsection 3.3.2.

3.4.2 PCM

Vervisch *et al.* [36] proposed the Presumed Conditional Moment (PCM) model, in which the heterogeneities of the reacting mixture are taken into consideration through PDFs. Initially developed in the context of partially premixed combustion, the PCM formalism was extended to turbulent self-ignited combustion by Galpin *et al.* [38]. In PCM, the mixture fraction and the normalised progress variable are assumed to be independent variables, allowing the joint PDF to be written as a product of two independent PDFs :

$$\widetilde{P}(Z,c) = \widetilde{P}(Z)\ \overline{P}(c) \tag{3.31}$$

Mean quantities of interest are calculated by integration of the independent PDFs product over Z and c.

Two different versions of the PCM approach are studied in the present work. In the first version, here referred to as "PCM-1", the fluctuations of the normalised progress variable are neglected and the normalised progress variable PDF is $\overline{P}(c) = \delta(c - \overline{c})$, where δ is the Dirac delta function. $\widetilde{P}(Z)$ can be approximated by a β distribution defined for $Z_{\min} \leq Z \leq Z_{\max}$ as :

$$\beta(Z) = \frac{\Gamma(a+b)}{\Gamma(a)\Gamma(b)}(Z - Z_{\min})^{a-1}(Z_{\max} - Z)^{b-1} \tag{3.32}$$

where Γ represents the general factorial function, and a and b are given by :

$$a = \frac{\widetilde{Z}}{\widetilde{Z''^2}}(\widetilde{Z} - \widetilde{Z}^2 - \widetilde{Z''^2}) \ , \ b = \frac{\widetilde{Z} - 2\widetilde{Z}^2 - \widetilde{Z}^3 - Z''^2 + \widetilde{Z}\widetilde{Z''^2}}{\widetilde{Z''^2}} \tag{3.33}$$

a and b parameters depend on the first and second moments of the mixture fraction distribution evaluated according to transport equations for mixture fraction mean $\widetilde{Z}$ and variance $\widetilde{Z''^2}$. The mixture fraction variance is conveniently normalised by the minimum and maximum values of Z to define unmixedness, as in Eq. (3.16). The model response is obtained as follows :

$$\widetilde{\dot{\omega}}_{Y_c} = \int_{Z_{\min}}^{Z_{\max}} \int_0^1 \dot{\omega}_{Y_c}^{\text{TAB}}(Z, c)\beta(Z)\delta(c - \overline{c}) \, \mathrm{d}Z \, \mathrm{d}c \tag{3.34}$$

In the second version, referred to as "PCM-2", $\overline{P}(c)$ is approximated by a β distribution whose first and second moments are computed according to transport equations for $\overline{c}$ and $\overline{c'^2}$, still assuming statistical independence between Z and c. The normalised progress variable variance $\overline{c'^2}$ is normalised to define a segregation factor $\overline{S_c}$, as for the unmixedness $\widetilde{S_Z}$, yielding :

$$\widetilde{\dot{\omega}}_{Y_c} = \int_{Z_{\min}}^{Z_{\max}} \int_0^1 \dot{\omega}_{Y_c}^{\text{TAB}}(Z, c)\beta(Z)\beta(c) \, \mathrm{d}Z \, \mathrm{d}c \tag{3.35}$$

The THR approach can be seen as a zero-order PCM model in which $\widetilde{S_Z}$ and $\overline{S_c}$ are equal to zero, or :

$$\widetilde{\dot{\omega}}_{Y_c} = \int_{Z_{\min}}^{Z_{\max}} \int_0^1 \dot{\omega}_{Y_c}^{\text{TAB}}(Z, c)\delta(Z - \widetilde{Z})\delta(c - \overline{c}) \, \mathrm{d}Z \, \mathrm{d}c \tag{3.36}$$

PCM model has been coupled with FPI approach for the simulation of premixed [38], partially premixed [125] and non-premixed turbulent flames [36].

3.4.3 ADF

The following briefly describes the Approximated Diffusion Flames (ADF) model ; for further details, the reader is referred to the article by Michel *et al.* [74]. The ADF model is based on the approximation of 1-D diffusion flames in a counterflow configuration, considering each element of a turbulent flame as a laminar diffusion flame, in order to take the micro-scale diffusion into account. For this purpose, the flamelet equation (3.22) introduced by Peters [105] is approximated solving Eq. (3.37) for the progress variable Y_c from the pure mixing state to the equilibrium state, extracting directly the source term $\dot{\omega}_{Y_c}^{\text{TAB}}$ from a look-up table.

$$\frac{\partial Y_c^{\text{ADF}}}{\partial t} = \dot{\omega}_{Y_c}^{\text{TAB}} \left(Z, \frac{Y_c^{\text{ADF}}}{Y_c^{\text{eq}}(Z)} \right) + \chi(Z,a) \frac{\partial^2 Y_c^{\text{ADF}}}{\partial Z^2} \tag{3.37}$$

The scalar dissipation rate $\chi = \mathcal{D}|\nabla Z|^2$ is modelled as follows :

$$\chi(Z,a) = a\ \mathcal{F}(Z) \tag{3.38}$$

where a is the strain rate of the approximated diffusion flame, and $\mathcal{F}(Z)$ is the classical expression for counterflow diffusion flames of Eq. (3.25) [69]. A library of approximated flamelets is built solving the Eq. (3.37) for various strain rates a, using combustion chemistry in tabulated form. This library gives access to the evolution of the equivalent progress variable $Y_c^{\text{ADF}}(Z,a,t)$ and consequently to $\dot{\omega}_{Y_c}^{\text{ADF}}(Z,a,t) = \partial Y_c^{\text{ADF}}(Z,a,t)/\partial t$.

Once the approximate diffusion flames are calculated, integration is performed at each flamelet time over PDFs of the mixture fraction Z. For this purpose, standardised β distributions are used, defined by the mixture fraction mean $\widetilde{Z}$, variance $\widetilde{Z''^2}$, as in Eq. (3.32). Variance $\widetilde{Z''^2}$ is conveniently normalised to define unmixedness S_Z, as in Eq. (3.16). Mean progress variable reaction rate $\widetilde{\dot{\omega}}_{Y_c}$ is thus obtained, taking into account both chemical and diffusive effects :

$$\widetilde{\dot{\omega}}_{Y_c}(\widetilde{Z}, Sz, a, t) = \int_{Z_{\text{min}}}^{Z_{\text{max}}} \frac{\partial Y_c^{\text{ADF}}(Z,a,t)}{\partial t}(Z,a,t)\beta(Z)\,\mathrm{d}Z \tag{3.39}$$

These quantities are finally written as functions of $\widetilde{Z}, S_Z, \widetilde{Y}_c$ and a using the bijective relation between time and mean progress variable and stored in a look-up table. Once the table has been generated, it can be read during the CFD calculation to obtain the tabulated values corresponding to the local values of $\widetilde{Z}, S_Z, \widetilde{Y}_c$ and a. These local values are obtained by transport equations.

ADF can be seen as an extension of the PCM approach with the additional assumption of a diffusion flamelet structure correlating Z and c. This approach has very low CPU requirements compared to the computation of an unsteady diffusion flame, as in RIF modelling [72], since only one equation is solved in the flamelet code (Eq. (3.37)). The ADF model has been applied with success on autoigniting non-premixed jets [40, 80] and single injection Diesel engines [30], coupled with the FPI tabulation approach.

3.5 Model evaluation methodology

The modelling approaches presented in Section 3.4 are evaluated on the basis of an *a priori* comparison with the DNS database results. The temporal evolution of mean values $\widetilde{Z}$ and $\overline{c}$, variances $\widetilde{Z''^2}$ and $\overline{c'^2}$, *etc.* corresponding to local (cell) values of transported variables in a RANS computation, are obtained by post-processing of the DNS cases, with a temporal sampling rate of one DNS solution every microsecond. These values are then treated by a model testing tool returning the model response, *i.e.* mass fractions and reaction rates, that are finally compared with the corresponding averaged DNS results (see Figure 3.3). This methodology allows an evaluation of the model predictivity and does not accumulate errors, since the model inputs are retrieved from DNS post-processing at every time-step of the model evaluation test (every microsecond). The chemistry tabulations, relating mass fractions and reaction rates to the mixture fraction Z and the normalised progress variable c, are generated with the CLOE [62] code. Both DNS and tabulated chemistry models use the same skeletal reaction mechanism (ERC mechanism [66]) ; therefore, the focus is exclusively put on the modelling assumptions. The evaluation of the models, based on the evolution of mean reaction rate of the progress variable $\widetilde{\dot{\omega}}_{Y_c}$, is presented, permitting to investigate the expected model behaviour in terms of autoignition delay and heat release in the context of CFD engine simulation.

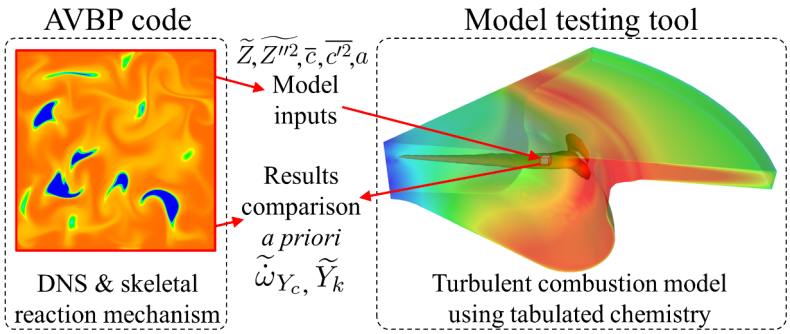

Figure 3.3: The principle of *a priori* model testing ; DNS of turbulent heterogeneous reactor (left hand side), model response tool corresponding to a RANS simulation cell (right hand side, Diesel combustion chamber 60° section).

Chapter 4

A representative DNS configuration

4.1 General overview

DNS can provide a detailed insight into turbulent non-premixed combustion and is an excellent tool for model development [126]. Since the computational cost of full engine DNS is prohibitive for the moment, small scale academic configurations are studied. Figure 4.1 illustrates the spacial scale of the DNSs performed in the present dissertation compared to an engine's combustion chamber.

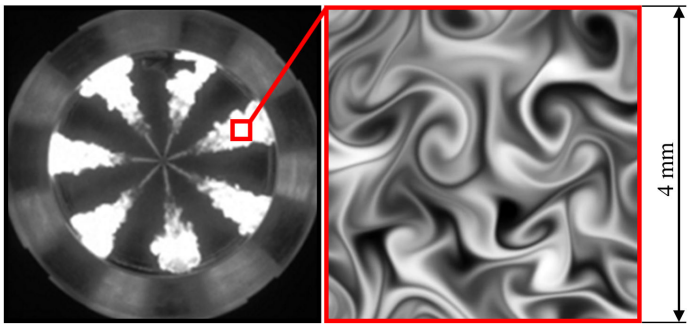

Figure 4.1: High-speed imaging of spray combustion [127] and DNS configuration.

This configuration has to be as representative of the physical problem addressed as possible. In order to obtain an estimation of the aerodynamic and the thermodynamic conditions inside the combustion chamber of a typical automotive Diesel engine during autoignition, preliminary RANS simulations are conducted. For this purpose, the code IFP-C3D [128] was used and a double injection, low load case ($\simeq$ 1500 rpm) was chosen from a benchmark database, validated against experimental data.

The evolutions of mean reaction rate $\overline{\dot{\omega}}$ and injected fuel mass m_{inj} are presented in Figure 4.2. As it can be seen, the pilot injection initiates combustion before TDC, increasing cylinder pressure and therefore improving the engine efficiency [129]. Additionally, temperature rises, leading to an earlier, smoother main injection autoignition, reducing combustion noise.

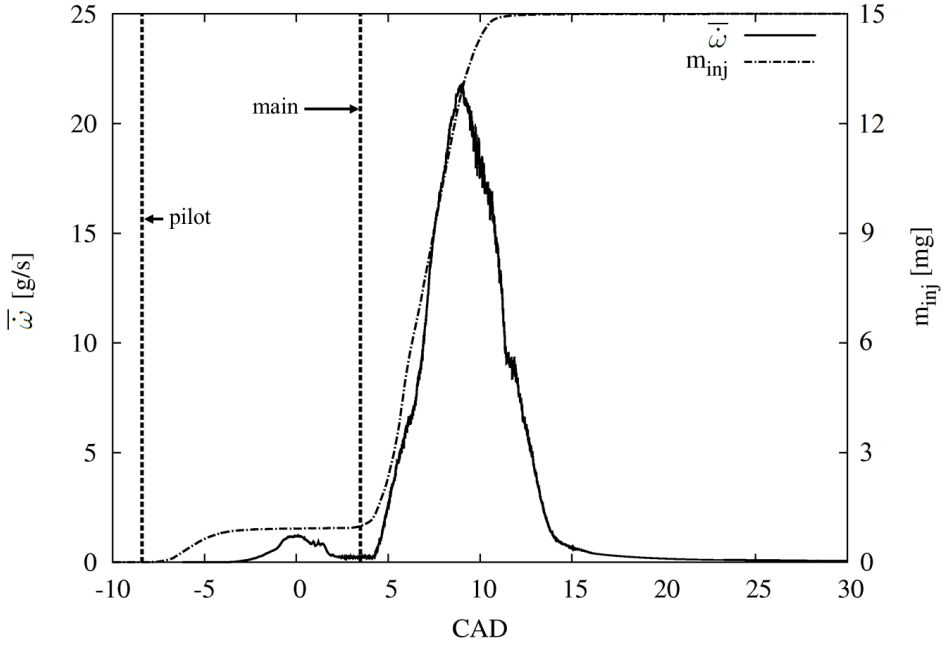

Figure 4.2: Evolution of mean reaction rate $\overline{\dot{\omega}}$ and injected fuel mass m_{inj} over a part of an engine cycle, pilot injection and main injection timings ; RANS simulation of double injection, low load Diesel cycle (IFP-C3D).

4.2 Turbulence characteristics

Turbulence is characterised by fluctuations in flow velocity. These fluctuations are associated with different length scales r ; a Reynolds number $Re(r)$ is then introduced for each turbulent length scale as :

$$Re(r) = \frac{u'(r)r}{\nu} \tag{4.1}$$

In homogeneous isotropic turbulence (HIT) all the statistical parameters of the fluctuating properties of the flow are uniform in space in every direction, independently of translations, rotations and reflections. Figure 4.3 displays the turbulence energy spectrum as one would deduce from analysis of experimental measurements ; energy spectral density E is plotted against wavenumber $K \propto 1/r$.

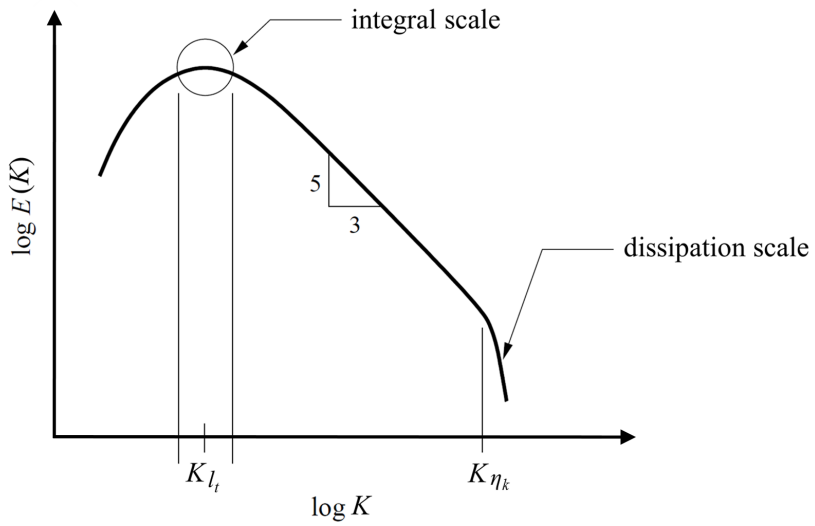

Figure 4.3: Turbulence energy spectrum plotted as a function of wavenumbers (log-log diagram).

The scale associated with the largest eddies (smaller wavenumbers) is the integral length scale l_t, usually considered as a fraction of the studied domain, no less than one-tenth of it. K_{l_t} is the wavelength corresponding to l_t, also called "most energetic wavelength". Integral length scale l_t is related to turbulence kinetic energy k, since these structures carry the biggest part of the total kinetic energy of the studied system, and its dissipation rate ε that indicates the rate of the continuous energy transfer from bigger to smaller patterns.

$$l_t = \frac{k^{3/2}}{\varepsilon} \tag{4.2}$$

The corresponding Reynolds number is the integral Reynolds number Re_t, else called "turbulent Reynolds number" :

$$Re_t = Re(l_t) = \frac{u' l_t}{\nu} \tag{4.3}$$

Turbulence kinetic energy k and its dissipation ε are deduced as :

$$k = \int_0^\infty E(K)\mathrm{d}K \propto u'(r)^2 \tag{4.4}$$

$$\varepsilon = \nu \int_0^\infty 2K^2 E(K)\mathrm{d}K \propto \frac{u'(r)^3}{r} \tag{4.5}$$

The smallest length scale considered in this analysis is the Kolmogorov (or "dissipation") length scale η_k, where the flow is mainly controlled by dissipation, *i.e.* by viscosity ν and by the dissipation rate ε of kinetic energy k :

$$\eta_k = (\nu^3/\varepsilon)^{1/4} \tag{4.6}$$

The ratio of the integral length scale l_t, to the Kolmogorov length scale η_k, comparing the largest and smallest turbulence fluctuations, is then expressed from Eqs. (4.2)-(4.5) :

$$\frac{l_t}{\eta_k} = Re_t^{3/4} \tag{4.7}$$

In DNS, the ensemble of the turbulence spectrum is explicitly resolved, covering all length scales. This means that the mesh size Δx must be of the order of Kolmogorov scale η_k and the size of the domain must be sufficiently big to include the biggest eddies, related with l_t. Considering a cube with a side length l_t as the computational domain, the number of elements N of the computational mesh should be equal to :

$$N = \left(\frac{l_t}{\eta_k}\right)^3 = Re_t^{9/4} \tag{4.8}$$

Thus, turbulent Reynolds number can be seen as an indicator of the CPU cost of a DNS study. Because computer resources are limited, DNS is often confined to simple geometries with two spatial dimensions, thereby missing all three-dimensional effects of real turbulence. The temporal evolution of 3-D turbulence is qualitatively different from that of 2-D turbulence due to the 3-D vortex-stretching effect [27, 47]. However, for fixed costs, the range of parameters explored with 2-D computations is wider. 2-D DNS parametric studies are valuable for the development and the validation of combustion models over a range of different conditions.

In the present study, decaying isotropic turbulence is superimposed on the heterogeneous distribution of chemical species. The velocity field in the numerical domain is initialised using a Passot-Pouquet turbulent kinetic energy spectrum function [130], correlating energy spectral density E with wavenumber K as following :

$$E(K) = C_s \sqrt{\frac{2}{\pi}} \frac{u'^2}{K_{l_t}} \left(\frac{K}{K_{l_t}}\right)^4 \exp\left[-2\left(\frac{K}{K_{l_t}}\right)^2\right] \tag{4.9}$$

where K_{l_t} is the most energetic wavenumber, u' is the RMS velocity fluctuation, and parameter C_s is equal to 32/3 for 2-D and 16 for 3-D fields.

The numerical results of the RANS simulation of double injection case are processed to extract approximate values of kinetic energy k and dissipation rate ε. Their evolution in the cylinder over a part of an engine cycle is presented in Figure 4.4. Combustion appears to have a strong impact on turbulent intensity. Kinetic energy increases after main autoignition since heat release induces strong flow accelerations. On the other hand, it diminishes due to the large changes in kinematic viscosity associated with temperature increase.

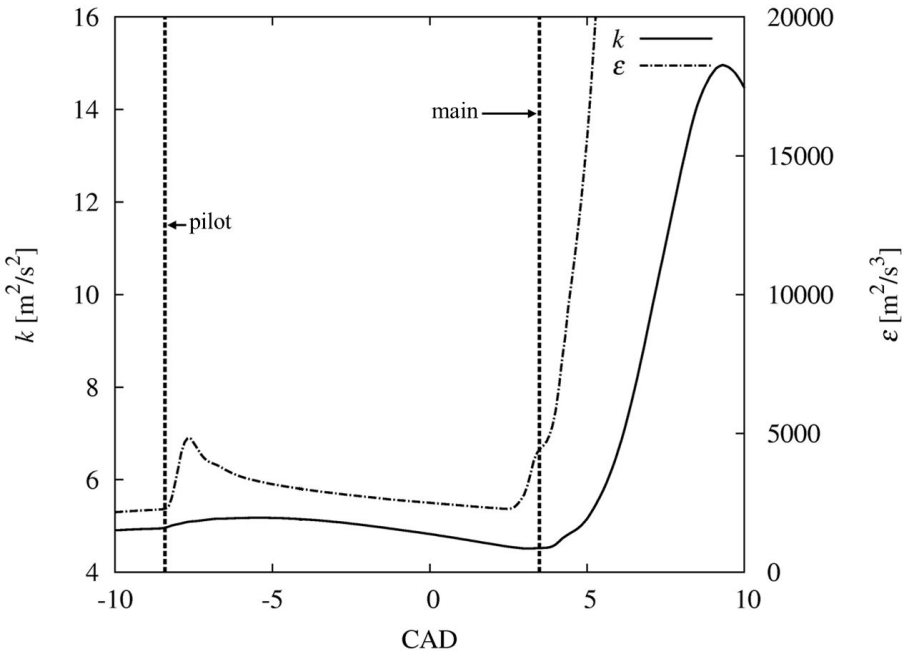

Figure 4.4: Evolution of mean kinetic energy k and dissipation rate ε over a part of an engine cycle, pilot injection and main injection timings ; RANS simulation of double injection, low load Diesel cycle (IFP-C3D).

In order to obtain a rough estimation of the level of kinetic energy and its dissipation rate in the reactive zones inside the domain, conditional probability density functions (PDF) of $k|_{\dot{\omega}>0}$ and $\varepsilon|_{\dot{\omega}>0}$ are extracted for positive values of local reaction rate $\dot{\omega}$ during autoignition. These PDFs are presented in Figure 4.5, along with the mean values of k and ε in the numerical domain. Nevertheless, these are rough approximations providing an order of magnitude of the parameters in question.

Based on the indicative turbulence characteristics extracted from the RANS simulation, the velocity fluctuation u' during autoignition is estimated at $\sqrt{2k/3} \simeq 1.8$ m/s and the integral length scale l_t is of the order of a millimetre, according to Eq. (4.2). The DNS domain should be a few times larger than l_t to provide converged statistics. A side length of 4 mm is chosen and

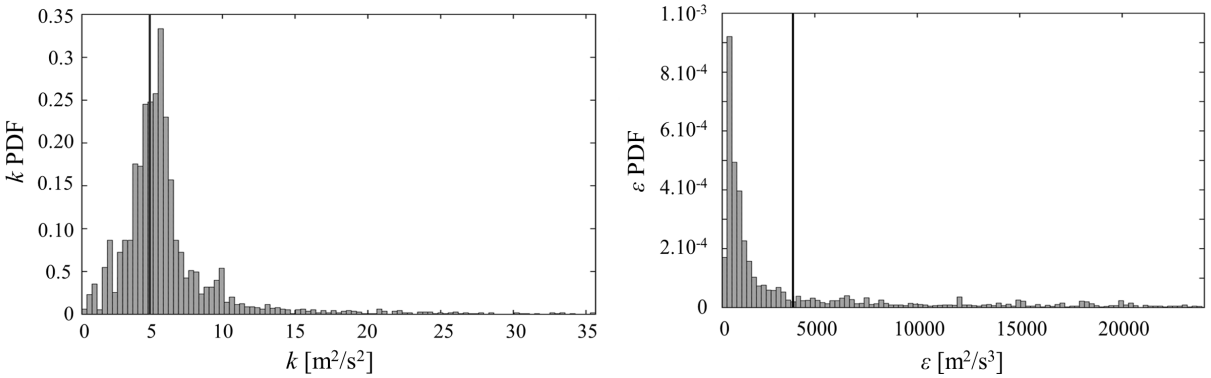

Figure 4.5: Conditional probability density functions of kinetic energy $k|_{\dot{\omega}>0}$ (left) and dissipation rate $\varepsilon|_{\dot{\omega}>0}$ (right) for positive values of local reaction rate $\dot{\omega}$ and mean values (solid lines). RANS simulation of double injection, low load Diesel cycle (IFP-C3D).

the grid resolution of the DNS domain is uniform. Mesh size Δx should allow the resolution of all turbulent scales down to the Kolmogorov length scale, that is approximately 10 µm according to Eq. (4.6).

4.3 Thermodynamic conditions

Initial thermodynamic conditions are chosen to correspond to those found during autoignition in the combustion chamber of an automotive engine. Mean in-cylinder pressure and temperature evolution over a part of the aforementioned double injection Diesel combustion cycle are presented in Figure 4.6 as calculated using RANS simulation. Pressure during autoignition is approximately 35 bar and temperature is around 890 K.

As the characteristic time of autoignition in Diesel engines is small compared to that of the pressure evolution, pressure can be considered locally quasi-constant during the beginning of autoignition. Consequently, a constant pressure DNS set-up is preferred. A periodic domain, commonly used in DNS, would restrict the study to a constant volume configuration. In the present work, a compressible CFD solver [55] is used. Preliminary tests showed that undesirable acoustic phenomena are amplified in a small periodic domain. More specifically, pressure waves generated by autoignition overlap while exiting and re-entering the domain through its periodic borders, creating high frequency modes that are not representative of the problem of interest. This effect is even more present at high pressures. For these reasons, the DNS domain containing the reactive mixture is enclosed in a larger domain (see Figure 4.7). The expansion

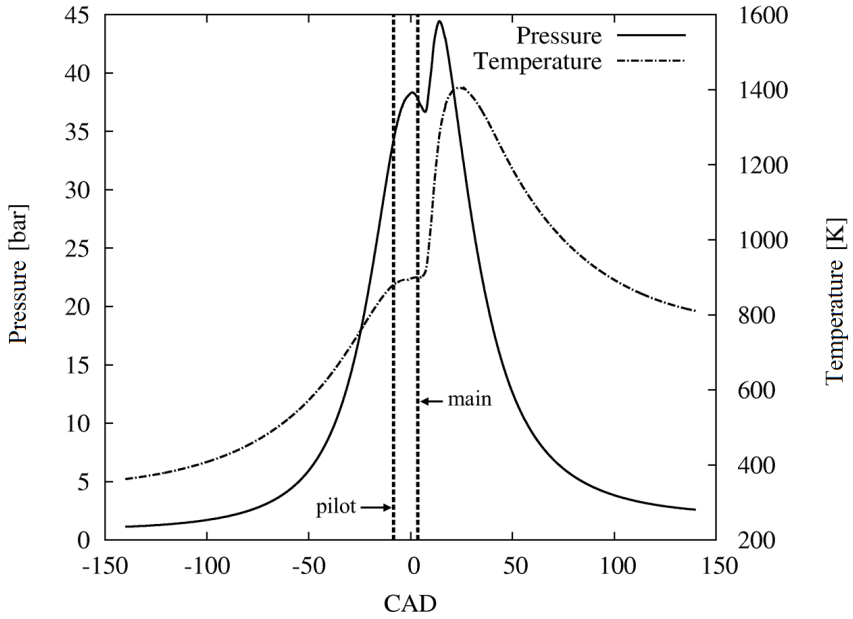

Figure 4.6: Evolution of pressure and temperature over a part of an engine cycle, pilot injection and main injection timings ; RANS simulation (IFP-C3D).

of the burnt gases inside the DNS domain is small compared to the volume of the outer domain. This approach allows autoignition simulation under quasi-constant pressure, including the local flame generated density fluctuations and eliminating any undesirable acoustic phenomena.

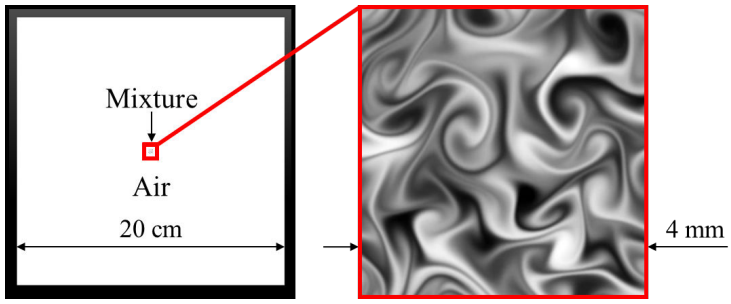

Figure 4.7: Large outer domain allowing quasi-constant pressure autoignition.

4.4 Chemical kinetics mechanism

N-Heptane (n-C_7H_{16}) is chosen as the fuel of this work because its cetane number[1] (CN $\simeq$ 56) is rather close to that of typical Diesel fuels (CN $\simeq$ 50). This fuel can exhibit both single-

[1] An inverse function of a fuel's ignition delay ; higher cetane fuels have shorter ignition delay periods.

stage and two-stage ignition, depending on the thermodynamic conditions and demonstrates a Negative Temperature Coefficient[2] (NTC) behaviour. The sketch in Figure 4.8(a) shows a NTC region for a hydrocarbon fuel ; within this region, ignition delay of a purely gaseous and homogeneous mixture increases with temperature. In addition to the NTC phenomenon, the transition between low and high temperature regimes of the fuel oxidation path also induces what is commonly called a cool flame (Figure 4.8(b), solid line). This refers to a two-step combustion ; a first increase of the mixture temperature of about 200 K (cool flame) precedes the final chemical runaway (main flame). The first step involves a small but sudden temperature increase. The temperature level remains constant during the second step since there is no significant heat release before the complete autoignition. In contrast, at higher initial gas temperatures (> 1000 K for p = 35 bar), no cool flame appears and only a single-step autoignition occurs (Figure 4.8(b), dashed line). NTC and cool flame are key phenomena in compression ignition (CI) engines.

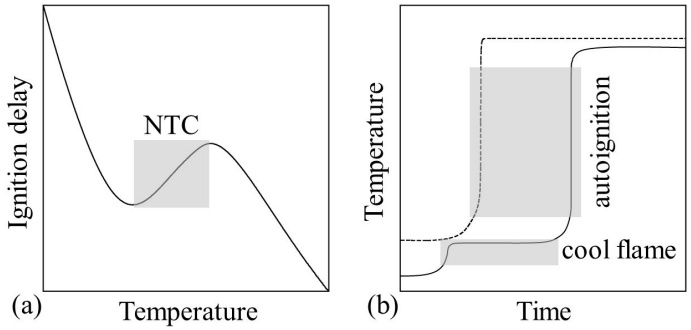

Figure 4.8: (a) Negative temperature coefficient (NTC) area (gray box): main ignition delay increases with respect to temperature. (b) Possible autoignition (AI) processes : cool flame AI before main AI (solid line) or direct main AI (dashed line).

The chemical kinetics mechanism chosen for this study is a skeletal mechanism for n-heptane/air mixture autoignition and flame propagation [66], henceforth called “ERC mechanism”. The mechanism consists of 29 species in 52 reactions and was developed and validated for multi-dimensional HCCI engine combustion simulations, with particular emphasis on the prediction of the ignition delay in high pressures (40-50 bar). It contains reactions that account for fuel decomposition, low-temperature oxidation, high-temperature oxidation and post-oxidation. The kinetic constants of two reactions of the original mechanism are updated as presented in Table 4.1, according to latest literature [131, 132] and respecting the uncertainties proposed by the authors.

[2]Ignition delay increases with initial temperature increase over a certain range of temperatures.

R_1	CH_2O	+	·OH	=	HCO	+ H_2O
R_2	$·CH_3$	+	HO_2	=	$CH_3O·$	+ ·OH

		A	β	Ea
R_1	original	5.563 E+10	1.095	-76.5
R_1	updated	3.430 E+09	1.180	-447.0
R_2	original	5.000 E+13	0.0	0.0
R_2	updated	6.800 E+12	0.0	0.0

Table 4.1: Updated constants for ERC mechanism [66].

As discussed in Section 4.2, the resolution of all length and time scales in turbulent flow on high turbulent Reynolds number Re_t can be very demanding in terms of CPU cost. However, depending on the thermodynamic conditions and the chemical kinetics mechanism, the stiffness associated with the determination of rates of chemical reactions can be even more costly. A high temporal resolution stems from the need to capture the effect of the quickest reactions, *e.g.* a hydroxyl radical OH peak with a very short duration. The temporal resolution requirements for the chosen initial conditions using ERC mechanism are investigated ; a series of tests in 0-D homogeneous reactor for different fuel-air equivalence ratios ϕ [3] and temperatures under constant pressure of 35 bar is conducted. The numerical solver used is the implicit solver DVODE [65] that resolves the ODE system using an adaptive time step, ensuring stability. The time step required, defined by the quickest reactions, *i.e.* the highest reaction rates, is found to fluctuate between 10^{-6} and 10^{-10} s, over 1 ns for the biggest part of the simulation.

4.5 Composition and temperature stratification

In the framework of this thesis, Diesel spray is locally represented in its evaporated form by a number of superposed Gaussian distributions of gaseous fuel mass fraction inside a decaying isotropic turbulence velocity field. No initial mean flow is imposed since the analysis of spray dynamics is beyond the scope of this study. The fuel mass fraction field is considered sufficiently far from the injector tip, out of the liquid penetration range of the injected fuel, as illustrated in the schematic Figure 4.9.

Some temperature stratification intrinsically exists inside the combustion chambers of a

[3] Ratio of the fuel-to-oxidizer ratio to the stoichiometric fuel-to-oxidizer ratio.

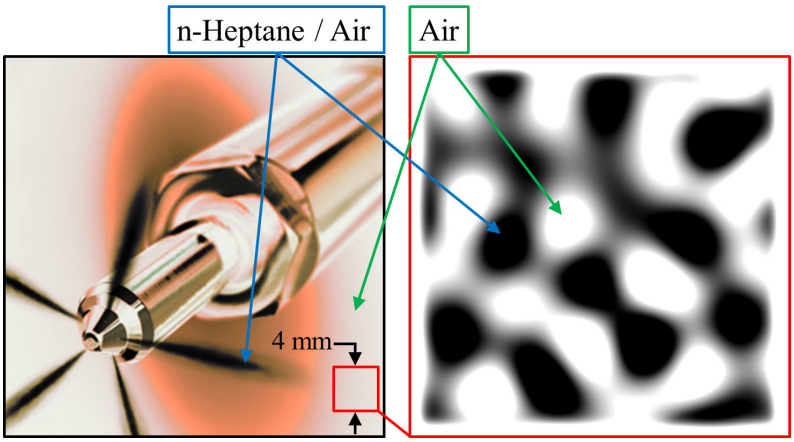

Figure 4.9: Diesel injector fuel spray and DNS fuel mass fraction field.

Diesel engine, due to wall heat losses and heat extracted from evaporating droplets (latent heat of evaporation). In this case, the studied domain represents an autoigniting stratified mixture inside the combustion chamber far from the chamber walls (see Figure 4.1). Thus, only the droplet evaporation cooling effect is taken into account ; temperature and composition stratifications are initially negatively-correlated, according to Eq. (4.10).

$$T(Z) = (1 - Z)T^{\text{air}} + ZT^{\text{fuel}} \tag{4.10}$$

where $T^{\text{air}} = 900$ K and $T^{\text{fuel}} = 500$ K are the air and gaseous fuel initial temperatures, respectively. The velocity field is assumed to be uncorrelated with temperature and composition fields.

Chemical phenomena that are crucial for the proper simulation of combustion take place in very short times over thin layers and are related to large gradients of temperature, density and species mass fractions. The spacial resolution required is indicated by the thinnest radical distribution profile in the combustion fronts. A series of 1-D simulations with different grid resolutions is performed to asses the DNS for the required grid resolution. The initial species mass fraction and temperature profiles are presented in Figure 4.10. These profiles correspond to a zone where n-heptane and pure air interact (diffusion and reaction) to give a diffusion flame. The tests are conducted under constant pressure of 35 bar. The maximum fuel mass fraction is chosen equal to 0.5, corresponding roughly to the saturation value of gas phase fuel concentration under the studied conditions.

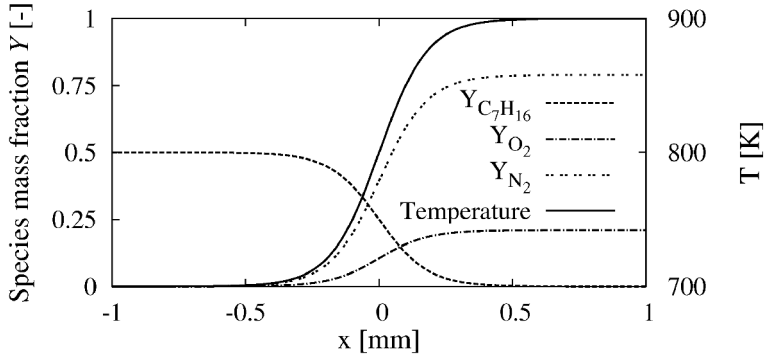

Figure 4.10: 1-D simulation initial profiles of species mass fraction and temperature.

Ignition delay is found to depend on the resolution of the 1-D domain ; grid convergence must therefore be sought. In Figure 4.11, ignition delay is plotted against the number of nodes in the reaction zone, here delimited by the hydroxyl radical OH peaks at its borders. Mesh independence is attained when these reaction layers are resolved with at least 25 grid points. This resolution corresponds to a mesh size Δx of 4 µm. Consequently, the resolution required to resolve the thinnest flame fronts under the studied conditions is 1000 grid points in each direction of the DNS domain. A 2-D configuration is adopted, as is the case for many contemporary DNS studies of autoignition [52, 53, 54, 133, 134]. Although differences between 2-D and 3-D autoignition synopses are to be expected [27, 47], 2-D turbulent heterogeneous reactors remain relevant for the evaluation of model hypotheses and permit the study of a wide range of conditions.

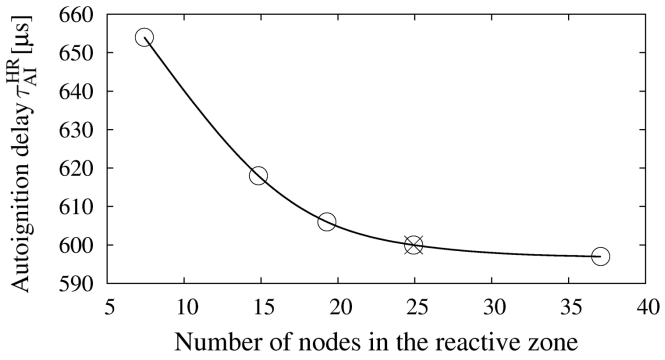

Figure 4.11: Ignition delay against number of nodes in the reaction zone (circles) and chosen resolution (x mark), 1-D simulation.

The aim of this work is the representation of the interaction between multiple Diesel injections and their impact on the combustion process. In this scope, gaseous fuel parcels are placed in a reacting environment. This mixture corresponds to a pilot injection that precedes the

main injection, represented here by the composition stratification inside the DNS domain[4]. The DNS configuration for multiple Diesel injections is presented on mixture fraction-normalised progress variable mixing lines in Figure 4.12(a) considering pure mixing of the reactants. The pilot injection is mixing with air and starts reacting before meeting the main injection (mark A). Combustion products, not necessarily at equilibrium, are computed in homogeneous reactor conditions (mark B), assuming that the pilot injection mixture is homogeneous. Thereafter, the DNS configuration is set up introducing a fuel mass fraction field inside an atmosphere of pilot injection combustion products. The initial composition and temperature at each node of the DNS domain is then found on the mixing line between pilot injection combustion products and maximum mixture fraction $Z_{\max}$ (mixing line B-C). It should be noted that fuel injection generally results in a highly heterogeneous mixture ; considering a homogeneous mixture to represent the pilot injection seems therefore questionable. Pitsch and Steiner [135], however, note that within the pilot injection stream of a piloted non-premixed methane/air diffusion flame (Sandia flame D) the mixture fraction gradient is zero. From a multiple injections' perspective, it can be considered that pilot injection combustion products are locally homogeneous, since the pilot injection fuel starts reacting with air and the combustion products start diffusing before they are reached by the fresh fuel of the main injection. If, additionally, these products are presumed to mix adiabatically with air before meeting the main injection fuel, a new composition is computed, as presented in Figure 4.12(b). Mixture fraction Z_0 and normalised progress variable c_0 refer to the homogeneous mixture representing the partially burnt gases of the pilot injection before mixing with the main injection fresh fuel. They correspond to different injection strategies and are key parameters in the present analysis since they are conditioning the initial composition and temperature stratifications of the DNS cases.

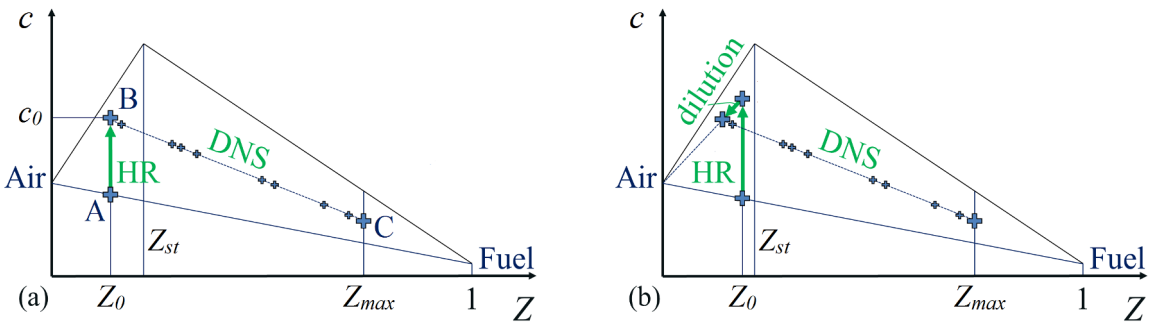

Figure 4.12: (a) Conceptual view of DNS for multiple Diesel injections on c-Z mixing lines ; pilot injection combustion products computed in homogeneous reactor (HR) (A-B), DNS local initial conditions on mixing line B-C. (b) Same concept with supplementary effect of pilot injection combustion products dilution with air.

[4]The same principle can be applied for the main injection-post injection interaction.

A generic DNS case is presented in Figure 4.13 as an example. The DNS domain is enclosed in a larger domain whose boundaries are all set to be adiabatic and free-slip. The expansion of the burned gases inside the DNS domain is small compared to the volume of the outer domain. This approach allows autoignition simulation under constant pressure, including the local flame generated density fluctuations, without penalising the computational efficiency, since the outer domain is discretised with a coarse mesh. The analysis of the following chapters is limited to the central well refined DNS domain.

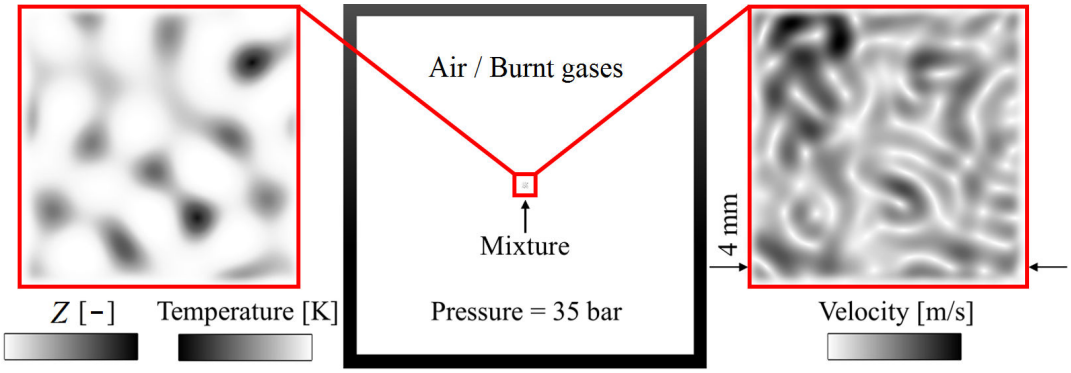

Figure 4.13: Generic DNS case : initial mixture fraction, temperature (left) and velocity field (right). The larger outer domain (middle) allows constant pressure autoignition.

Chapter 5

Simulations and modelling under single injection conditions

This chapter is dedicated to the analysis of DNS results corresponding to single Diesel injection conditions and the *a priori* evaluation of the studied combustion models against these DNS results.

5.1 Phenomenological analysis

Two reference 2-D DNSs of autoigniting stratified turbulent mixtures are carried out, corresponding to local conditions in a low load single injection Diesel cycle. The two cases, namely a_0 and b_0, differ in the characteristics of the decaying isotropic turbulence initially imposed. The physical parameters of the two single injection cases are presented in Table 5.1.

Case	u'	l_t	η_k	τ_{AI}	τ_t	τ_c	Da
a_0	1.12	1.4	10	287	1052	1.7	621
b_0	5.60	0.3	2	311	42	1.7	25
	[m/s]	[mm]	[µm]	[µs]	[µs]	[µs]	[-]

Table 5.1: Physical parameters of the two single injection cases.

The DNS configuration consists of pockets of fuel randomly distributed within hot air subjected to a turbulent field, as described in Chapter 4. The initial mean equivalence ratio ϕ is 1 for both cases, that is $\widetilde{Z} = Z_{\mathrm{st}} \simeq 0.062$ according to the definition of Eq. (3.12). The maximum mixture fraction corresponds to a rough estimation of the saturation value of gas phase mixture fraction under the studied conditions $Z_{\mathrm{max}} = 0.5$. Unmixedness $\widetilde{S_Z}$ (Eq. (3.16)) is 0.33 for both reactors, corresponding to a highly heterogeneous initial mixture, in compliance with Diesel combustion conditions. Initial temperature stratification T^{init} is linearly correlated to Z, varying from 700 K on the fuel side to 900 K on the air side (see Figure 4.10).

Velocity fluctuation levels u' and integral length scales l_t are chosen of the same order as the indicative values extracted from the preliminary RANS, that is $u' \simeq 1.8$ m/s and $l_t \simeq 1$ mm, as presented in Chapter 4. A low and and a high level of turbulence intensity are chosen so to investigate the effects of the turbulent mixing on autoignition. Initial integral l_t and Kolmogorov η_k length scales are estimated according to Eqs. (4.2) and (4.6), based on preliminary non-reactive tests. The mesh used is deemed adequate to provide converged statistics and to resolve all turbulent structures, from the biggest to the smallest. Turbulent Reynolds number Re_t (Eq. (4.3)) is 630 for both cases.

A main ignition delay τ_{AI} can be estimated for every DNS as the time needed for the mean normalised progress variable to reach half its maximum, *i.e.* $\tau_{\mathrm{AI}} = t|_{\tilde{c}\,=\,0.5}$. This delay is indicative of the reactivity of the heterogeneous reactor. Figure 5.1 shows the main ignition delay of n-heptane/air homogeneous mixtures at 35 bar as a function of the mixture fraction Z, with a Z dependent initial temperature, as in the single injection cases. This curve is obtained by a series of 0-D homogeneous reactor calculations with ERC mechanism [66], using the same criterion to define the autoignition delay $\tau_{\mathrm{AI}}^{\mathrm{HR}} = t|_{c\,=\,0.5}$. The shortest ignition delay ($\simeq$ 186 µs) is associated with a specific most reactive mixture fraction ($Z_{\mathrm{MR}} \simeq 0.13$) and can be used as a reference to be compared with the ignition delay of stratified turbulent mixtures τ_{AI}. $\tau_{\mathrm{AI}}^{\mathrm{HR}}$ can be considered as the minimum possible autoignition time of mixtures created by fuel and oxidant streams of the given initial temperatures [136]. The decaying effect of turbulence and of temperature and composition stratifications can be measured by the ratio of the two ignition times, $\tau_{\mathrm{AI}}/\tau_{\mathrm{AI}}^{\mathrm{HR}} \simeq 1.5$ for the lower turbulence intensity case a_0 and 1.7 for the higher turbulence intensity case b_0.

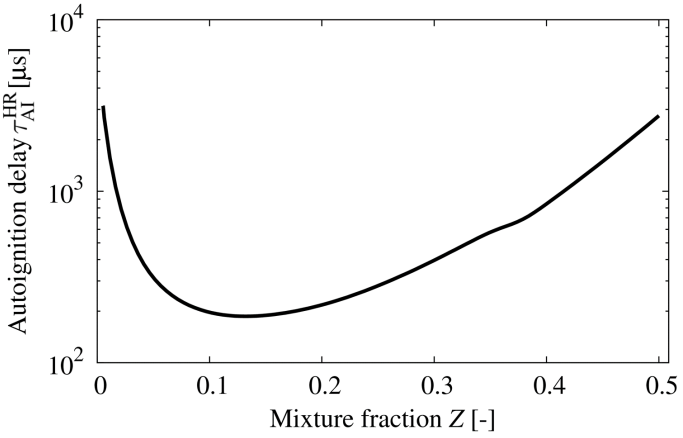

Figure 5.1: 0-D ignition delay $\tau_{\mathrm{AI}}^{\mathrm{HR}}$ of n-heptane/air homogeneous mixtures at 35 bar as a function of mixture fraction Z, with the Z dependent initial temperature of Eq. (4.10), using the ERC mechanism [66].

$\tau_t = k/\varepsilon$ is a characteristic turbulent time scale that can be compared with a chemical time scale τ_c for the classification of the presented results under a certain combustion regime. A chemical time scale is estimated as the inverse of the maximum value of the mean reaction rate of the normalised progress variable $\widetilde{\dot{\omega}}_{c\ \max}$, conditioned at the stoichiometric mixture fraction.

$$\tau_c = \frac{1}{\widetilde{\dot{\omega}}_{c\ \max}\big|_{Z=Z_{\mathrm{st}}}} \tag{5.1}$$

According to these estimates, the Damköhler number Da (Eq. (3.26)), comparing turbulent τ_t with the chemical τ_c time scales, is $\simeq 621$ for case a_0 and $\simeq 25$ for case b_0. The laminar flamelet concept, viewing the turbulent diffusion flame as an ensemble of laminar diffusion flamelets [105], is only valid for high Damköhler numbers. Based on the extracted values, this concept seems more adapted for the modelling of the lower turbulence intensity conditions of case a_0 than the conditions of case b_0 where turbulent and chemical time scales are similar.

The evolution of the mean reaction rate of the progress variable $\widetilde{\dot{\omega}}_{Y_c}$ is plotted against the mean normalised progress variable $\overline{c}$ in Figure 5.2 for the DNS cases a_0 (left) and b_0 (right). A two-step combustion is clearly illustrated : the first peak that appears corresponds to the cool flame autoignition and the second, larger peak corresponds to the main ignition. The effect of higher turbulence intensity can be seen from the wider spread of mean reaction rate over progress variable in case b_0.

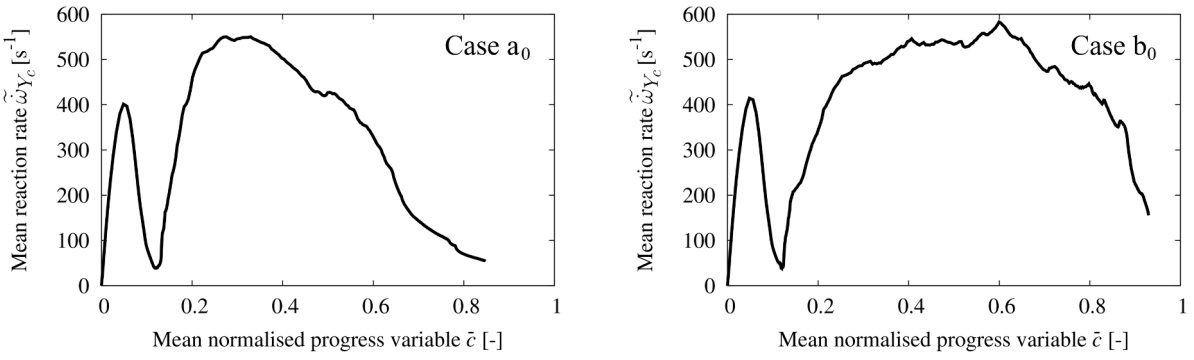

Figure 5.2: DNS cases a_0 (left) and b_0 (right) ; evolution of mean reaction rate of the progress variable $\widetilde{\dot{\omega}}_{Y_c}$ with mean normalised progress variable $\overline{c}$.

The effect of turbulent mixing on the progress of combustion is also visible in Figure 5.3 comparing the temporal evolution of the mean temperature $\widetilde{T}$ (left) and of the normalised progress variable $\overline{c}$ (right) of the two single injection DNS cases. The higher turbulence intensity of case b_0 results in a slightly longer ignition delay than in case a_0. Once initiated,

however, the combustion process advances faster than in the low turbulence intensity case a_0, due to enhanced mixing.

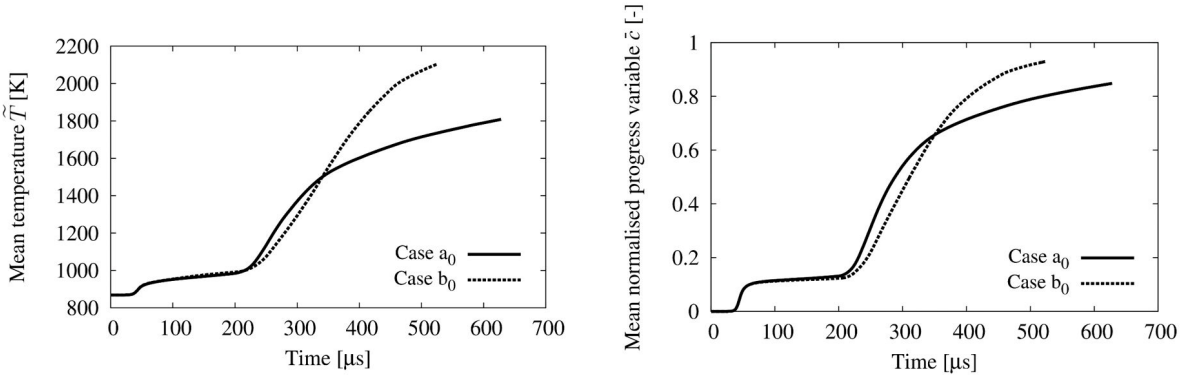

Figure 5.3: Temporal evolution of mean temperature $\widetilde{T}$ (left) and mean normalised progress variable $\bar{c}$ (right) for single injection cases a_0 (solid line) and b_0 (dashed line).

Mixture fraction Z and normalised progress variable c fields of DNS case a_0 are presented in Figure 5.4. The initial composition and temperature stratifications define the areas where cool flame appears, occurring at 50 µs approximately. In parallel, turbulence accelerates the formation of local mixing layers and enhances heat transfer between hot, lean and cold, rich regions, leading to the main autoignition, arriving at 287 µs. The structure of the flame seems mildly affected by the initial turbulence and mainly defined by the composition and temperature stratification, as established during the autoignition delay.

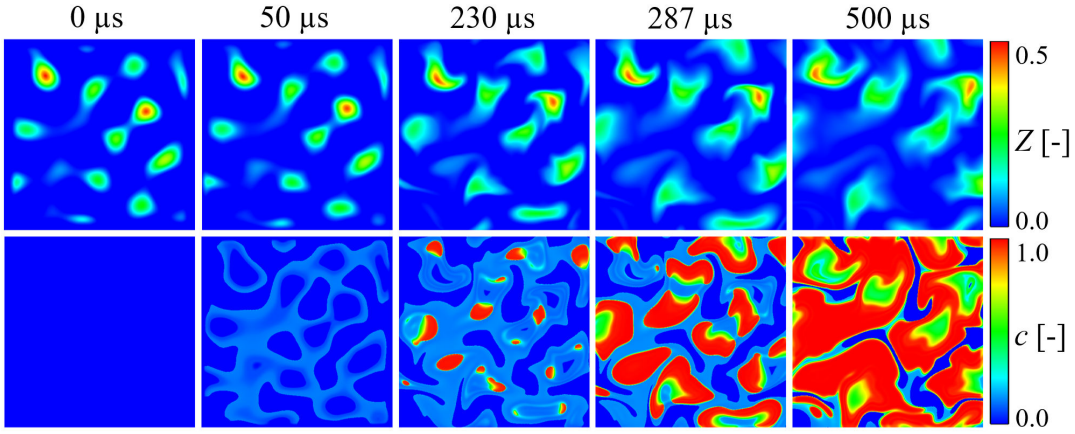

Figure 5.4: Instantaneous views for a sequence of times ; mixture fraction Z (first row) and normalised progress variable c (second row) fields of DNS case a_0.

Figure 5.5 shows the evolution of mixture fraction Z and normalised progress variable c fields of DNS case b_0. The cool flame timing is almost identical to that of case a_0, practically unaffected by the flow. By contrast with case a_0, after the cool flame turbulent structures wrinkle strongly the mixture fraction field. Main ignition occurs at 311 µs. Subsequently, the flame structures are strained by the turbulent flow.

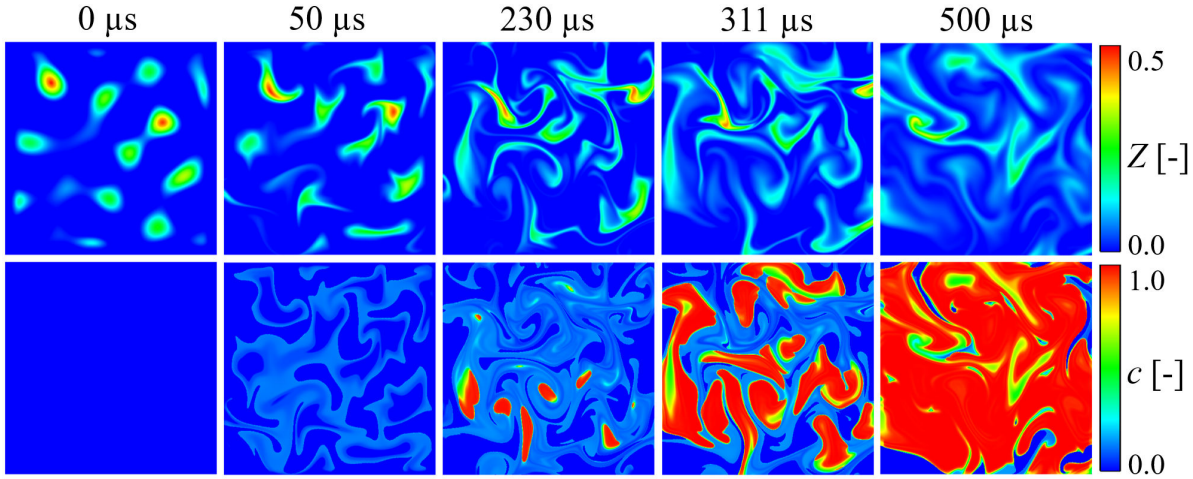

Figure 5.5: Instantaneous views for a sequence of times ; mixture fraction Z (first row) and normalised progress variable c (second row) fields of DNS case b_0.

As can be seen in Figure 5.6, the imposed turbulence plays a decisive role in the formation of the mixing layers but is also strongly impacted by the burnt gases expansion during ignition. The flow fields are expanding in the ambient environment due to the heat release of combustion, since there are no boundaries on the domain where the turbulent spectrum is initially imposed (see Figure 4.7). Thus, turbulent mixing and autoignition process are in strong interaction : the decaying isotropic turbulence affects autoignition delay and the flame structures after ignition of the stratified mixtures have an impact on the velocity field.

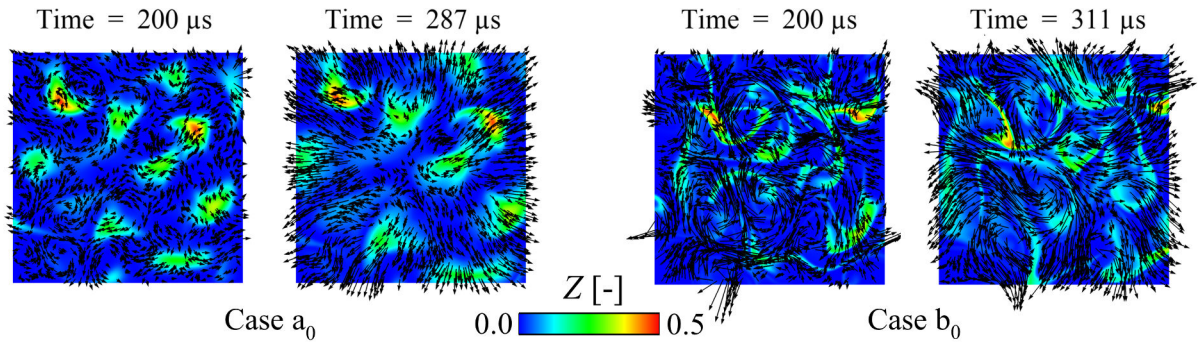

Figure 5.6: Contours of mixture fraction Z and velocity vectors in cases a_0 (left) and b_0 (right).

To further elucidate the mechanisms of autoignition in turbulent mixing flows, a series of scatterplots of progress variable Y_c against mixture fraction Z is presented in Figure 5.7 for DNS case a_0. The progress variable of the DNS $\widetilde{Y_c|_Z}$ averaged over classes of Z (green line) is compared with the progress variable values of a 1-D unsteady strained laminar diffusion flame. The strain rate a of the diffusion flame is chosen based on an estimated value during autoignition in the DNS, according to the following :

$$a = \frac{\widetilde{\chi}}{\int \mathcal{F}(Z)\widetilde{P}(Z)\,\mathrm{d}Z} \tag{5.2}$$

where $\mathcal{F}(Z)$ is the classical expression for counterflow diffusion flames of Eq. (3.25) [69]. The mean scalar dissipation rate $\widetilde{\chi}$ is a Favre-average of local χ values obtained according to the definition of Equation (3.23). The laminar diffusion flame follows relatively well the evolution of combustion in the heterogeneous reactor in terms of average progress variable. This agreement can be further improved using more adapted strain rate values that evolve in time. From this perspective, the assumption of a diffusion flamelet structure, which is the basis of numerous combustion models such as ADF [74], RIF [108] and CMC [137], seems coherent for the modelling of such turbulent heterogeneous reactors.

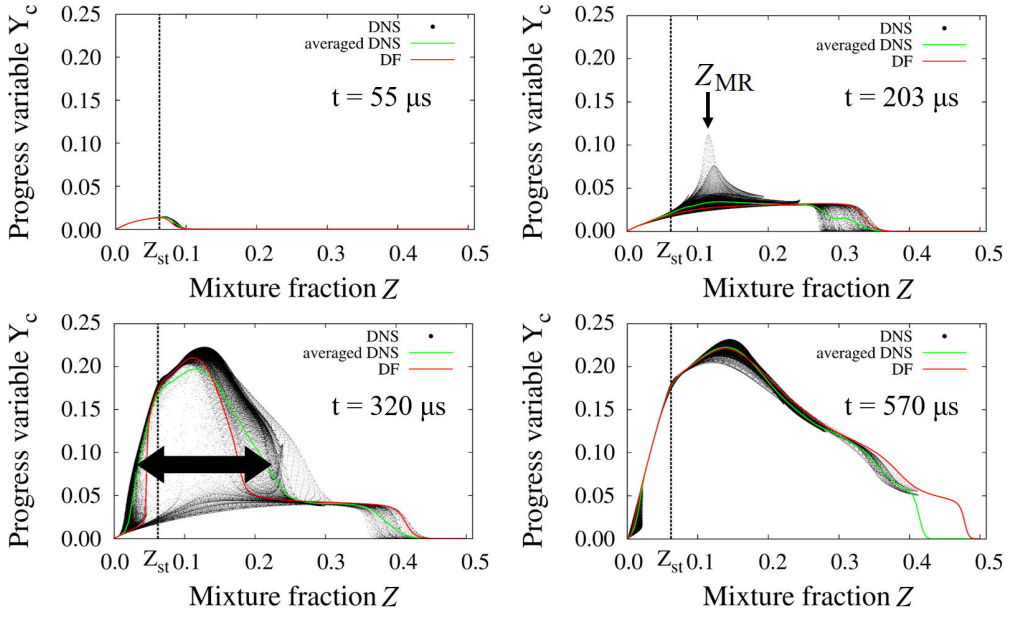

Figure 5.7: DNS case a_0 ; scatterplots of progress variable Y_c against mixture fraction Z (black points). Comparison between the progress variable of the DNS $\widetilde{Y_c|_Z}$ averaged over classes of Z (green line) and a 1-D unsteady strained laminar diffusion flame (red line).

Some more observations are possible in Figure 5.7. The effect of turbulence on the evolution of the combustion process is visible ; there are regions with the same mixture fraction that react at different moments. Additionally, main autoignition spots first appear around a well-defined mixture fraction value $Z_{\mathrm{MR}} \simeq 0.13$, already identified by means of 0-D homogeneous reactor calculations (see Figure 5.1). Thereafter, scatterplots spread around Z_{MR}, indicating that reaction fronts propagate towards both leaner and richer mixtures after ignition. This observation is consistent with the conclusions of Thevenin and Candel [138], obtained by constant-density numerical solutions for one-dimensional laminar autoigniting layers.

Figure 5.8 shows scatterplots of reaction rate of the progress variable $\dot{\omega}_{Y_c}$ against scalar dissipation rate $\chi|_{Z_{\mathrm{MR}}}$ conditioned in the range $0.12 < Z_{\mathrm{MR}} < 0.14$ bracketing Z_{MR}, for two consecutive instants of DNS case a_0. First ignition spots originate in areas where scalar dissipation rate is low, since the only points exceeding the threshold of 20.000 s^{-1} are those with a scalar dissipation rate value under 3 s^{-1}.

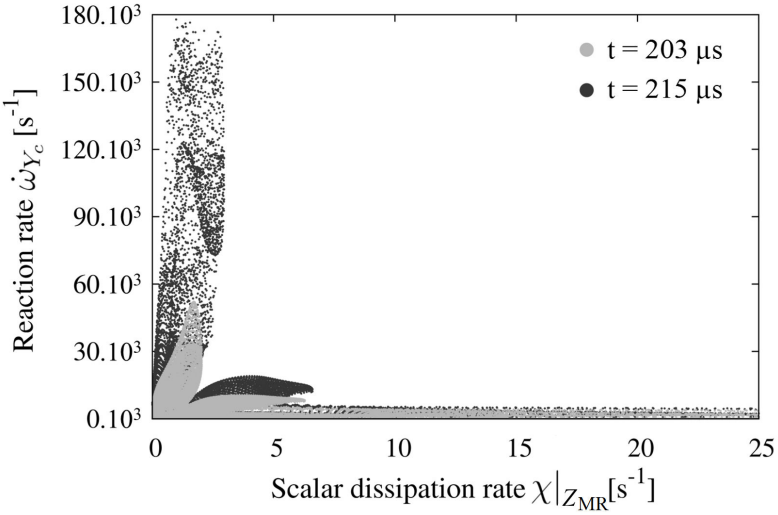

Figure 5.8: DNS case a_0 ; conditional scatter plots of reaction rate of the progress variable $\dot{\omega}_{Y_c}$ against scalar dissipation rate $\chi|_{Z_{\mathrm{MR}}}$ conditioned in $0.12 < Z_{\mathrm{MR}} < 0.14$.

Consequently, the most favourable spots for ignition are those which contain a mixture fraction around a well-defined, most reactive value Z_{MR}, and are found at locations where scalar dissipation rate χ is low. The *sine qua non* conditions of Z_{MR} and low χ are not sufficient to accurately predict the first autoignition spots ; there are regions in the DNS domain with low scalar dissipation rate χ and same mixture fraction Z_{MR} that autoignite in different moments (see Figures 5.7 and 5.8). This remark illustrates the importance of the evolution of the turbulent reacting flow in space and time during the autoignition delay.

The presented results are in agreement with previous 2-D DNS computations with semi-detailed chemistry [45, 139, 140] as well as 3-D DNS [47, 141].

5.2 *A priori* model evaluation

The three modelling approaches presented in Section 3.4 (THR, PCM [74] and ADF [38]) are evaluated on the basis of an *a priori* comparison with the DNS results, as detailed in Section 3.5. 0-D homogeneous reactor tabulations are used, as in the FPI [78] tabulation approach. Mass fractions and reaction rates of homogeneous mixtures autoigniting under constant pressure of 35 bar are tabulated, covering the mixture fraction range $Z \in [0, 0.5]$, with the same initial temperature-mixture fraction $T^{\text{init}}(Z)$ correlation as in the DNS single injection cases a_0 and b_0 (see Table 5.1). Tabulated reaction rate of the progress variable $\dot{\omega}_{Y_c}^{\text{TAB}}(Z, c)$ values are illustrated in Figure 5.9.

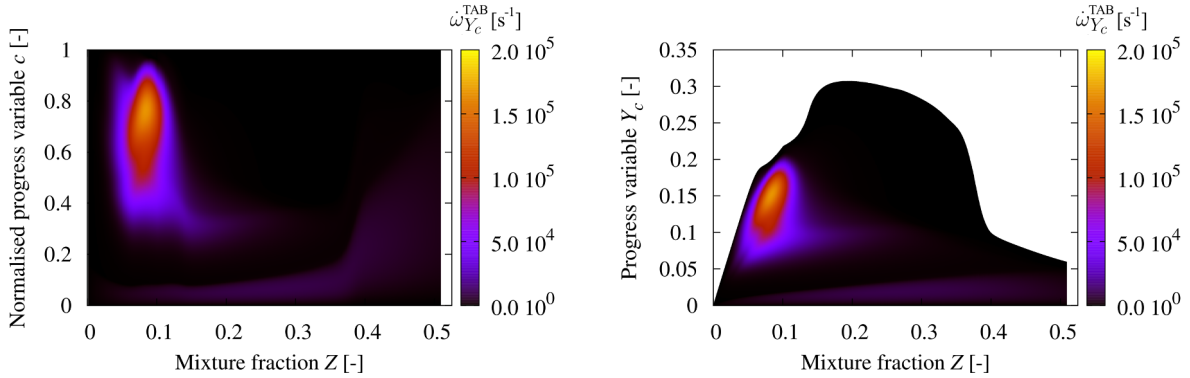

Figure 5.9: 0-D homogeneous reactor tabulation of reaction rate of the progress variable $\dot{\omega}_{Y_c}^{\text{TAB}}$ with mixture fraction Z and normalised progress variable c (left), and with mixture fraction Z and progress variable Y_c (right).

The mean reaction rate of the progress variable $\widetilde{\dot{\omega}}_{Y_c}$ according to the THR approach is shown in Figure 5.10, compared to averaged DNS results for the single injection cases a_0 (left) and b_0 (right), using the tabulation of Figure 5.9. The THR approach fails to predict the evolution of the combustion process. The cool flame reaction rate peak arrives prematurely in progress variable terms, and the maximum reaction rate is strongly overestimated. This kind of behaviour would lead to highly overestimated heat release rates in the context of engine simulation.

These results are accompanied by the response of a zero-order model, denoted here as "Arrhenius" : the DNS results are post-processed at every time-step of the model evaluation test (every microsecond) to obtain the mean mass fractions $\widetilde{Y}_k$ of all 29 chemical species transported. Then, chemical kinetics are resolved for one chemical time-step under constant pressure homogeneous reactor conditions, to obtain the reaction rate $\dot{\omega}_{Y_c}$ of this average composition. This test corresponds to a direct integration of chemical kinetics into the CFD simulation [92], without considering any interaction of the turbulent mixing with the chemical kinetics below the grid level. This is a quite popular approach that necessitates, however, the transport of as many

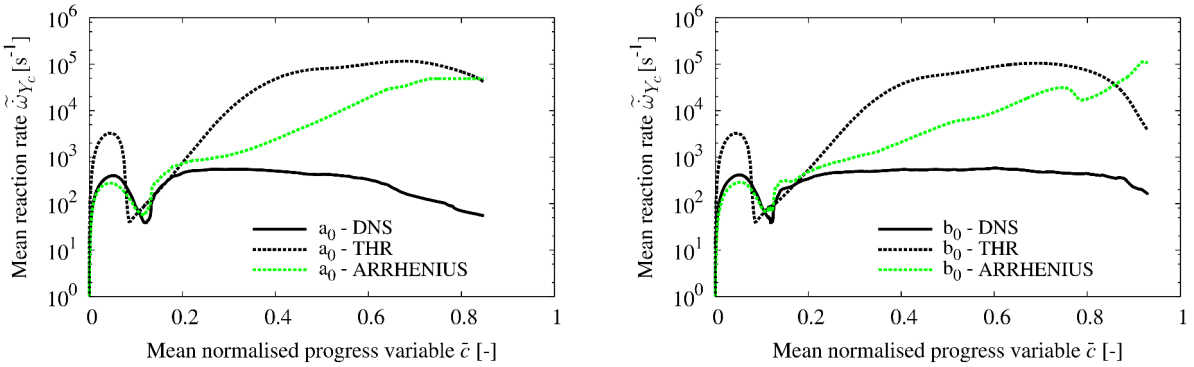

Figure 5.10: Evolution of mean reaction rate of the progress variable $\widetilde{\omega}_{Y_c}$ with mean normalised progress variable $\overline{c}$; comparison between DNS results (solid lines), THR approach (dashed black lines) and Arrhenius approach (dashed green lines), single injection cases a_0 (left) and b_0 (right).

additional variables as species contained in the chemical kinetics mechanism and the parallel resolution of chemistry in every computational cell, demands that can drastically increase CPU cost. The comparison of this method with the THR approach and the DNS results helps quantifying the part of the discrepancies that are due to the assumption of a homogeneous mixture, and to the chemistry tabulation itself. At the beginning of the test, the biggest part of the observed error of the THR model can be attributed to the chemistry tabulation, since the Arrhenius approach is significantly closer to the averaged DNS results. Once the velocity field starts acting on the mixing process, however, discrepancies become important and the zero-order model approaches the THR results. These observations show that the homogeneous mixture assumption is an important source of error, especially when simulating highly heterogeneous turbulent mixtures.

Figure 5.11 illustrates a comparison between DNS results and the two versions of PCM model for cases a_0 (left) and b_0 (right). The first version PCM-1, that is considering only the mixture fraction heterogeneity through a presumed β distribution, clearly overestimates $\widetilde{\omega}_{Y_c}$. PCM-2, taking into account the progress variable heterogeneity independently of the mixture fraction, is an improvement compared to PCM-1. It remains inaccurate, however, since it overestimates by a factor of 10 the mean reaction rate over the largest part of the combustion process. This behaviour is consistent with previous results [29, 39].

The main model assumptions of PCM-type models will now be evaluated ; first, the presumed PDF approach and then, the chemistry tabulation itself.

To investigate the impact of the approximation of $\widetilde{P}(Z)$ and $\overline{P}(c)$ by presumed β distributions, model prediction is estimated for PCM-2 model by integrating over the actual PDFs,

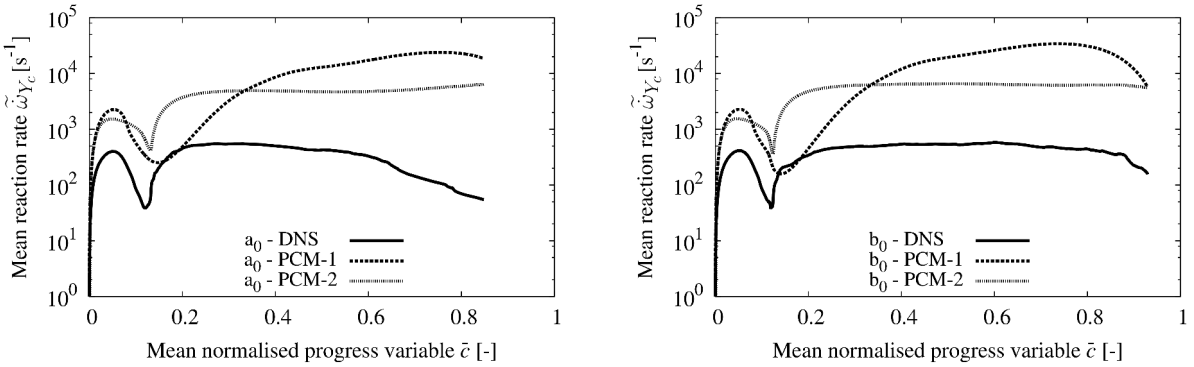

Figure 5.11: Evolution of mean reaction rate of the progress variable $\widetilde{\omega}_{Y_c}$ with mean normalised progress variable $\bar{c}$; comparison between DNS results (solid lines) and the two versions of PCM model (dashed lines), single injection cases a_0 (left) and b_0 (right).

retrieved from post-processing of the DNS results, instead of the presumed β distributions of Eq. (3.35). This investigation reveals that the presumed $\beta(c)$ may fail if the kinetics include some stagnation of c, *e.g.* in the case of the cool flame, as reported in [29]. This can be observed in Figure 5.12(a) comparing the actual $\overline{P}(c)$ with the presumed β distribution during cool flame (mark *I*) and main autoignition (mark *II*) in case a_0. DNS averaged results, PCM-2 prediction and the direct integration of $\overline{P}(c)$ for case a_0 are compared in Figure 5.12(b). Indeed, an important part of the model discrepancies is due to the inaccurate approximation of the PDF of c by a β distribution. The accuracy of the standardised β distribution approximating the PDF of Z was found to be satisfactory. These tendencies are common for both single injection cases.

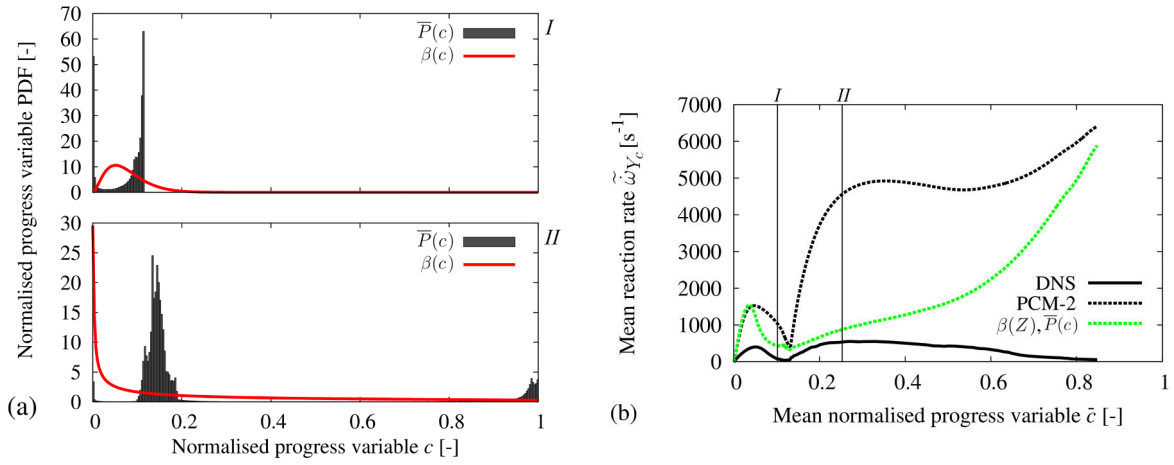

Figure 5.12: (a) Comparison of the actual $\overline{P}(c)$ with the presumed β distribution during cool flame (mark *I*) and main autoignition (mark *I*). (b) Evolution of mean reaction rate of the progress variable $\widetilde{\omega}_{Y_c}$ with mean normalised progress variable $\bar{c}$; comparison between DNS results (solid line), PCM-2 model (dashed black line) and the direct integration of the $\overline{P}(c)$ (dashed green line), case a_0.

To further understand the mismatch between the DNS and PCM-type models, DNS results are post-processed to obtain the evolution of the joint probability density function $\widetilde{P}(Z,c)$. The latter is directly integrated over Z and c, as in Equation (3.29). The evolution of $\widetilde{\dot{\omega}}_{Y_c}$ with $\overline{c}$ is presented in Figure 5.13 for the single injection cases a_0 (left) and b_0 (right) ; the averaged DNS results (solid lines) are compared with the mean values obtained by direct integration of the independent probability density functions $\widetilde{P}(Z)$ and $\overline{P}(c)$ (dashed black lines), and of the joint probability density function $\widetilde{P}(Z,c)$ (dashed red lines).

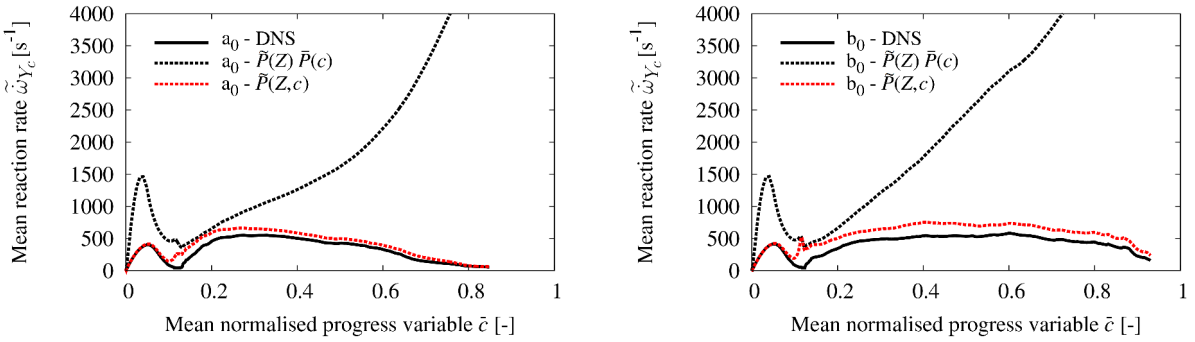

Figure 5.13: Evolution of mean reaction rate of the progress variable $\widetilde{\dot{\omega}}_{Y_c}$ with mean normalised progress variable $\overline{c}$; comparison between DNS results (solid lines), the direct integration of the independent $\widetilde{P}(Z)$ and $\overline{P}(c)$ (dashed black lines), and the direct integration of the joint $\widetilde{P}(Z,c)$ (dashed red lines) using 0-D homogeneous reactor tabulation, cases a_0 (left) and b_0 (right).

The direct integration of the joint $\widetilde{P}(Z,c)$ leads to much smaller discrepancies compared to the integration of the independent $\widetilde{P}(Z)$ and $\overline{P}(c)$, in both cases. Thus, the assumption of independence between the mixture fraction Z and the progress c variable (see Equation (3.31)) is inexact. This assumption appears to be one of the main responsibles for the discrepancies of the PCM model, as concluded in [29].

The impact of the chemistry tabulation will now be adressed. As discussed in Section 5.1, the autoignition of the turbulent heterogeneous reactors simulated with DNS presents some similarities with the autoignition of a laminar diffusion flame. On the basis of this observation, a 1-D unsteady strained laminar diffusion flame tabulation is tested, resulting in a FGM-like tabulation [81]. The strain rate a of the tabulated diffusion flame is chosen based on an estimated value during autoignition of the DNS case a_0, as in Eq. (5.2). Figure 5.14 illustrates the evolution of $\widetilde{\dot{\omega}}_{Y_c}$ with $\overline{c}$ for cases a_0 (left) and b_0 (right). The 1-D unsteady strained laminar diffusion flame tabulation is used for the direct integration of the joint probability density

function $\widetilde{P}(Z,c)$ (dashed red lines). The comparison of these results with those obtained using the 0-D homogeneous reactor tabulation (dashed black lines) highlights that the 1-D diffusion flame tabulation is more suitable than the 0-D homogeneous reactor tabulation for the modelling of autoignition of such stratified turbulent mixtures. The relatively better results of case a_0, as opposed to those of case b_0, can be attributed to the choice of the value of the strain rate a of the tabulated unsteady laminar diffusion flame based on case a_0 results. These results can be further improved using more adapted strain rate values that evolve in time.

This methodology cannot be considered as a feasible modelling approach, since the joint $\widetilde{P}(Z,c)$ is not available in the context of RANS simulation ; it defines, nonetheless, the maximum precision of combustion models using chemistry tabulations relating all quantities to mixture fraction Z and normalised progress variable c.

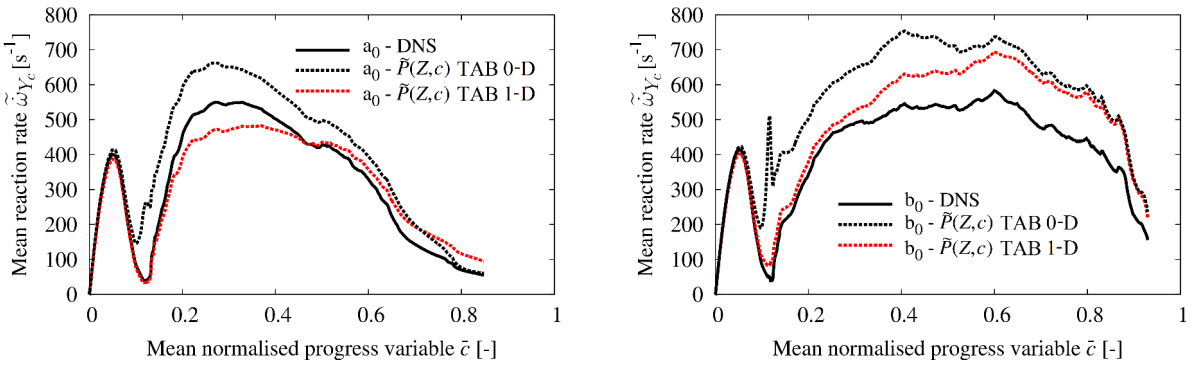

Figure 5.14: Evolution of mean reaction rate of the progress variable $\widetilde{\dot{\omega}}_{Y_c}$ with mean normalised progress variable $\overline{c}$; comparison between DNS results (solid lines) and the direct integration of the joint probability density function $\widetilde{P}(Z,c)$ using 0-D homogeneous reactor tabulation (dashed black lines), or 1-D unsteady strained laminar diffusion flame tabulation (dashed red lines), cases a_0 (left) and b_0 (right).

The evaluation of THR and PCM models was repeated using the 1-D unsteady strained laminar diffusion flame tabulation ; the general tendencies of the models' response were similar and discrepancies with averaged DNS results remained important, indicating that a diffusion flame tabulation does not counterbalance the errors due to the model assumptions. Nevertheless, the computation of unsteady diffusion flames, either for the generation of chemistry tabulations or during CFD runs, as in RIF [108] modelling, comes at a high CPU cost.

An interesting alternative is the ADF [74] model, introducing a statistical correlation of Z and c through the approximation of strained diffusion flames (see 3.4.3). DNS results are post-processed to obtain the evolution of strain rate a estimate ; ADF tables are then generated, relating mean mass fractions $\widetilde{Y_i}$, reaction rates $\widetilde{\dot{\omega}}_{Y_i}$, *etc.* to $\widetilde{Z}$, $\widetilde{S_Z}$, $\overline{c}$ and a, covering the range of strain rate values of interest. The ADF model response is presented in Figure 5.15 for the single injection cases a_0 (left) and b_0 (right), along with the respective DNS results. This approach considerably improves mean reaction rate $\widetilde{\dot{\omega}}_{Y_c}$ predictions during cool flame (first peak) and is able to follow the general trend of the evolution of combustion process, readily decreasing reactivity while approaching $\overline{c} = 1$. Although improved, $\widetilde{\dot{\omega}}_{Y_c}$ remains overestimated over a large part of the test, especially in the high turbulence intensity case b_0, in which the maximum reaction rate is overestimated by a factor of 7.

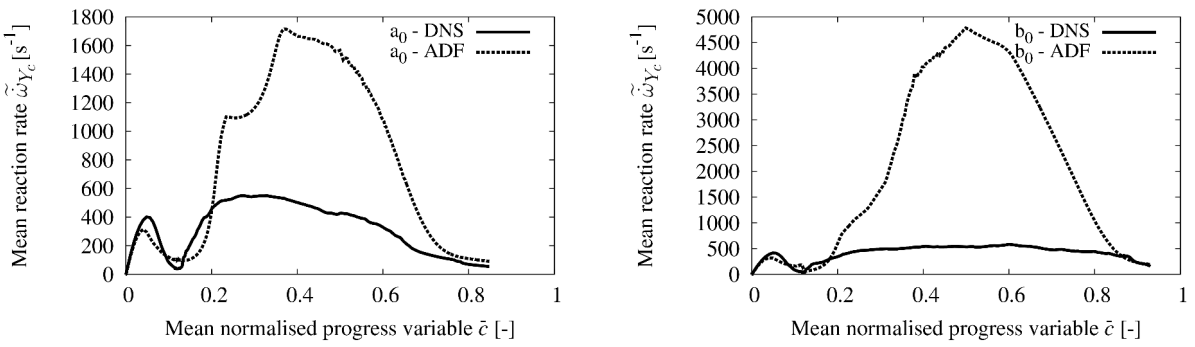

Figure 5.15: Evolution of mean reaction rate of the progress variable $\widetilde{\dot{\omega}}_{Y_c}$ with mean normalised progress variable $\overline{c}$; comparison between DNS results (solid lines) and ADF model (dashed lines) using 0-D homogeneous reactor tabulation, cases a_0 (left) and b_0 (right).

The fact that the ADF model response is closer to the DNS results in the lower turbulence case a_0 than in b_0 can be attributed to the difference of Damköhler number values, $\simeq 621$ and $\simeq 25$, respectively. Indeed, the laminar flamelet concept, viewing the turbulent diffusion flame as an ensemble of laminar diffusion flamelets [105], is only valid for high Damköhler numbers. This concept is also the basis of several other combustion models : Representative Interactive Flamelet [108] and Conditional Moment Closure [137] models consider a diffusion flame structure averaged at each time over a probability density function of the mixture fraction. Consequently, these models are expected to behave similarly to ADF. The eventual differences would be mainly attributed to the discrepancies between approximated and exact laminar diffusion flamelets.

All three evaluated models are regrouped and compared with DNS results in Figure 5.16 for cases a_0 (left) and b_0 (right). This comparison illustrates that the PCM approach can be significantly ameliorated following the additional assumption of a diffusion flamelet structure correlating Z and c, as for ADF model.

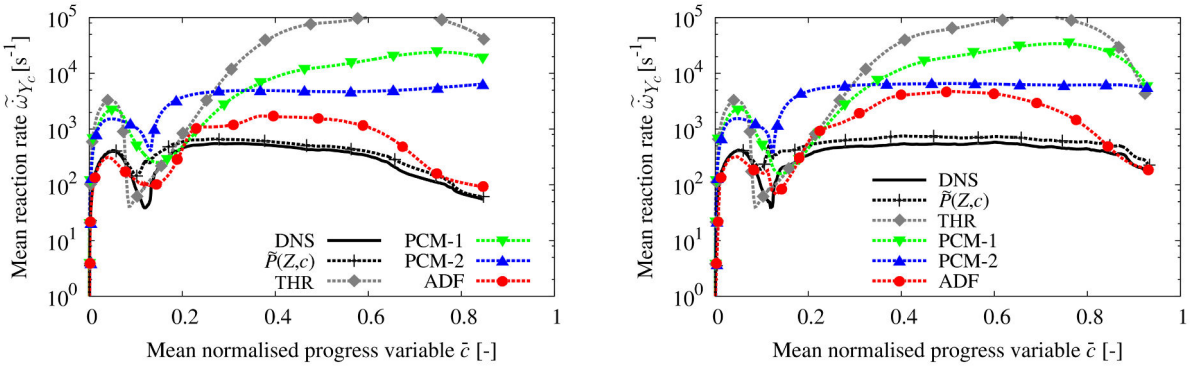

Figure 5.16: Evolution of mean reaction rate of the progress variable $\widetilde{\omega}_{Y_c}$ with mean normalised progress variable $\overline{c}$; comparison between DNS results (solid lines) and evaluated models (dashed lines) using 0-D homogeneous reactor tabulation, cases a_0 (left) and b_0 (right).

In order to obtain estimations of autoignition delay predictions of the tested models, the above results are stored as functions of $\widetilde{\omega}_{Y_c}(\widetilde{Y}_c)$ and integrated as following :

$$\widetilde{\omega}_{Y_c} = \frac{\partial \widetilde{Y}_c}{\partial t} \Rightarrow t = \int \frac{1}{\widetilde{\omega}_{Y_c}} \mathrm{d}\widetilde{Y}_c \tag{5.3}$$

Based on this approximation, a temporal evolution of $\overline{c}(t)$ is obtained for every studied model and presented in Figure 5.17 for cases a_0 (left) and b_0 (right). THR and PCM-1 models give a quasi-instantaneous cool flame ignition (first step in $\overline{c}(t)$ evolution) very far from the DNS results. A main ignition delay can be defined as the time needed for this reconstructed mean normalised progress variable to reach half of its maximum, *i.e.* $\overline{c} = 0.5$. According to this criterion, PCM models underestimate autoignition delay by at least a factor of four in the tested conditions. The THR approach gives a better estimation of autoignition delay, underestimating it by no more than a factor of two, but a very steep progress of combustion during main autoignition is observed. ADF model gives more satisfactory results that are closer to the DNS progress variable evolution and the most precise prediction of autoignition delay among the tested models, with approximately 25% of error for case a_0 and 35% for case b_0. The fact that, in terms of progress variable evolution, the results of ADF are closer to the DNS than the direct integration of the joint probability density function $\widetilde{P}(Z,c)$ can only be interpreted as a favourable accumulation of modelling errors.

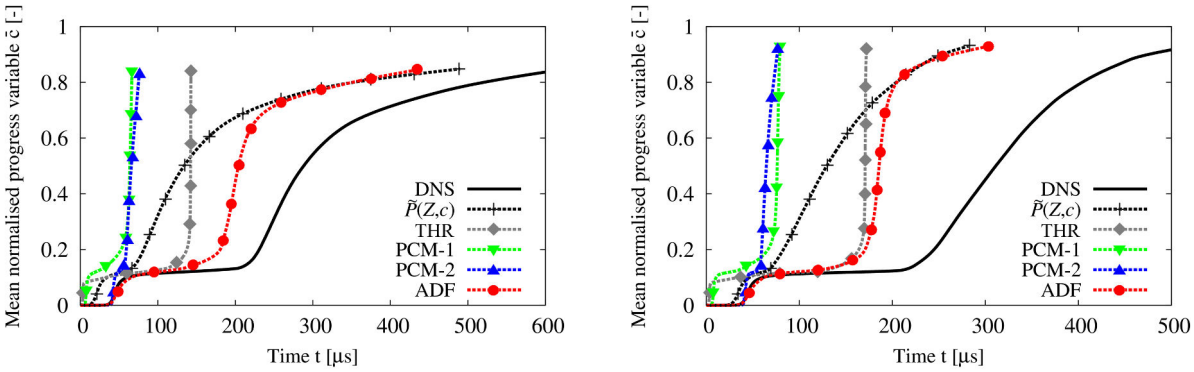

Figure 5.17: Temporal evolution of mean normalised progress variable $\overline{c}$; comparison between DNS results (solid lines) and evaluated models (dashed lines), cases a_0 (left) and b_0 (right).

5.3 Conclusions

The numerical results of two 2-D DNS single injection cases were presented and discussed. The first autoignition spots were found to originate where the instantaneous composition corresponds to a most reactive mixture fraction Z_{MR} together with low scalar dissipation rates. Additionally, the reaction fronts were found to propagate towards leaner as well as richer mixtures after the autoignition. These results are in agreement with previous 2-D [45, 139, 140] as well as 3-D [47, 141] DNS computations.

Autoignition of the turbulent heterogeneous reactors presented some similarities with the autoignition of a laminar diffusion flame. From this perspective, the assumption of a diffusion flamelet structure, which is the basis of numerous combustion models such as ADF [74], RIF [108] and CMC [137], seems coherent for the modelling of such turbulent heterogeneous reactors.

Turbulent combustion models using tabulated chemistry were evaluated on the basis of an *a priori* comparison with the DNS results. Both DNS and combustion models used the same skeletal reaction mechanism, therefore, the focus was exclusively put on the modelling assumptions. Three modelling approaches were tested : the Tabulated Homogeneous Reactor approach, which is a direct exploitation of the chemistry tabulation ignoring any local mixture heterogeneity ; (2) the Presumed Conditional Moment (PCM) model, which includes a separate statistical description for the mixture and the combustion progress ; (3) the Approximated Diffusion Flame (ADF) model, which considers the heterogeneous turbulent reactor as a diffusion flame.

The direct use of tabulation values based on the evolution of the mean values $\widetilde{Z}$ and $\overline{c}$, under the assumption of a homogeneous mixture (THR approach), led to extremely inaccurate results. The comparison of this approach with a zero-order model, involving the direct resolution of chemistry, also assuming a homogeneous mixture, revealed that an important part of these discrepancies at the beginning of the test is due to the chemistry tabulation itself. The zero-order model also gave very inaccurate results once the turbulent velocity field started acting more substantially on the mixing process. This behaviour could be extended to all models assuming a complete homogeneity of the computational cell.

Considering only the mixture fraction heterogeneity, as in PCM-1, only slightly ameliorated the model predictions. PCM-2, that takes into account the progress variable heterogeneity independently of the mixture fraction, was an improvement compared to PCM-1, it remained, nonetheless inaccurate under the studied conditions. Further investigation revealed that the presumed β distribution, approximating the progress variable PDF through the normalised progress variable mean $\overline{c}$ and variance $\overline{c'^2}$, may fail if the kinetics include some stagnation of c, *e.g.* in the case of the cool flame. The statistical independence of Z and c was identified as the main cause of the discrepancies of the PCM model.

The best results were obtained with the ADF model for both DNS single injection cases, illustrating the coherence of its modelling assumptions, namely the approximation of the mixture fraction PDF by a β distribution, the diffusion flamelet structure and the consequent Z and c correlation. These results are in agreement with those reported by Chevillard *et. al.* [29]. The ADF model response was generally more accurate in the lower turbulence case a_0 than in the higher turbulence case b_0, behaviour that can be attributed to the difference of Damköhler number values, $\simeq 621$ and $\simeq 25$, respectively, making case a_0 more suitable for a flamelet modelling type approach.

Chapter 6

Simulations and modelling under multiple injection conditions

This chapter presents the analysis of DNS results corresponding to multiple Diesel injections conditions. A DNS split injection database is generated and studied. Combustion models are then evaluated against these DNS results.

6.1 Phenomenological analysis

A total of 10 2-D DNSs were carried out by varying two parameters : (1) the progress of the hypothetical pilot injection combustion c_0, and (2) the velocity fluctuations level u'. The objective is to study independently the effects of chemical progress and turbulent mixing corresponding to different split injection strategies. The physical parameters of the 10 split injection cases are summarised in Table 6.1.

Case	$\boldsymbol{c_0}$	T^{init}	$\widetilde{S_Z}$	$\boldsymbol{u'}$	l_t	η_k	τ_{AI}	τ_t	τ_c	Da
a_1	0.05	701 - 942	0.39	1.12	1.4	10	323	947	1.7	549
a_2	0.10	702 - 967	0.41	1.12	1.6	11	418	1129	1.7	648
a_3	0.25	705 - 1034	0.44	1.12	1.8	13	333	1310	1.8	738
a_4	0.50	715 - 1158	0.51	1.12	2.2	15	49	1546	1.8	855
a_5	0.75	790 - 1350	0.53	1.12	2.7	19	-	1875	1.7	1102
a_6	1.00	818 - 1537	0.54	1.12	3.4	24	-	2419	1.5	1562
b_1	0.05	701 - 942	0.39	5.60	0.3	2	292	46	1.7	27
b_2	0.10	702 - 967	0.41	5.60	0.3	2	459	47	1.7	27
b_3	0.25	705 - 1034	0.44	5.60	0.4	3	335	52	1.8	30
b_4	0.50	715 - 1158	0.51	5.60	0.4	3	49	62	1.8	34
	[-]	[K]	[-]	[m/s]	[mm]	[µm]	[µs]	[µs]	[µs]	[-]

Table 6.1: Physical parameters of the different cases.

The DNS configuration consists of segregated "main injection" fuel parcels randomly distributed within "pilot injection" partially burnt gases subjected to a turbulent field. The initial mean equivalence ratio ϕ is 1 for all DNS cases, that is $\widetilde{Z} = Z_{\text{st}} \simeq 0.062$ according to the definition of Eq. (3.12). Before mixing with the fresh main injection fuel, the pilot injection partially burnt gases composition and temperature are calculated in homogeneous reactor conditions under a constant pressure of 35 bars. The pilot injection homogeneous mixture has an equivalence ratio ϕ_0 of approximately 0.27 ($Z_0 = 0.0175$) and an initial temperature $T^{\text{init}}(Z_0) =$ 893 K. The temporal evolution of normalised progress variable c of the pilot injection homogeneous mixture is shown in Figure 6.1. A two-step combustion is clearly illustrated : the first increase of the normalised progress variable, corresponding to a cool flame, is followed by a plateau leading to the main ignition, at approximately 1.14 ms. The various progress variable c_0 levels of the DNS database are marked with coloured lines. Composition at $c_0 = 0.05$ corresponds to a mixture at cool flame ignition and $c_0 = 0.1$ is found in the midst of the cool flame. These mixtures contain large quantities of species participating in NTC and cool flame chemistry, with reactions accounting for fuel decomposition and low temperature oxidation. $c_0 =$ 0.25 is found right before main ignition and $c_0 = 0.5$ during main ignition, containing species participating in the ignition and high temperature oxidation process. $c_0 = 0.75$ mixture consists mainly of species that participate in high temperature oxidation and post-oxidation reactions. $c_0 = 1$ corresponds to fully burnt gases at the equilibrium state, a case that can be associated with exhaust gas recirculation (EGR) conditions from an engine perspective. All these different compositions are expected to behave very differently when mixed with fresh fuel, as discussed further on.

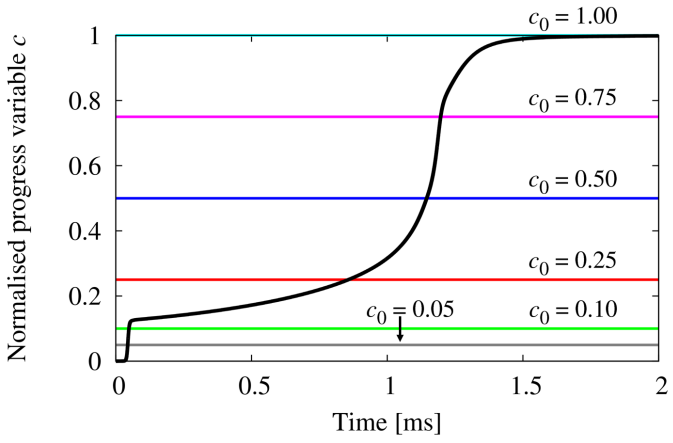

Figure 6.1: Temporal evolution of normalised progress variable c of the pilot injection homogeneous mixture. The various c_0 levels of the split injection database marked with coloured lines.

Initial temperature stratification T^{init} in the DNSs is linearly correlated to Z, as presented in

Table 6.1. The initial temperature of the oxidiser, which in this study refers to the pilot injection partially burnt gases, is equal to the adiabatic temperature of the pilot injection homogeneous mixture burning up to $c = c_0$. The temperature of the main injection fuel side is chosen so that the mean total enthalpy is the same for all the DNS cases. The maximum mixture fraction Z_{max} is calculated according to the adiabatic mixing of a main injection stream at Z_{sat}, with a pilot injection burnt gases stream at Z_0, as in Eq. (6.1), using a rough estimation of the saturation value of gas phase mixture fraction under the studied conditions $Z_{\text{sat}} = 0.5$. Unmixedness $\widetilde{S_Z}$ values, varying from 0.39 up to 0.54, indicate that the studied reactors are highly heterogeneous, in compliance with Diesel combustion conditions.

$$Z_{\text{max}} = Z_{\text{sat}} + (1 - Z_{\text{sat}})\, Z_0 = 0.50875 \tag{6.1}$$

As in the previous chapter, two levels of turbulence intensity are tested for a-cases and b-cases, respectively. Velocity fluctuations levels u' and integral length scales l_t are chosen of the same order as the indicative values extracted from the preliminary RANS simulation, that is $u' \simeq 1.8$ m/s and $l_t \simeq 1$ mm. Kolmogorov η_k length scale values are estimated according to Eq. (4.6), based on preliminary non-reactive tests. The mesh used is deemed adequate to resolve all turbulent structures. Turbulent Reynolds number Re_t is 630 for all cases.

Figure 6.2 shows the ignition delay $\tau_{\text{AI}}^{\text{HR}} = t|_{c\,=\,0.5}$ of homogeneous mixtures at 35 bar as a function of mixture fraction Z. Every curve is obtained by a series of 0-D homogeneous reactor calculations with the ERC mechanism [66], considering mixtures of fuel and partially burnt gases. Initial temperature and composition are linearly correlated with Z, as in the respective DNS cases.

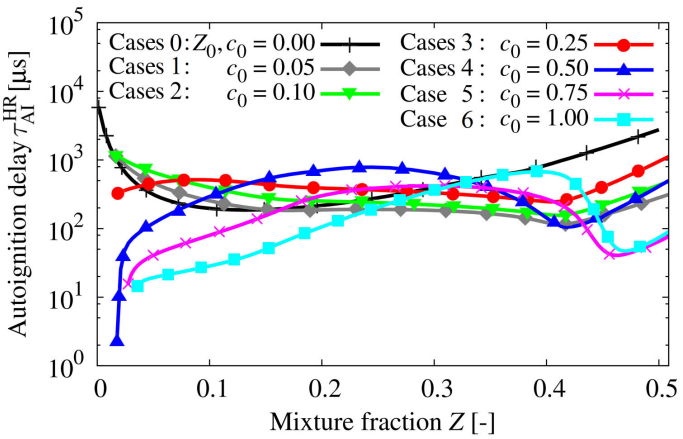

Figure 6.2: 0-D ignition delay $\tau_{\text{AI}}^{\text{HR}}$ of main injection fuel-pilot injection partially burnt gases homogeneous mixtures at 35 bar as a function of mixture fraction Z with Z dependent initial temperature using the ERC mechanism [66].

These results should be taken with caution since the skeletal reaction mechanism [66] used was developed for n-heptane/air mixture autoignition and flame propagation under high pressure and with a certain level of exhaust gas recirculation (EGR), but has not been validated for fuel-partially burnt gases mixtures and for very rich mixtures ($\phi \simeq 16$ at $Z = Z_{\text{max}}$). Nonetheless, the evaluation of the studied models should not be largely impacted by this fact, since both DNS and tabulated chemistry models use the ERC mechanism [66] ; therefore, the focus is exclusively put on the modelling assumptions.

The mixture fraction distributions $\widetilde{P}(Z)$ in the initial fields of DNS cases a_1 and a_6 are presented in Figure 6.3. Combining the fact that the heterogeneous reactors are mostly lean (low Z) with the general tendencies of the 0-D ignition delay of Figure 6.2 and ignoring the decaying effect of turbulence and of temperature stratifications, a first indication of the reactivity of the heterogeneous reactors can be obtained. Cases a_4, b_4, a_5 and a_6 are expected to be much more reactive than cases a_1, b_1, a_2 and b_2, with much shorter chemical time scales τ_c and autoignition delays τ_{AI}.

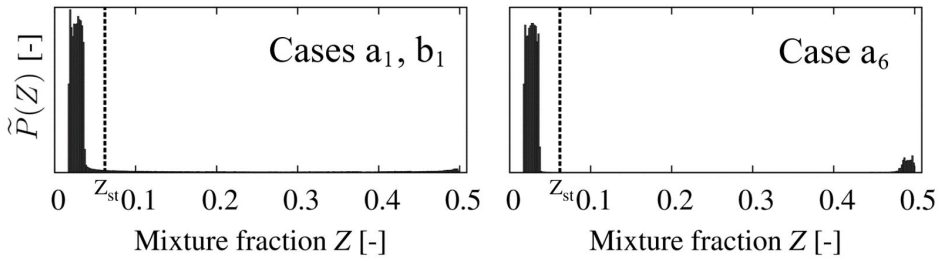

Figure 6.3: Mixture fraction distributions $\widetilde{P}(Z)$ in the initial fields of DNS cases a_1, b_1 and a_6.

Ignition delays τ_{AI} are estimated for all split injection DNS cases and are regrouped in Table 6.1. It should be noted that the criterion of the mean normalised progress variable reaching half of its maximum, *i.e.* $t|_{\widetilde{c}=0.5}$ cannot be applied in cases a_5 and a_6 since initial mean normalised progress variable in these cases is greater than 0.5.

The temporal evolution of the mean temperature $\widetilde{T}$ (left) and of the normalised progress variable $\widetilde{c}$ (right) of several DNS cases is presented in Figure 6.4. The reactivity of these heterogeneous reactors is found to present a multi-mode nature depending on c_0. Mixing partially burnt gases of $c_0 = 0.1$ with fresh fuel (green lines) gives reactors that autoignite slower than the equivalent fuel-air mixtures (black lines). Split injection cases a_3 and b_3 (red lines) present slightly longer ignition delays than single injection cases a_0 and b_0 (black lines). Once initiated, however, the combustion process advances faster in these cases than in cases a_0 and b_0. Mix-

tures of cases a_4, b_4, a_5 and a_6 are very reactive and burn almost instantaneously, regardless of the turbulent flow, and that is the reason of their exemption from Figure 6.4. The evolution of mean normalised progress variable $\overline{c}$, mean reaction rate of the progress variable $\widetilde{\dot{\omega}}_{Y_c}$ and strain rate a of all DNS cases are regrouped in Appendix I.

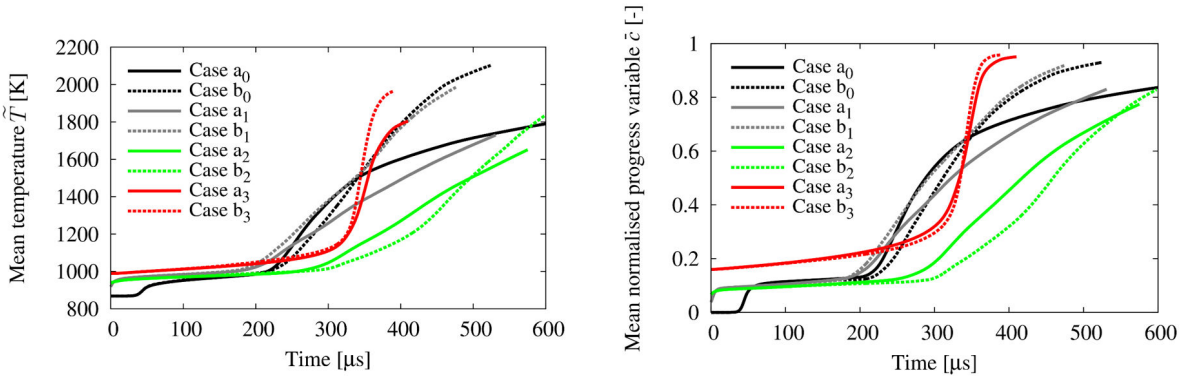

Figure 6.4: Temporal evolution of mean temperature $\widetilde{T}$ (left) and mean normalised progress variable $\overline{c}$ (right) of several DNS cases.

Turbulent time scales $\tau_t = k/\varepsilon$ and chemical time scales $\tau_c = 1/\widetilde{\dot{\omega}}_{c\ \max}|_{Z=Z_{\text{st}}}$ (see Section 5.1) are estimated for all the cases. According to these estimates, Damköhler number Da varies between 27 and 1562, depending on the case. This means that in some cases (low Da) the internal structure of the flame is potentially affected by turbulent mixing, whereas others ($Da >> 1$) are more propitious for flamelet modelling (see Section 3.2).

To highlight the differences between cases with higher and lower Damköhler number, cases a_3 and b_2, with $Da \simeq 738$ and $\simeq 27$, respectively, are chosen to be contrasted with one another. Mixture fraction Z and normalised progress variable c fields of DNS case a_3 are presented in Figure 6.5. Turbulence drives the formation of local mixing layers and enhances heat transfer between hot, lean and cold, rich regions, leading to the main autoignition ($\overline{c} = 0.5$), arriving at 333 µs. Combustion progresses uniformly over a large range of Z : at $\overline{c} = 0.5$ few regions of the mixture have reached chemical equilibrium but most of them have started to react.

Figure 6.6 shows the evolution of mixture fraction Z and normalised progress variable c fields of DNS case b_2. Turbulent structures wrinkle strongly the mixture fraction field and strain the flame structures. Main ignition occurs at 459 µs. By contrast with case a_3, combustion progresses in a segregated way : at $\overline{c} = 0.5$ many regions of the heterogeneous mixture have already reached chemical equilibrium, whereas others have hardly started to react.

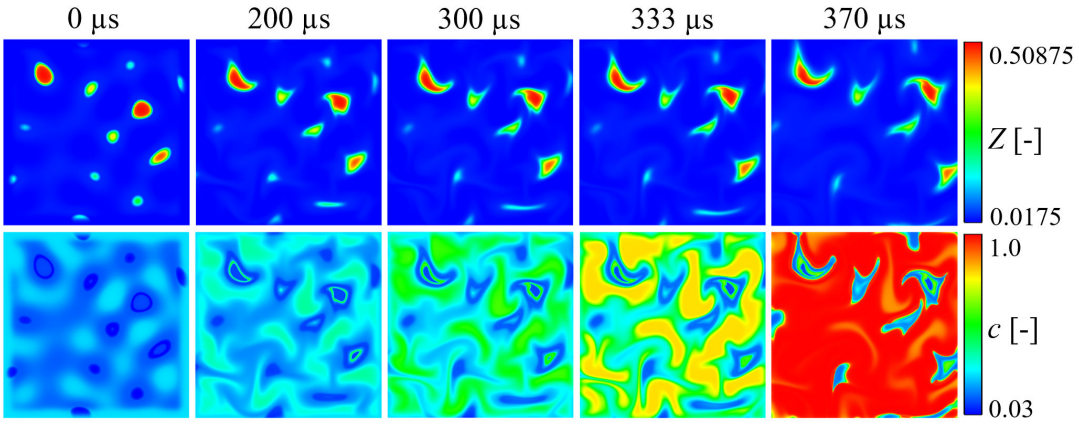

Figure 6.5: Instantaneous views for a sequence of times ; mixture fraction Z (first row) and normalised progress variable c (second row) fields of DNS case a_3.

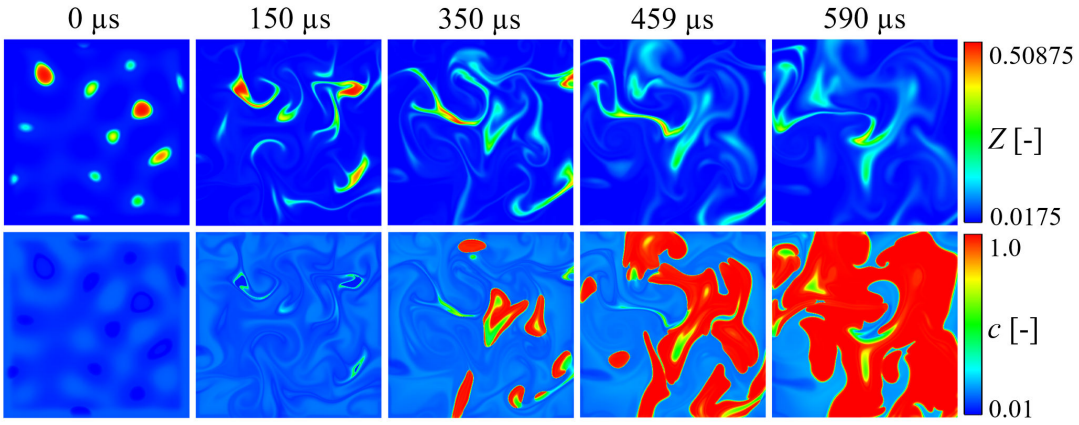

Figure 6.6: Instantaneous views for a sequence of times ; mixture fraction Z (first row) and normalised progress variable c (second row) fields of DNS case b_2.

When the Damköhler number is large, the burning rate can be quantified in terms of turbulent mixing. This assumption is only valid for combustion regimes where turbulence does not have an impact on the inner structure of the flame. In geometrical terms, this would mean that reaction zones' thickness is small compared to turbulent mixing length scales. Estimates of these length scales are proposed and compared for the DNS cases a_3 and b_2 at $\overline{c} = 0.7$. A reaction zone can be defined around every local reaction rate peak, considering the thickness $\delta\dot{\omega}_c$ of the region in which reaction rate $\dot{\omega}_c$ values are higher than 10% of the local maximum.

A turbulent mixing length scale δZ is defined based on the gradients of mixture fraction Z, as follows :

$$\delta Z = \frac{Z_{\text{max}}^{\text{loc}} - Z_{\text{min}}^{\text{loc}}}{|\nabla Z|} \tag{6.2}$$

where $Z_{\text{min}}^{\text{loc}}$ and $Z_{\text{max}}^{\text{loc}}$ are the local minimum and maximum values of a studied mixing layer, respectively. Fields of $|\nabla Z|$ and $\dot{\omega}_c$ of case a_3 at t = 350 µs or $\overline{c} = 0.7$ are presented in Figure 6.7. A region combining a strong gradient of Z with a local peak of $\dot{\omega}_c$ is found in the upper left corner of the DNS domain (red dashed circle). A line passing through the abscissa of this region is chosen (black dashed line). Values of $|\nabla Z|$ and $\dot{\omega}_c$ along this line are presented accompanied by values of Z (green line). Estimated values $\delta\dot{\omega}_c = 58$ µm and $\delta Z = 100$ µm are calculated based on the above definitions. According to these values, the thickness of this reaction zone is a few times smaller than the mixing length scale.

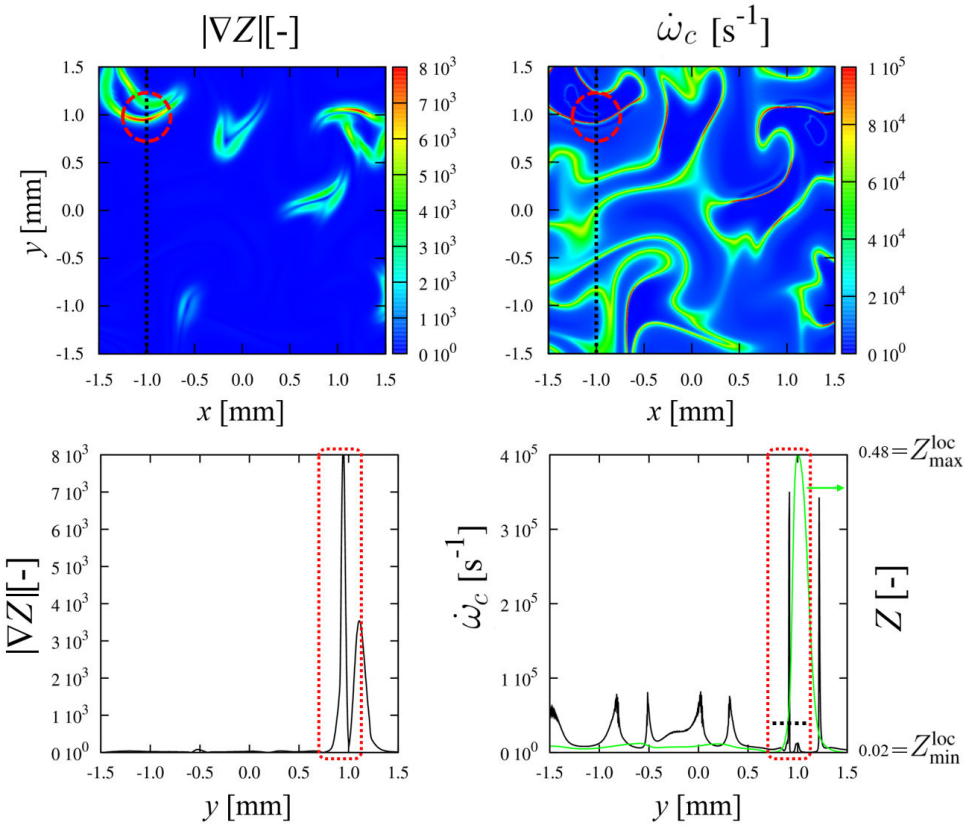

Figure 6.7: Fields of $|\nabla Z|$ and $\dot{\omega}_c$ (upper figures), a region combining a strong gradient of Z with a local peak of $\dot{\omega}_c$ (red dashed circle), a line passing through the abscissa of this region (black dashed line), and respective values of $|\nabla Z|$ and $\dot{\omega}_c$ along this line (lower figures) accompanied by values of Z (green line) for case a_3 at t = 350 µs or $\overline{c} = 0.7$.

The same procedure is repeated for case b_2. Figure 6.8 illustrates fields of $|\nabla Z|$ and $\dot{\omega}_c$ of this case at t = 530 µs or $\overline{c} = 0.7$. A region is again chosen (red dashed circle). Values of $|\nabla Z|$ and $\dot{\omega}_c$ on a line cutting through this region (black dashed line) are presented along with the distribution of Z (green line). The estimates obtained are $\delta\dot{\omega}_c = 20$ µm and $\delta Z = 20$ µm, meaning that the thickness of the reaction zone is of the same size as the mixing length scale. Hence, the internal structure of the flame is potentially affected by turbulent mixing.

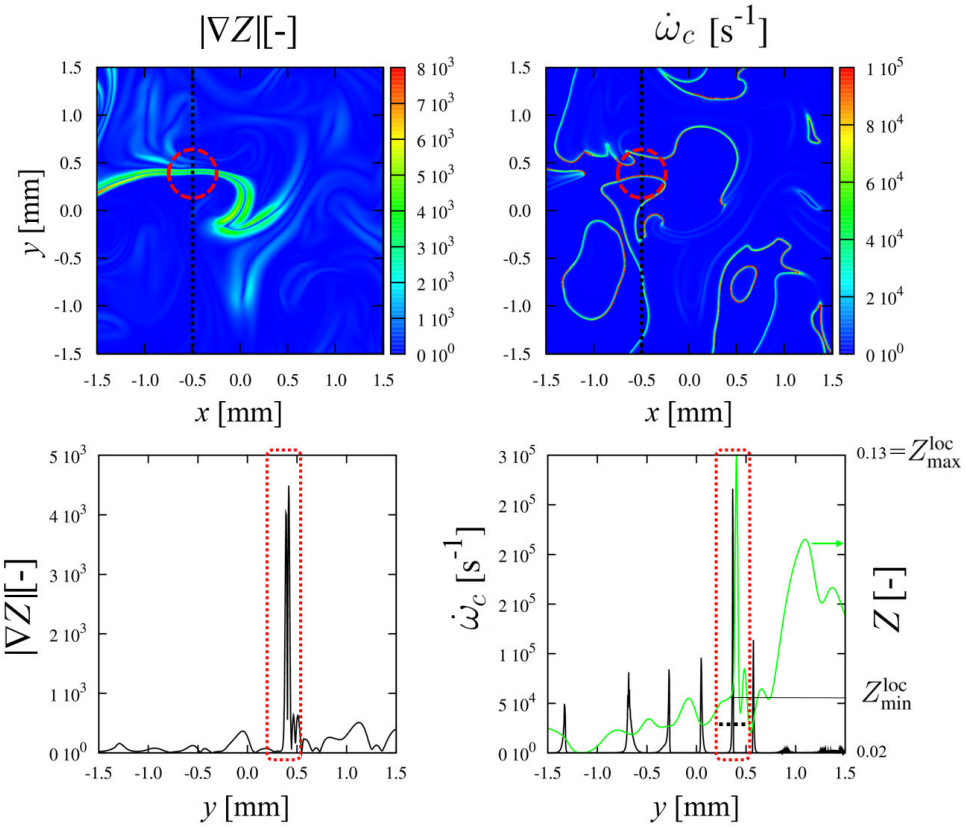

Figure 6.8: Fields of $|\nabla Z|$ and $\dot{\omega}_c$ (upper figures), a region combining a strong gradient of Z with a local peak of $\dot{\omega}_c$ (red dashed circle), a line passing through the abscissa of this region (black dashed line), and respective values of $|\nabla Z|$ and $\dot{\omega}_c$ along this line (lower figures) accompanied by values of Z (green line) for case b_2 at t = 530 µs or $\overline{c} = 0.7$.

This instantaneous comparison is not a complete demonstration allowing the classification of the two cases under different combustion regimes. It serves, nonetheless, as evidence for the interpretation of model response later on. Based on these observations, the ADF model, which is based on the assumption of the flamelet structure, is expected to give more satisfactory results in case a_3 than in case b_2.

6.2 *A priori* model evaluation

6.2.1 Influence of chemistry tabulation

The three modelling approaches presented in Section 3.4 are evaluated on the basis of an *a priori* comparison with the DNS results, as detailed in Section 3.5. The behaviour of the models in the split injection cases is examined omitting the effects of c_0 on the combustion chemistry, using the tabulation of Figure 5.9 that corresponds to the single injection cases. Taking the example of split injection case a_3, the evolution of the mean reaction rate of the progress variable $\widetilde{\dot{\omega}}_{Y_c}$ with the mean normalised progress variable $\overline{c}$ is illustrated in Figure 6.9(a), comparing averaged DNS results with model response, accompanied by the results of the direct integration over Z and c of the joint probability density function $\widetilde{P}(Z,c)$, as in Eq. (3.29). The ranking of the evaluated models in terms of accuracy is the same as in the single injection cases. However, all approaches give largely overestimated values of mean reaction rate. Even using the exact joint probability density function $\widetilde{P}(Z,c)$, extracted directly from the DNS results, the modelled mean reaction rate does not follow the trend of the DNS at the beginning of the test. This behaviour is due to the tabulated kinetics based on fuel-air mixtures, returning high reaction rate values for non-zero progress variable input.

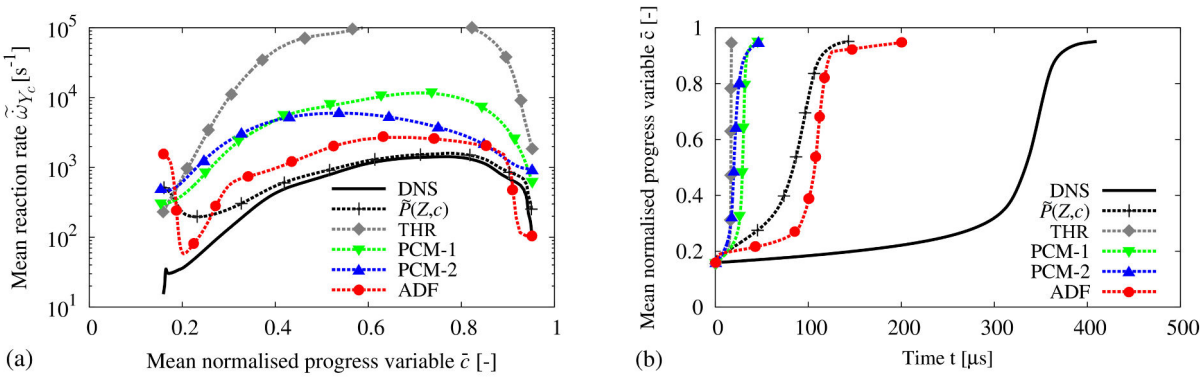

Figure 6.9: Comparison between DNS results (solid lines) and evaluated models (dashed lines) using 0-D homogeneous reactor tabulation of fuel-air mixtures for split injection case a_3. (a) Evolution of mean reaction rate of the progress variable $\widetilde{\dot{\omega}}_{Y_c}$ with mean normalised progress variable $\overline{c}$. (b) Temporal evolution of mean normalised progress variable $\overline{c}$.

In order to obtain an *a priori* estimation of the temporal evolution of the normalised progress variable $\overline{c}(t)$, and therefore of the autoignition delay predictions of the tested models, the above results are stored as functions of $\widetilde{\dot{\omega}}_{Y_c}(\widetilde{Y}_c)$ and integrated as in Eq. (5.3). Based on this approxi-

mation, a $\overline{c}(t)$ evolution is obtained for every studied model and presented in Figure 6.9(b) for case a_3. According to the aforementioned criterion $\tau_{\mathrm{AI}} = t|_{\overline{c}\,=\,0.5}$, all evaluated models largely underestimate autoignition delay, by at least a factor of three.

The progress of the pilot injection combustion c_0, corresponding to different injection timings, is the key parameter in the present work, since it is conditioning the composition of the partially burnt gases surrounding the fresh fuel parcels. The progress variable related to an initial state of fresh fuel-air mixtures is no longer valid since an additional quantity of fuel is injected into the system while the combustion process is ongoing. Thus, special attention should be paid to elaborating a strategy for the treatment of the chemistry tabulation for models used in multiple injection configurations. As discussed in Section 6.1, the progress of combustion in the split injection cases is found to be strongly dependent on c_0. The behaviour of pure air and fuel mixtures is very different from that of mixtures of partially burnt gasses (pilot injection) reacting with fresh fuel (main injection). For this reason, 0-D homogeneous reactor tabulations are created using adiabatic mixtures between a pilot injection burnt gases stream and a mixed pilot injection burnt gases-main injection fresh fuel stream. The initial temperature-mixture fraction correlation $T^{\mathrm{init}}(Z)$ is the same as in the respective DNS split injection cases (see Table 6.1). Six different split injection tabulations are generated, one for each tested value of c_0. Tabulated reaction rate of the progress variable $\dot{\omega}_{Y_c}^{\mathrm{TAB}}(Z, c)$ values of autoigniting homogeneous mixtures, with initial conditions corresponding to cases a_3 and b_3 ($c_0 = 0.25$), are illustrated in Figure 6.10.

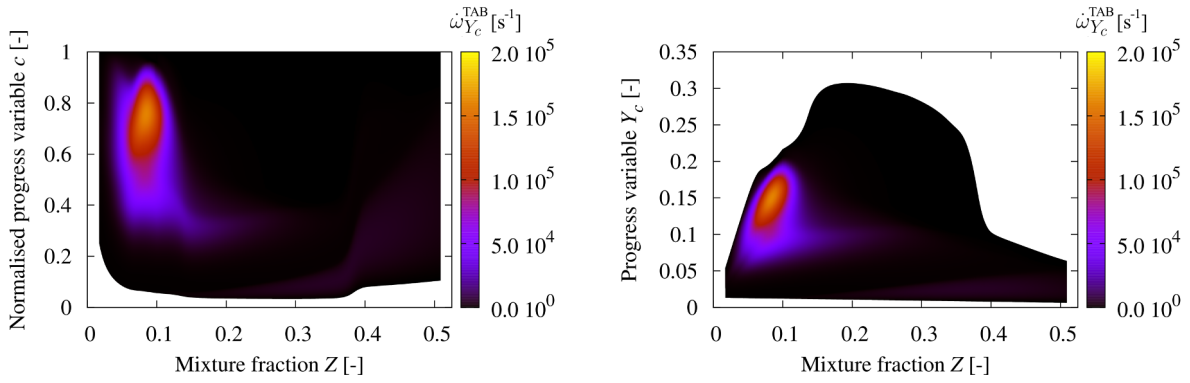

Figure 6.10: 0-D homogeneous reactor tabulation of reaction rate of the progress variable $\dot{\omega}_{Y_c}^{\mathrm{TAB}}$ with mixture fraction Z and normalised progress variable c (left), and with mixture fraction Z and progress variable Y_c (right), using autoigniting main injection fuel-pilot injection partially burnt gases mixtures, adapted to cases a_3 and b_3 ($c_0 = 0.25$).

The evolution of the joint probability density function $\widetilde{P}(Z,c)$ is obtained for all split injection cases by post-processing of the DNS results. The latter is directly integrated as in Eq. (3.29), using different tabulations, such as the ones presented in Figures 5.9 and 6.10. This method is repeated to cover the complete split injection database, testing all the available tabulations (one single injection and six split injection tabulations), so to unveil the impact of c_0 on the precision of PCM-type combustion models. All tabulations used in this work are regrouped in Appendix III.

A relative error of the mean reaction rate of the progress variable $\widetilde{\dot{\omega}}_{Y_c}$ model predictions can be defined as:

$$\delta(\widetilde{\dot{\omega}}_{Y_c}) = \frac{\int |\ \widetilde{\dot{\omega}}_{Y_c}^{\mathrm{DNS}} - \widetilde{\dot{\omega}}_{Y_c}^{\mathrm{MODEL}}\ |\ \mathrm{d}\bar{c}}{\int \widetilde{\dot{\omega}}_{Y_c}^{\mathrm{DNS}}\ \mathrm{d}\bar{c}} \tag{6.3}$$

The relative error of the direct integration of $\widetilde{P}(Z,c)$ in the prediction of the mean reaction rate of the progress variable $\widetilde{\dot{\omega}}_{Y_c}$ is calculated for all cases and tabulations tested, according to the above definition. These values correspond to minimum discrepancies estimates for PCM-type models.

Figure 6.11 regroups relative errors of the direct integration of $\widetilde{P}(Z,c)$ in the prediction of the mean reaction rate of the progress variable $\widetilde{\dot{\omega}}_{Y_c}$ using a fuel-air mixtures tabulation (TAB I) and adapted split injection tabulations (TAB II) for the corresponding DNS case. The best agreement is observed when using the tabulation corresponding to the pilot injection normalised progress variable c_0 of the respective studied case (TAB II).

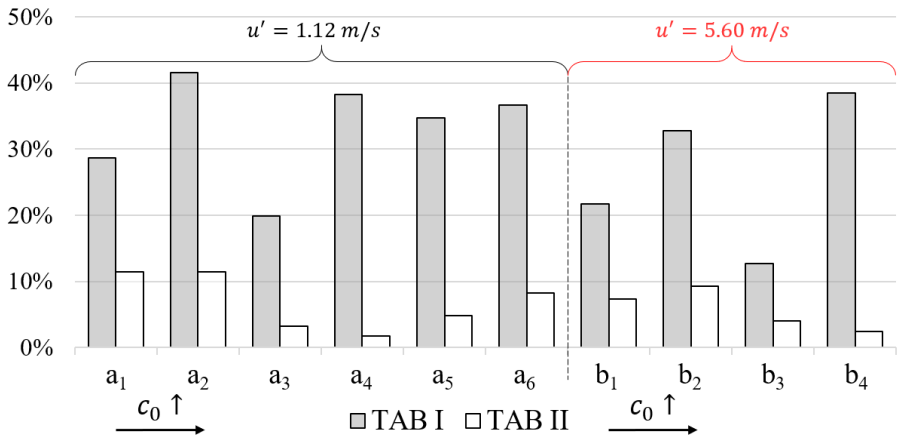

Figure 6.11: Relative errors of the direct integration of $\widetilde{P}(Z,c)$ in the prediction of the mean reaction rate of the progress variable $\widetilde{\dot{\omega}}_{Y_c}$ using a fuel-air mixtures tabulation (TAB I) and adapted split injection tabulations (TAB II) for the corresponding DNS case.

This analysis demonstrates the need for additional dimensions (c_0 and possibly Z_0) on the tabulations used by the combustion models for multi-injection Diesel engine applications. Furthermore, it helps quantifying the part of the observed discrepancies between the evaluated combustion models and the DNS results that stems from the tabulated chemistry approach itself. When an adapted chemistry tabulation is used, this error does not exceed 11%. Therefore, turbulent combustion models based on tabulations of homogeneous reactors, regrouped under the general description of Eq. (3.29), appear to be a solid choice for the simulation of such conditions, as long as the effect of multiple injections is taken into account in the chemistry tabulation.

Model predictions in the split injection case a_3 are recalculated using the split injection tabulation of Figure 6.10 and compared with the averaged DNS results in Figure 6.12(a). Discrepancies between the THR approach and the averaged DNS results remain very important, despite the more adapted chemistry tabulation. The predictions of PCM and ADF models, however, are significantly ameliorated. The tendencies of the DNS results are approximatively followed, with low reaction rate values for non-zero progress variable input and a reduction of reactivity while progress variable tends to unity. For PCM-type models, the maximum reaction rate is highly overestimated, which would lead to a strong overestimation of heat release rate in the context of engine simulation. The ADF model gives the best results among the tested models : it overestimates the small first peak of reactivity observed in the DNS and then follows its evolution throughout the test. The relative error of the ADF prediction in this case is approximately 89%, as opposed to 123% of error using the tabulation of Figure 5.9 that corresponds to single injection cases, without taking into account Z_0 and c_0.

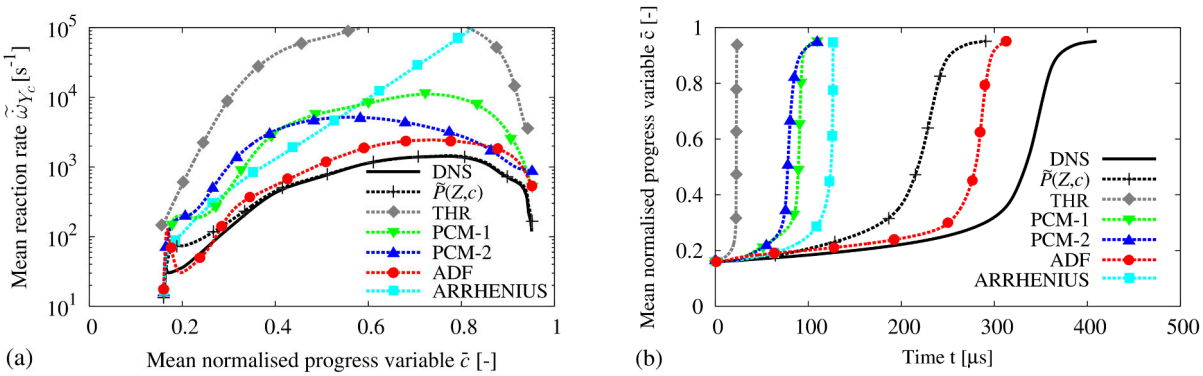

Figure 6.12: Comparison between DNS results (solid lines) and evaluated models (dashed lines) using adapted 0-D homogeneous reactor tabulation for split injection case a_3. (a) Evolution of mean reaction rate of the progress variable $\widetilde{\omega}_{Y_c}$ with mean normalised progress variable $\bar{c}$. (b) Temporal evolution of mean normalised progress variable $\bar{c}$.

These results are accompanied by the response of a zero-order model, here denoted as "Arrhenius" : like in the previous chapter, the DNS results are post-processed at every time-step of the model evaluation test (every microsecond) to obtain the mean mass fractions $\widetilde{Y}_k$ of all 29 chemical species transported. Then, chemical kinetics are resolved for one chemical time-step under constant pressure homogeneous reactor conditions, to obtain the reaction rate $\dot{\omega}_{Y_c}$ of this average composition. This test corresponds to a direct integration of chemical kinetics into the CFD simulation [92], without considering any interaction of the turbulent mixing with the chemical kinetics below the grid level. Initially, the Arrhenius approach is in agreement with DNS results. Once the velocity field starts acting on the mixing process, discrepancies become important and the zero-order model fails to follow the trend of the DNS results.

Estimates of the temporal evolution of the normalised progress variable $\overline{c}(t)$ are obtained for every studied model by integration of $\widetilde{\dot{\omega}}_{Y_c}(\widetilde{Y}_c)$, as in Eq. (5.3). The results of case a_3 are presented in Figure 6.12(b). The THR approach gives a very sharp quasi-instantaneous combustion. PCM models still strongly underestimate autoignition delay with approximately 75% of error. ADF gives the more satisfactory results with approximately 25% of error on the estimation of the autoignition delay. Once again, the fact that, in terms of progress variable evolution, the results of ADF are closer to the DNS than the direct integration of the joint probability density function $\widetilde{P}(Z,c)$ can only be interpreted as a favourable accumulation of errors.

6.2.2 Influence of *Z* and *c* statistical independence

It was demonstrated that, in multi-injection configurations, taking into account the progress of the pilot injection c_0 in the chemistry tabulation improves significantly the model predictions. However, there are other possible sources of discrepancies to be understood and dealt with. To better understand the mismatch between the DNS and PCM-type models, DNS results are post-processed to obtain the PDFs of Z and c as well as the joint $\widetilde{P}(Z,c)$. The evolution of $\widetilde{\dot{\omega}}_{Y_c}$ with $\overline{c}$ is presented in Figure 6.13 for the split injection cases a_3 (left) and b_1 (right) ; the averaged DNS results (solid lines) are compared with the mean values obtained by direct integration of the independent probability density functions $\widetilde{P}(Z)$ and $\overline{P}(c)$ (dashed black lines), and of the joint probability density function $\widetilde{P}(Z,c)$ (dashed red lines), using adapted split injection tabulations. As for the single injection cases, the direct integration of the joint $\widetilde{P}(Z,c)$ gives a lot smaller discrepancies compared to the integration of the independent $\widetilde{P}(Z)$ and $\overline{P}(c)$, in both cases. Thus, the assumption of independence between the mixture fraction Z and the progress c variable (see Eq. (3.31)) is again shown to be inexact.

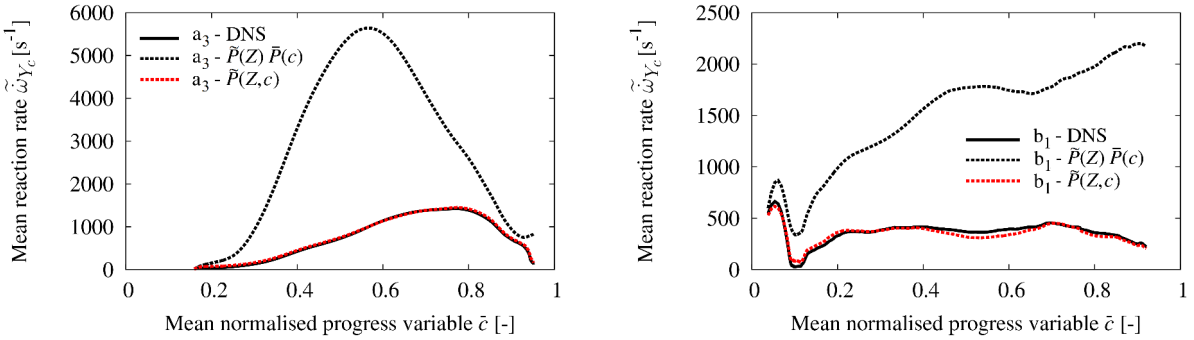

Figure 6.13: Evolution of mean reaction rate of the progress variable $\widetilde{\dot{\omega}}_{Y_c}$ with mean normalised progress variable $\overline{c}$; comparison between DNS results (solid lines), the direct integration of the independent probability density functions $\widetilde{P}(Z)$ and $\overline{P}(c)$ (dashed black lines), and the direct integration of the joint probability density function $\widetilde{P}(Z,c)$ (dashed red lines), cases a_3 (left) and b_1 (right).

The relative errors (see Eq. (6.3)) in the prediction of the mean reaction rate of the progress variable $\widetilde{\dot{\omega}}_{Y_c}$, using either the joint $\widetilde{P}(Z,c)$ or the independent $\widetilde{P}(Z)$ and $\overline{P}(c)$ are calculated for all the split injection DNS cases and regrouped in Figure 6.14. According to these results, the assumption of the statistical independence can be assumed to be the main responsible for the discrepancies of the PCM model, as concluded in Section 5.2 and in [29] for single injection configurations.

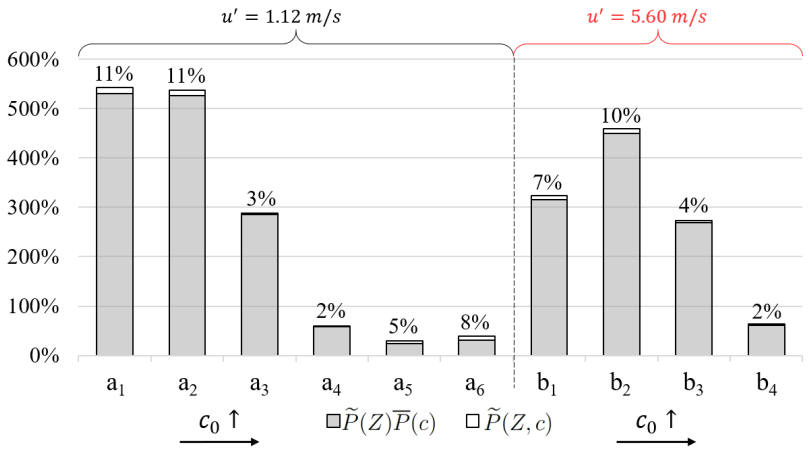

Figure 6.14: Relative errors in the prediction of the mean reaction rate of the progress variable $\widetilde{\dot{\omega}}_{Y_c}$ using either the joint $\widetilde{P}(Z,c)$ or the independent $\widetilde{P}(Z)$ and $\overline{P}(c)$, for all the split injection DNS cases.

6.2.3 Influence of PDF approximation

As seen in Section 5.2, the approximation of the mixture fraction and progress variable PDFs by presumed β distributions is also a possible source of error for PCM and ADF models. To investigate the impact of this approximation, theoretical model predictions can be obtained by integrating over the actual PDFs, retrieved from post-processing of the DNS results, instead of the presumed β distribution of Eqs. (3.35) and (3.39). In Figure 6.15(a) a comparison between averaged DNS results (solid lines) and ADF model using either a standardised β distribution (dashed black line) or the actual $\widetilde{P}(Z)$ (dashed green line) for split injection case a_3 is presented as an example. Indeed, an important part of the model discrepancies is due to the inaccurate approximation of the PDF of Z by a β distribution. More specifically, when the evolution of the $\widetilde{P}(Z)$ is used, the relative error of the ADF model is reduced from 89% down to 26% for this case. Further investigation reveals that the presumed $\beta(Z)$ may be insufficient if initial fields include some stagnation of Z, as is the case here for $Z = Z_0$ (see Figure 6.15(b)).

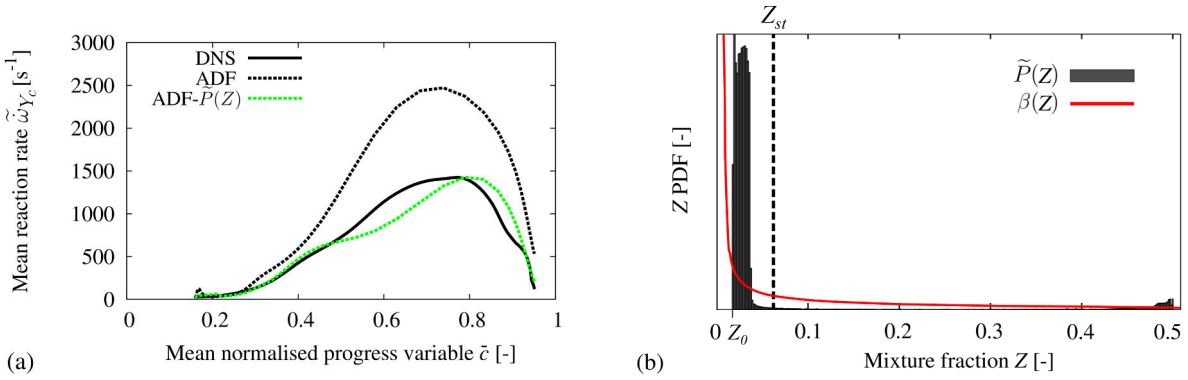

Figure 6.15: (a) Evolution of mean reaction rate of the progress variable $\widetilde{\dot{\omega}}_{Y_c}$ with mean normalised progress variable $\overline{c}$; comparison between averaged DNS results (solid lines) and ADF model using either a standardised β distribution (dashed black line) or the actual $\widetilde{P}(Z)$ (dashed green line) for split injection case a_3. (b) Comparison of the actual $\widetilde{P}(Z)$ with the presumed β distribution at the beginning of the test.

The relative errors (see Eq. (6.3)) of the PCM and ADF models in the prediction of the mean reaction rate of the progress variable $\widetilde{\dot{\omega}}_{Y_c}$, using either β distributions or the actual PDFs, are calculated for all the split injection DNS cases and regrouped in Figure 6.16. This analysis helps quantifying the part of the observed discrepancies between the models and the DNS results that is due to the approximation of the Z and c PDFs by standardised β distributions. As can be observed, the inaccurate approximation of the PDFs contributes considerably to model

discrepancies. PCM-2 model in case a_3 and ADF model in case a_4 give smaller discrepancies when using standardised β distributions instead of the actual PDFs. It should be noted that these results are most probably accidental in the sense that the accumulation of errors due to chemistry tabulation and the PDF approximation inadvertently lead to smaller relative errors.

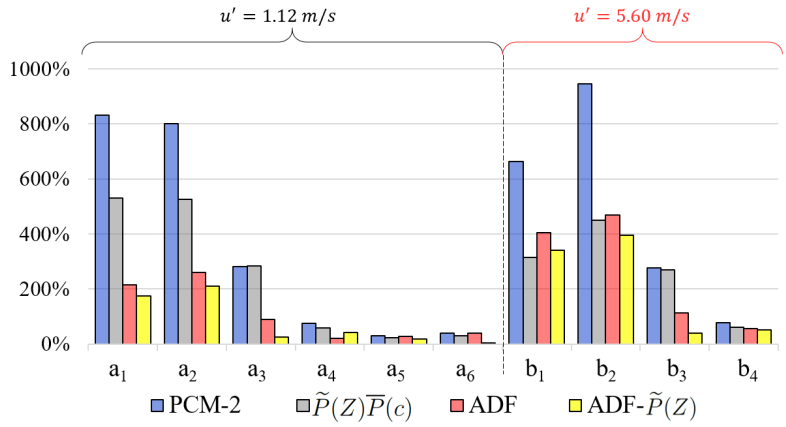

Figure 6.16: Relative errors of the PCM and ADF models in the prediction of the mean reaction rate of the progress variable $\widetilde{\omega}_{Y_c}$, using either standardised β distributions or the actual PDFs, for all the split injection DNS cases.

Nevertheless, $\widetilde{P}(Z)$ and $\overline{P}(c)$ are not available in the context of RANS simulation when using PCM or ADF models. There exist alternatives for a more precise approximation of the PDFs, such as the presumed mapping function approach used in [142]. Their use in RANS simulation of multi-injection Diesel cycles can be an interesting perspective work.

6.2.4 Influence of progress of pilot injection combustion

Cases a_1 - a_6 correspond to different split injection strategies (see Table 6.1), varying the progress of the pilot injection combustion c_0. The initial mean equivalence ratio ϕ is 1 and the initial velocity fluctuations level u' is 1.12 m/s for all the presented cases. As discussed in 6.1, the reactivity of these heterogeneous reactors is found to present a multi-mode nature depending on c_0 (see Figure 6.4). Case a_1, corresponding to fresh fuel mixing with a lean mixture at cool flame ignition ($c_0 = 0.05$), presents a slightly smoother autoignition, compared to the single injection case a_0. The reactor of case a_2, resulting from the mixing of fresh fuel with partially burnt gases in the midst of the cool flame ($c_0 = 0.1$), autoignites slower than the single injection a_0. Case a_3, with pilot injection right before main ignition ($c_0 = 0.25$) presents a longer ignition delay than a_0, but advances remarkably faster than the single injection case

once initiated. Mixtures of cases a_4 - a_6 are very reactive and burn almost instantaneously. The evolution of mean normalised progress variable $\overline{c}$, mean reaction rate of the progress variable $\widetilde{\dot{\omega}}_{Y_c}$ and strain rate a of all DNS cases are regrouped in Appendix I.

These different behaviours, depending on c_0, have an effect on the accuracy of the evaluated models' predictions. Having demonstrated the necessity to take the progress of the pilot injection combustion into account in the chemistry tabulation (see Subsection 6.2.1), the studied models are evaluated over the split injection cases a_1 - a_6, using the corresponding adapted tabulations. Estimates of the temporal evolution of the normalised progress variable $\overline{c}(t)$ are obtained for every studied model by integration of $\widetilde{\dot{\omega}}_{Y_c}(\widetilde{Y}_c)$, as in Eq. (5.3). The averaged DNS results and the model response are accompanied by the results obtained by direct integration of the joint $\widetilde{P}(Z,c)$, representing the maximum (theoretical) precision of a PCM-type combustion model.

The evolution of mean reaction rate of the progress variable $\widetilde{\dot{\omega}}_{Y_c}$ with mean normalised progress variable $\overline{c}$ (left) and the temporal evolution of mean normalised progress variable $\overline{c}$ (right) are presented in Figures 6.17 and 6.18 for cases a_1 and a_2, respectively. The response of the studied models is compared to the DNS results. The THR approach, assuming a homogeneous mixture and making direct use of the chemistry tabulation, leads to overly inaccurate results in terms of reaction rate in both these cases. Especially in case a_2, the THR model completely fails to predict the cool flame mean reaction rate peak. The THR predictions of the autoignition delay, based on the criterion $t|_{\overline{c}=0.5}$ of the reconstructed $\overline{c}(t)$ (see Eq. (5.3)), are interestingly close to the respective DNS results. However, the progress of combustion during the main ignition is extremely steep, unlike in the DNS results.

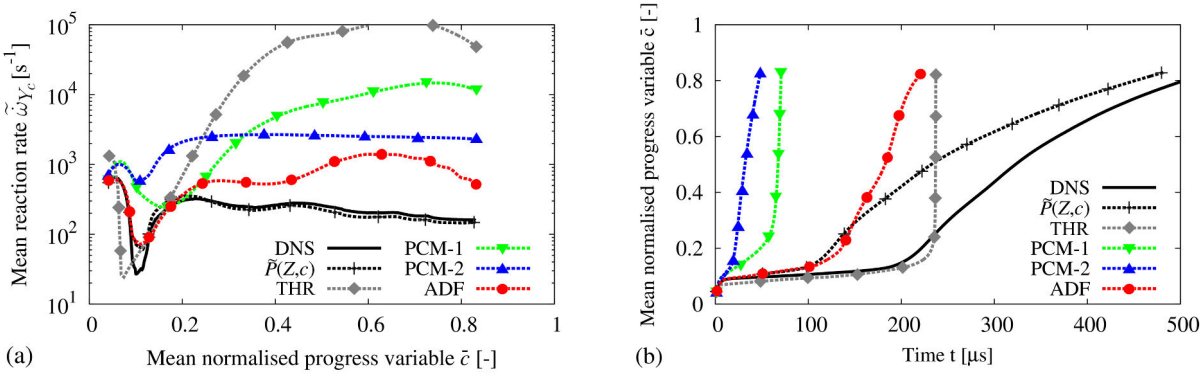

Figure 6.17: Comparison between DNS results (solid lines) and evaluated models (dashed lines) for split injection case a_1. (a) Evolution of mean reaction rate of the progress variable $\widetilde{\dot{\omega}}_{Y_c}$ with mean normalised progress variable $\overline{c}$. (b) Temporal evolution of mean normalised progress variable $\overline{c}$.

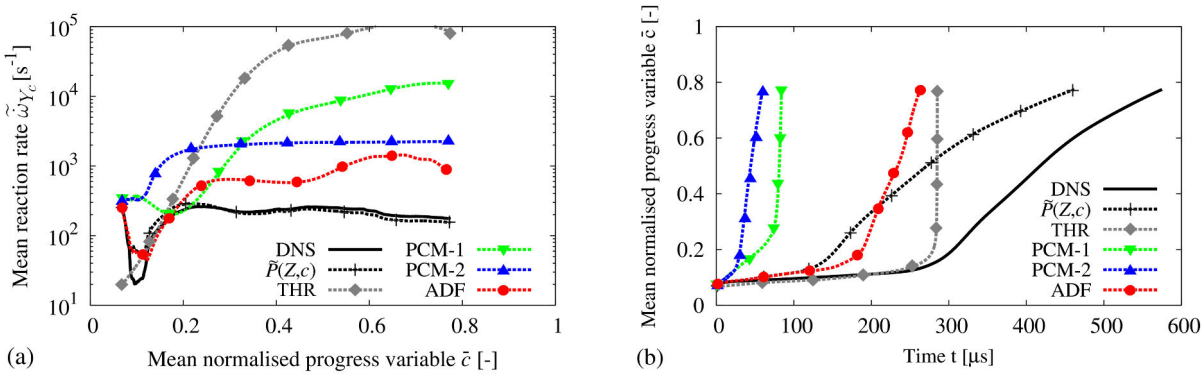

Figure 6.18: Comparison between DNS results (solid lines) and evaluated models (dashed lines) for split injection case a_2. (a) Evolution of mean reaction rate of the progress variable $\widetilde{\omega}_{Y_c}$ with mean normalised progress variable $\bar{c}$. (b) Temporal evolution of mean normalised progress variable $\bar{c}$.

The two versions of the PCM model also give important discrepancies in the prediction of the mean reaction rate of the progress variable $\widetilde{\omega}_{Y_c}$, overestimating it by at least a factor of 10 over the largest part of the test in both cases a_1 and a_2. PCM-1, considering only the mixture fraction heterogeneity through a presumed β distribution, gives larger discrepancies in the prediction of the maximum $\widetilde{\omega}_{Y_c}$ values than PCM-2, taking into account the progress variable heterogeneity independently of the mixture fraction. However, PCM-1 is closer to the DNS than PCM-2 at the beginning of the test, resulting in a slightly better estimation of the autoignition delay. The ADF model gives the best results among the tested models : it predicts with good precision the first peak of mean reaction rate corresponding to cool flame reactions, and generally gives the smallest discrepancies in both cases.

Model predictions in the split injection cases a_3 - a_6 are compared with the averaged DNS results in Figures 6.19 - 6.22, respectively. Moving from lower to higher c_0 values, discrepancies are generally diminishing. A possible explanation for this may be that, as c_0 increases, especially over 0.5, the DNS cases become more reactive and the ignition process evolves increasingly faster, compared to the turbulent mixing, making the latter less important ; the heterogeneous reactors then resemble more and more a conglomerate of homogeneous reactors and are more effectively modelled by the tabulated combustion models with a lower level of complexity.

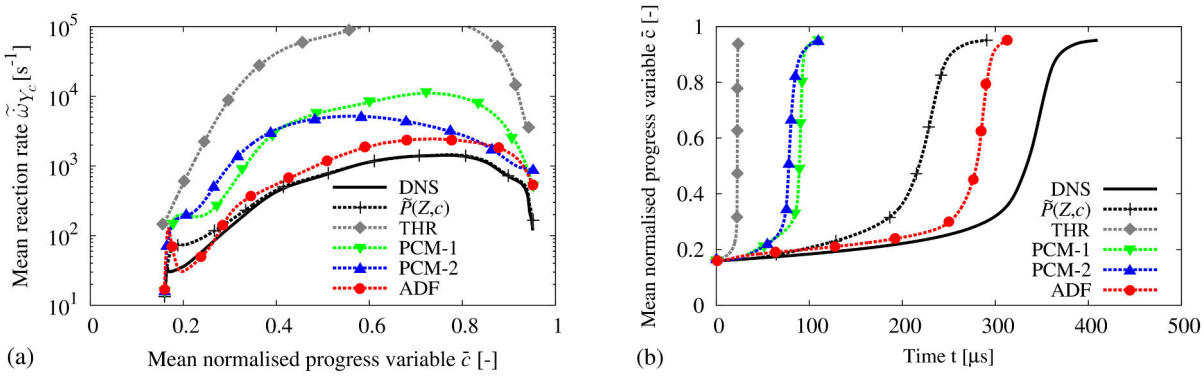

Figure 6.19: Comparison between DNS results (solid lines) and evaluated models (dashed lines) for split injection case a_3. (a) Evolution of mean reaction rate of the progress variable $\widetilde{\omega}_{Y_c}$ with mean normalised progress variable $\bar{c}$. (b) Temporal evolution of mean normalised progress variable $\bar{c}$.

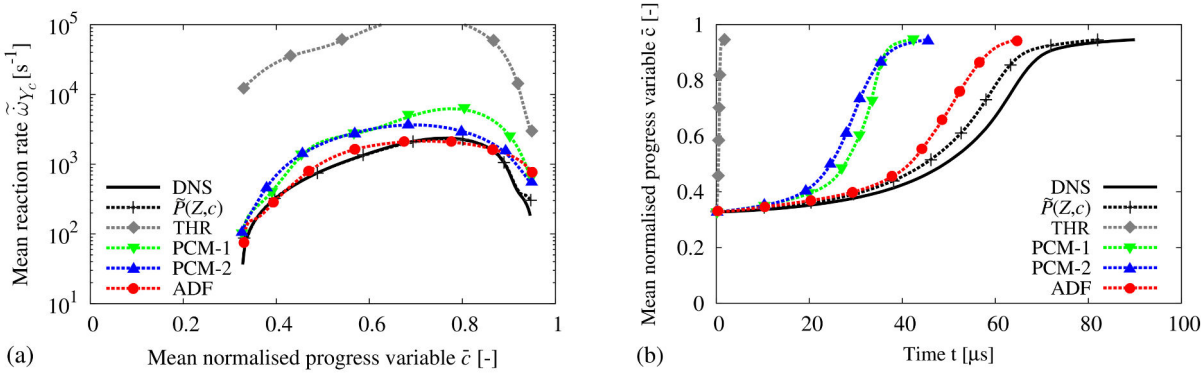

Figure 6.20: Comparison between DNS results (solid lines) and evaluated models (dashed lines) for split injection case a_4. (a) Evolution of mean reaction rate of the progress variable $\widetilde{\omega}_{Y_c}$ with mean normalised progress variable $\bar{c}$. (b) Temporal evolution of mean normalised progress variable $\bar{c}$.

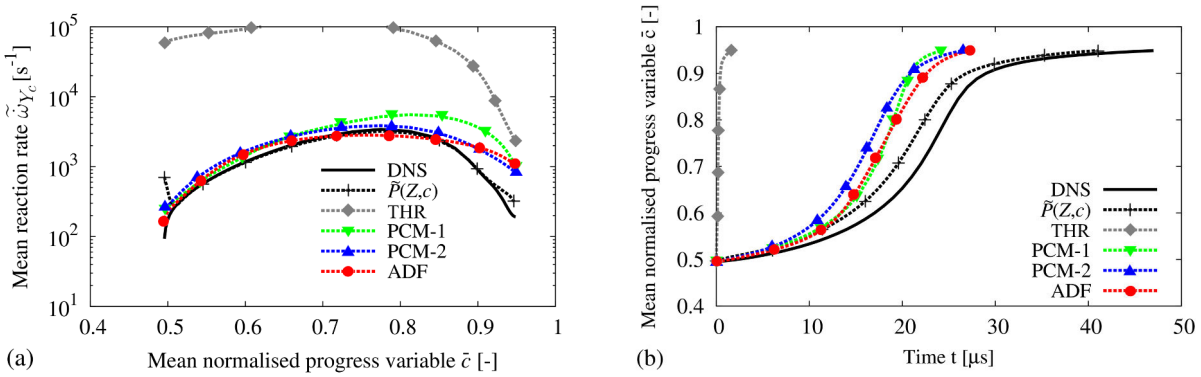

Figure 6.21: Comparison between DNS results (solid lines) and evaluated models (dashed lines) for split injection case a_5. (a) Evolution of mean reaction rate of the progress variable $\widetilde{\dot{\omega}}_{Y_c}$ with mean normalised progress variable $\bar{c}$. (b) Temporal evolution of mean normalised progress variable $\bar{c}$.

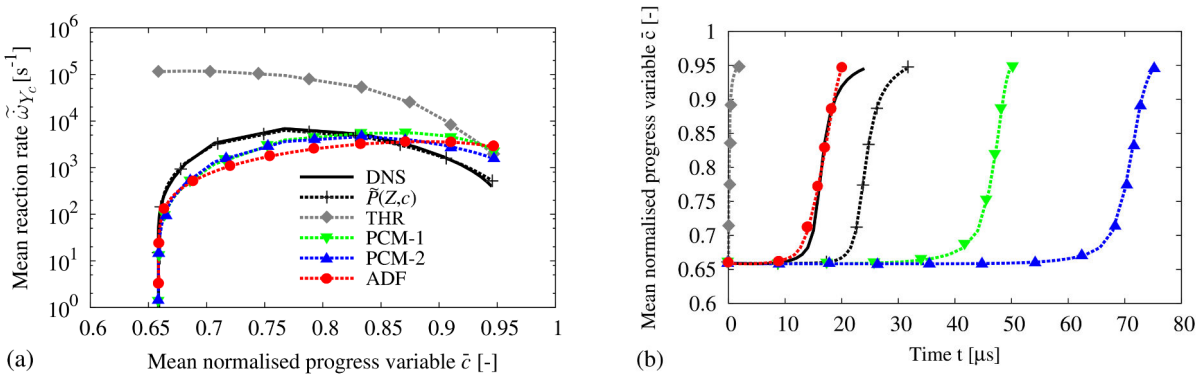

Figure 6.22: Comparison between DNS results (solid lines) and evaluated models (dashed lines) for split injection case a_6. (a) Evolution of mean reaction rate of the progress variable $\widetilde{\dot{\omega}}_{Y_c}$ with mean normalised progress variable $\bar{c}$. (b) Temporal evolution of mean normalised progress variable $\bar{c}$.

The ranking of the models in terms of mean reaction rate prediction accuracy is generally the same, with THR model giving the most inaccurate results, followed by PCM, and ADF model giving the smallest discrepancies among the tested approaches. The THR model systematically overestimates the mean reaction rate by at least an order of magnitude and completely fails to predict its initial level for high c_0 values. PCM and ADF models, however, substantially approximate the averaged DNS results as c_0 increases. The fact that, in some cases (*e.g.* a_3 or a_6), the results of ADF model are closer to the DNS than the direct integration of the $\widetilde{P}(Z,c)$ in terms of reconstructed progress variable evolution can only be understood as a favourable

accumulation of errors. In case a_6, corresponding to hot burnt gases ($c_0 = 1$) of a lean pilot injection mixture ($Z_0 = 0.0175$ or $\phi_0 \simeq 0.27$) mixing with fresh fuel, PCM-type models tend to underestimate the mean reaction rate, as can be seen in Figure 6.22 for the direct integration of the joint $\widetilde{P}(Z, c)$.

6.2.5 Influence of turbulence intensity

Two levels of turbulence intensity are tested, 1.12 m/s for a-cases, and 5.60 m/s for b-cases, respectively. Integral length scale values l_t are chosen of the same order as the indicative value extracted from the preliminary RANS simulation, that is $\simeq$ 1 mm (see Table 6.1). Turbulent Reynolds number Re_t is 630 for all cases.

The studied models are evaluated over the high turbulence intensity cases b_1 - b_4, using the corresponding adapted tabulations. The averaged DNS results and the model response are accompanied by the results obtained by direct integration of the joint $\widetilde{P}(Z, c)$, representing the maximum (theoretical) precision of a PCM-type combustion model. The model predictions of the mean reaction rate of the progress variable $\widetilde{\dot{\omega}}_{Y_c}$ in cases a_1 - a_4 are compared with those in cases b_1 - b_4 in Figures 6.23 - 6.26, respectively.

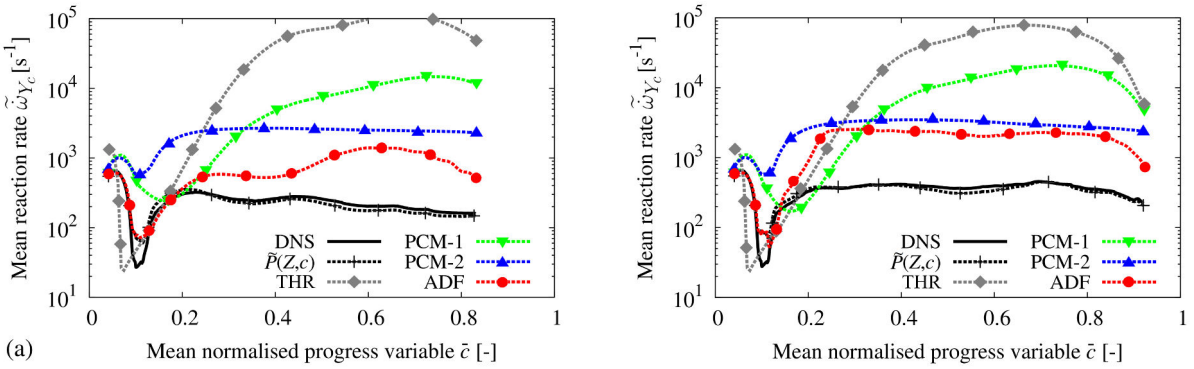

Figure 6.23: Evolution of mean reaction rate of the progress variable $\widetilde{\dot{\omega}}_{Y_c}$ with mean normalised progress variable $\bar{c}$; comparison between DNS results (solid lines) and evaluated models (dashed lines) for cases a_1 (left) and b_1 (right).

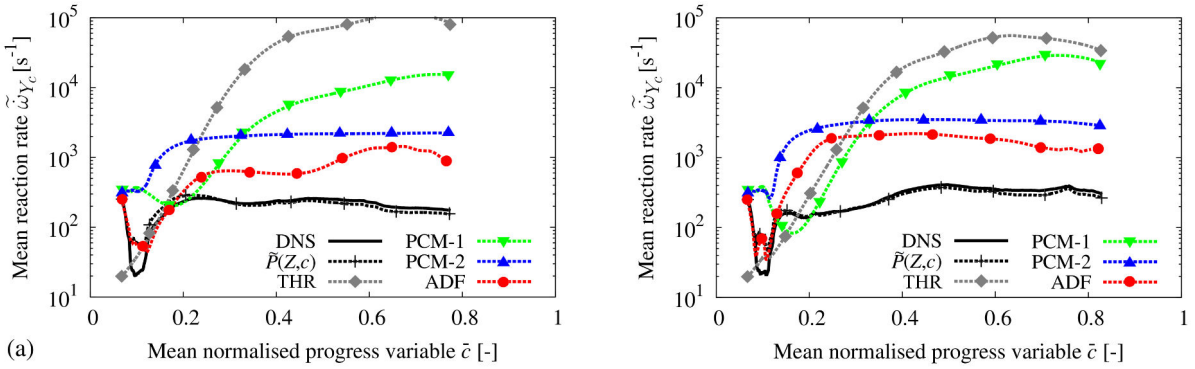

Figure 6.24: Evolution of mean reaction rate of the progress variable $\widetilde{\omega}_{Y_c}$ with mean normalised progress variable $\bar{c}$; comparison between DNS results (solid lines) and evaluated models (dashed lines) for cases a_2 (left) and b_2 (right).

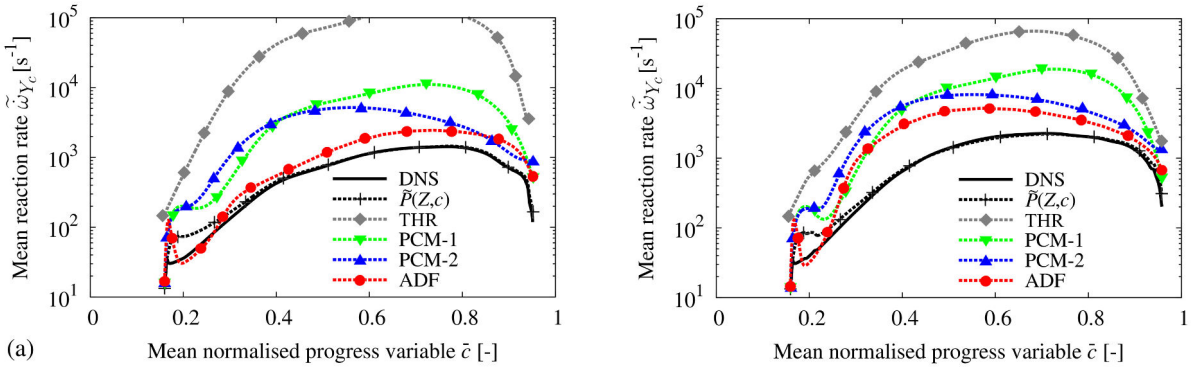

Figure 6.25: Evolution of mean reaction rate of the progress variable $\widetilde{\omega}_{Y_c}$ with mean normalised progress variable $\bar{c}$; comparison between DNS results (solid lines) and evaluated models (dashed lines) for cases a_3 (left) and b_3 (right).

The THR model gives more accurate results in the high than in the low turbulence intensity cases. PCM model response is generally indistinguishable between the two groups. A Damköhler number Da is estimated for every DNS case (see Table 6.1), based on time scale $\tau_t = k/\varepsilon$ and chemical time scale $\tau_c = 1/\widetilde{\dot{\omega}}_{c\,\max}|_{Z=Z_{\rm st}}$ (see Section 5.1). As discussed in Section 6.1, in low Da cases the internal structure of the flame is potentially affected by turbulent mixing, whereas in high Da cases ($Da >> 1$), may be more propitious for flamelet modelling (see Section 3.2). Indeed, ADF model discrepancies are systematically higher in the high turbulence intensity and low Da b-cases than in the low turbulence intensity and higher Da a-cases.

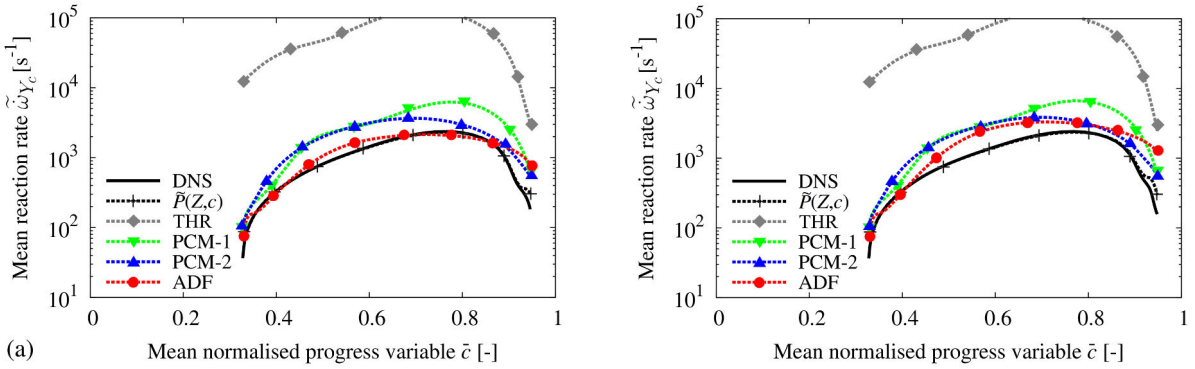

Figure 6.26: Evolution of mean reaction rate of the progress variable $\widetilde{\omega}_{Y_c}$ with mean normalised progress variable $\bar{c}$; comparison between DNS results (solid lines) and evaluated models (dashed lines) for cases a_4 (left) and b_4 (right).

The relative errors of all the studied approaches in the prediction of the mean reaction rate of the progress variable $\widetilde{\omega}_{Y_c}$ (see Eq. (6.3)) are regrouped in Table 6.2 for all the DNS cases. The zero-order model, denoted here as "Arrhenius", corresponds to a direct integration of chemical kinetics into the CFD simulation [92], without considering any interaction of the turbulent mixing with the chemical kinetics below the grid level, a popular and relatively costly approach. As expected, relative errors obtained following this approach are generally smaller than those obtained by THR model, since the latter includes discrepancies that are due to the chemistry tabulation additionally to those associated with the homogeneous reactor hypothesis. PCM-1 model gives results of a comparable accuracy with those obtained with the Arrhenius method at a CPU cost that is expected to be significantly lower in 3D CFD simulations. PCM-2 gives better results than the simpler version of PCM-1. ADF model gives the smallest discrepancies among the tested approaches for all cases. Moving from lower to higher c_0 values, discrepancies of PCM and ADF models are generally diminishing in both low and high turbulence intensity cases.

Case	Arrhenius	THR	PCM-1	PCM-2	ADF	
a_0	3053	15273	3140	1190	156	[%]
a_1	1628	21060	2564	832	216	[%]
a_2	955	23696	2848	800	260	[%]
a_3	6822	8332	601	283	89	[%]
a_4	2991	5253	148	75	22	[%]
a_5	9400	4326	71	30	27	[%]
a_6	479	1728	51	40	40	[%]
b_0	2963	9804	3439	1155	403	[%]
b_1	3465	9243	2465	663	405	[%]
b_2	1503	9074	4341	945	468	[%]
b_3	4267	2316	614	278	115	[%]
b_4	3393	4931	155	78	56	[%]

Table 6.2: Relative errors of the studied approaches in the prediction of the mean reaction rate of the progress variable $\widetilde{\dot{\omega}}_{Y_c}$ for all the DNS cases.

6.3 Conclusions

Self-ignited combustion in turbulent heterogeneous reactors under multi-injection Diesel engine-relevant conditions was examined by means of DNS simulation. The DNS configuration consists of segregated "main injection" fuel parcels randomly distributed within "pilot injection" partially burnt gases subjected to a turbulent field. A 2-D DNS database was generated, varying the progress of the pilot injection c_0 and the velocity fluctuation level u' of the imposed isotropic decaying turbulence, corresponding to different split injection strategies.

The numerical results of all the DNS split injection cases were presented and discussed. The progress of combustion was found to present a multi-mode nature depending on c_0. Mixing partially burnt gases with fresh fuel can potentially give reactors that autoignite slower than equivalent fuel-air mixtures with same richness and total enthalpy. It can also result in mixtures presenting similar ignition delays with the fuel-air mixtures that advance faster once initiated. Finally, it can give very reactive heterogeneous mixtures burning much faster than fuel-air mixtures. An analysis of time and length scales of the DNS cases revealed that some of the studied cases (high c_0, low u', high Da) are more propitious for flamelet modelling than others (low c_0, high u', low Da).

Turbulent combustion models using tabulated chemistry were evaluated on the basis of an *a priori* comparison with the DNS results. Three modelling approaches were tested : the Tabulated Homogeneous Reactor approach, which is a direct exploitation of the chemistry tabulation ignoring any local mixture heterogeneity ; (2) the Presumed Conditional Moment (PCM) model, which includes a separate statistical description for the mixture and the combustion progress ; (3) the Approximated Diffusion Flame (ADF) model, which considers the heterogeneous turbulent reactor as a diffusion flame. Once again, the same skeletal reaction mechanism was used for the DNSs and the chemistry tabulation used by the combustion models ; therefore, the focus was exclusively put on the modelling assumptions.

The direct use of the joint probability density function $\widetilde{P}(Z, c)$ of the DNSs (see Eq. (3.29)), representing the maximum (theoretical) precision of a PCM-type combustion model, combined with different tabulations, permitted to quantify the part of the observed discrepancies between the evaluated combustion models and the DNS results that stems from the tabulated chemistry approach itself. Additionally, it revealed the need to take into account the effects of the progress of the pilot injection c_0 in the chemistry tabulation in order to yield satisfactory model predictions. Adapted split injection tabulations were produced, with an additional dimension c_0. This approach permitted a slight improvement of THR results but significantly ameliorated PCM and ADF model response.

Possible sources of error, other than the chemistry tabulation, were investigated. A comparison of the DNS results with the direct integration of the joint $\widetilde{P}(Z,c)$ and of the independent $\widetilde{P}(Z)$ and $\overline{P}(c)$ indicated that the hypothesis of the independence of Z and c is the main cause of the discrepancies of the PCM model in the split injection cases, similarly to the single injection cases. Furthermore, the part of the observed discrepancies between the PCM and ADF models and the DNS results that is due to the approximation of the Z and c PDFs by standardised β distributions was quantified.

The generated split injection DNS database was exploited so to study the effect of the progress of the pilot injection c_0 on the accuracy of the evaluated models' predictions. The ranking of the models in terms of mean reaction rate prediction accuracy was generally the same, with ADF model giving the smallest discrepancies among the tested approaches, followed by PCM and THR models. ADF thus appeared as the main candidate amongst the evaluated approaches for modern multi-injection Diesel engine RANS simulation. Moving from lower to higher c_0 values, discrepancies were generally diminishing.

The effect of turbulence intensity u' on the accuracy of the evaluated models was investigated by comparison of two groups of low and high u', respectively. THR model gave more accurate results in the high than in the low turbulence intensity cases. PCM model precision was generally indistinguishable between the two groups. ADF model discrepancies, however, were found systematically higher in the high turbulence intensity and low Da b-cases than in the low turbulence intensity and higher Da a-cases, in agreement with the analysis of time and length scales of the DNS results.

Chapter 7

An extended modelling approach for prospective multiple injection simulations

Injection systems such as Common Rail are very flexible and allow the splitting of the fuel injection into several pulses. A typical application of multiple injections in Diesel engines is to use a small pilot injection quantity for noise reduction, a main injection that contains most of the injected mass, and a small post injection quantity for better late stage mixing and soot oxidation. The temporal evolution of injected fuel mass rate $\dot{m}_{inj}$ and local mean mixture fraction $\widetilde{Z}$ of this injection strategy are schematically presented in Figure 7.1 as an example.

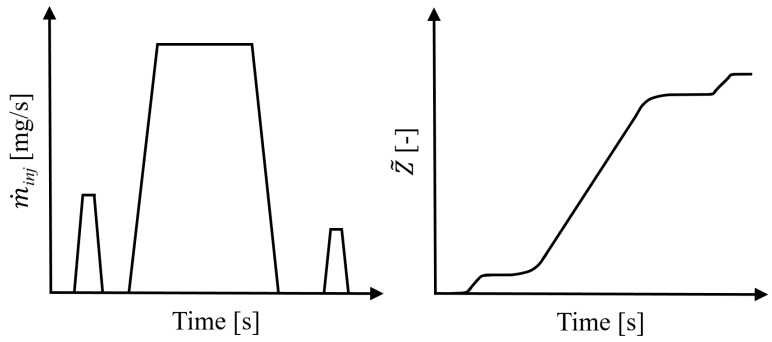

Figure 7.1: Temporal evolution of injected fuel mass rate $\dot{m}_{inj}$ and mean mixture fraction $\widetilde{Z}$.

In order to account for the effect of the interaction between the different fuel injections on the progress of combustion, an extended modelling approach for multiple injection simulations is proposed. The description that follows is done in a generic way, so to cover the implementation of two turbulent combustion models based on tabulated chemistry : (1) the 3-zones Extended Coherent Flame Model (ECFM3Z) [113] (see 3.3.2), representing the mixing state by three mixing zones accounting for pure fuel zone, pure air and possible residual gases, and mixed zone, respectively, and (2) the Approximated Diffusion Flame (ADF) [74] model (3.4.3), considering the heterogeneous turbulent reactor as a diffusion flame. These two approaches

are chosen in continuity with works undertaken over the past few years within IFPEN focusing on the development of turbulent combustion models for rigorous and affordable RANS simulation of internal combustion engines, gas turbines and furnaces. ECFM3Z is a model that is widely used in the context of industrial applications and is likely to be the first to be tested in multi-injection Diesel engine simulations, based on the formulation described hereafter. The ADF model will also be tested, in consistence with the results of the *a priori* model evaluation presented in the previous sections.

7.1 TKI-ECFM3Z

A detailed description of the original ECFM3Z model is available in [113]. In order to take into account the autoignition mechanisms, ECFM3Z is often coupled with the Tabulated Kinetics of Ignition (TKI) approach [114, 115]. An autoignition precursor is traced in the flow, helping to quantify the autoignition delay, and the autoignition chemistry is accounted for using constant pressure homogeneous reactor tabulations. Like the standard version from which it is derived, the TKI-ECFM3Z model for multiple injection applications includes a description of the local mixture stratification by considering three homogeneous sub-regions in every computational cell (see Figure 7.2). The first region contains pure fuel (region F). The evaporation of the spray droplets reaching the computational cell is accounted for using a source of gaseous fuel mass in this region. The second region (region O) contains air or partially burnt gases, depending on the use or not of exhaust gas recirculation (EGR) and on whether the computational cell in question has been reached by a single injection or more.

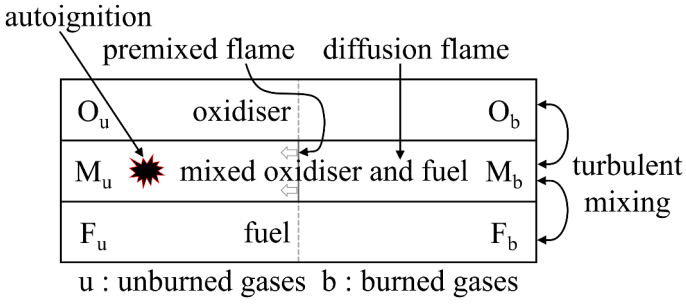

Figure 7.2: Scheme of TKI-ECFM3Z combustion model.

In the latter case, this region represents the reactive environment resulting from the mixing of previous injections with the ambient air. The third region (region M) represents the mixing of the fresh fuel of region F with the oxidiser (air or partially burnt gases) of region O, at a rate that depends on a turbulent mixing time. A mixing model is introduced via transport equations for region F fuel tracer $\widetilde{Y}_{Fu}^{F}$ and region O oxygen tracer $\widetilde{Y}_{O_2}^{O}$:

$$\frac{\partial \overline{\rho}\widetilde{Y}_{Fu}^{F}}{\partial t} + \frac{\partial}{\partial x_i}\left(\overline{\rho}\widetilde{u_i}\widetilde{Y}_{Fu}^{F}\right) = \frac{\partial}{\partial x_i}\left(\overline{\rho}(\mathcal{D}+\mathcal{D}_t)\frac{\partial \widetilde{Y}_{Fu}^{F}}{\partial x_i}\right) + \overline{\rho}\dot{S}_{Fu} + \overline{\rho}\dot{E}_{Fu}^{F\to M} \tag{7.1}$$

$$\frac{\partial \overline{\rho}\widetilde{Y}_{O_2}^{O}}{\partial t} + \frac{\partial}{\partial x_i}\left(\overline{\rho}\widetilde{u_i}\widetilde{Y}_{O_2}^{O}\right) = \frac{\partial}{\partial x_i}\left(\overline{\rho}(\mathcal{D}+\mathcal{D}_t)\frac{\partial \widetilde{Y}_{O_2}^{O}}{\partial x_i}\right) + \overline{\rho}\dot{E}_{O_2}^{O\to M} \tag{7.2}$$

where $\overline{\rho}$ is the mean density, $\widetilde{u_i}$ the Favre averaged mean velocity, $\mathcal{D}$ an averaged diffusion coefficient, $\mathcal{D}_t$ the turbulent diffusivity, $\dot{S}_{Fu}$ the source term of gaseous fuel mass fraction for the evaporation of liquid fuel droplets, and $\dot{E}_{Fu}^{F\to M}$, $\dot{E}_{O_2}^{O\to M}$ are the mixing source terms from regions F to M and O to M, respectively. These mixing source terms are based on a characteristic mixing time τ_m :

$$\dot{E}_{Fu}^{F\to M} = -\frac{1}{\tau_m}\widetilde{Y}_{Fu}^{F}(1-\widetilde{Y}_{Fu}^{M}) \tag{7.3}$$

$$\dot{E}_{O_2}^{O\to M} = -\frac{1}{\tau_m}\widetilde{Y}_{O_2}^{O}(1-\widetilde{Y}_{O_2}^{M}) \tag{7.4}$$

where $\widetilde{Y}_{Fu}^{M}$ and $\widetilde{Y}_{O_2}^{M}$ are respectively the fuel and oxygen mass fractions in region M. In the standard version of the ECFM3Z this mixing time scale τ_m is proportional to the turbulent time scale given by the $k-\varepsilon$ turbulence model [143] :

$$\tau_m^{-1} = \beta_m \frac{\varepsilon}{k} \tag{7.5}$$

where k is the turbulent kinetic energy, ε its dissipation rate and β_m is a constant set to 1 [113].

To account for combustion chemistry in a detailed manner, the studied modeling approach uses a tabulation containing values of mean progress variable reaction rate and mean mass fractions of certain species as functions of quantities available in the CFD simulation. Previous works have proposed the extension of the TKI-ECFM3Z model to variable volume [85] and variable pressure [42] environments for internal combustion engine simulations, using adapted chemistry tabulation techniques. In this work, the extension of the model to multiple injection applications is presented, omitting such effects, focusing on the additional look-up table di-

mensions needed to take into account the interaction of the different injections. Two quantities are chosen to represent the effect of multiple injections in the chemistry tabulation : a mixture fraction Z_0 and a normalised progress variable c_0, characterising the partially burnt gases of previous injections interacting with fresh fuel. Thus, the final tabulation input parameters are pressure p_0 and initial temperature T_0, characterising the thermodynamic conditions, mixture fraction Z and partially burnt gases mixture fraction Z_0, characterising the mixing, progress variable c and partially burnt gases normalised progress variable c_0, characterising the reaction progress.

Markers are used in the CFD code to differentiate every injection event n from the $n-1$ injections preceding it. An averaged conservation equation is solved in every computational cell for the mean mixture fraction $\widetilde{Z}_n$ of every injection n :

$$\frac{\partial \overline{\rho}\widetilde{Z}_n}{\partial t} + \frac{\partial}{\partial x_i}\left(\overline{\rho}\widetilde{u_i}\widetilde{Z}_n\right) = \frac{\partial}{\partial x_i}\left(\overline{\rho}(\mathcal{D}+\mathcal{D}_t)\frac{\partial \widetilde{Z}_n}{\partial x_i}\right) + \overline{\rho}\dot{S}_{\widetilde{Z}_n} \tag{7.6}$$

The source terms $\dot{S}_{\widetilde{Z}_n}$, corresponding to the evaporation of the spray droplets of the respective injections, are estimated using the expressions proposed by Demoulin and Borghi [144]. Global mean mixture fraction $\widetilde{Z}$ is calculated as the sum of the separate injections' mixture fractions $\widetilde{Z}_n$:

$$\widetilde{Z} = \sum_{n=1}^{N} \widetilde{Z}_n \tag{7.7}$$

where N corresponds to the last injection having reached the computational cell ($Z_N \neq 0$). The partially burnt gases mixture fraction Z_0 is then evaluated as the sum of the mixture fractions of the previous $N-1$ injections.

$$Z_0 = \sum_{n=1}^{N-1} \widetilde{Z}_n \tag{7.8}$$

Global mean normalised progress variable $\overline{c}$ is modelled as following :

$$\overline{c} = 1 - \frac{\widetilde{Y}_{Fb}}{\widetilde{Z}} \tag{7.9}$$

where $\widetilde{Y}_{Fb}$ is the mean burnt fuel mass fraction. $\widetilde{Y}_{Fb}$ is calculated as the sum of the separate injections' burnt fuel mass fractions $\widetilde{Y}^n_{Fb}$:

$$\widetilde{Y}_{Fb} = \sum_{n=1}^{N} \widetilde{Y}_{Fb}^{n} \tag{7.10}$$

obtained by resolution of transport equations for $\widetilde{Y}_{Fb}^{n}$ of every injection n :

$$\frac{\partial \overline{\rho} \widetilde{Y}_{Fb}^{n}}{\partial t} + \frac{\partial}{\partial x_i}\left(\overline{\rho}\widetilde{u_i}\widetilde{Y}_{Fb}^{n}\right) = \frac{\partial}{\partial x_i}\left(\overline{\rho}(\mathcal{D}+\mathcal{D}_t)\frac{\partial \widetilde{Y}_{Fb}^{n}}{\partial x_i}\right) \tag{7.11}$$

The partially burnt gases normalised progress variable c_0 is then modelled as follows :

$$c_0 = 1 - \frac{Y_{Fb}^{0}}{Z_0} \tag{7.12}$$

where Y_{Fb}^{0} is the burnt fuel mass fraction of the partially burnt gases, evaluated as the sum of the progress variables of the previous $N-1$ injections.

$$Y_{Fb}^{0} = \sum_{n=1}^{N-1} \widetilde{Y}_{Fb}^{n} \tag{7.13}$$

The tabulation input parameters, that is pressure p_0, initial temperature T_0, mean mixture fraction $\widetilde{Z}$, partially burnt gases mixture fraction Z_0, mean normalised progress variable $\overline{c}$ and partially burnt gases normalised progress variable c_0, are hence gathered. The corresponding tabulated values (*e.g.* $\dot{\omega}_{Y_c}^{\text{TAB}}(p_0, T_0, \widetilde{Z}, Z_0, \overline{c}, c_0)$) are extracted from the look-up tables for every computational cell and used in the CFD simulation at every time-step.

7.2 ADF

In the ECFM3Z model, the local mixture heterogeneity is represented using three descrete zones, with no description of the flamelet structure. As a consequence, this representation does not allow to account for the effect of strain on the ignition delay, heat release, and species [69]. As presented in Subsection 3.4.3, the ADF [74] model is able to account for the diffusion flame structure while maintaining CPU times compatible with industrial requirements. Originally developed for constant pressure and adiabatic configurations, the model was extended by Michel *et. al.* [145] to a variable pressure environment for internal combustion engine simulations.

The ADF model for multiple injection applications is presented here omitting any variable pressure effects, focusing on the extension of the model to account for the interaction of dif-

ferent injections. For this purpose, two quantities, are introduced : a mixture fraction Z_0 and a normalised progress variable c_0, characterising the partially burnt gases of previous injections interacting with fresh fuel. Therefore, the chemistry tabulation used for the calculation of the approximated flamelets includes these two dimensions, additionally to the original input parameters (mixture fraction Z, progress variable Y_c and strain rate a). Hence, the flamelet equation becomes :

$$\frac{\partial Y_c}{\partial t} = \dot{\omega}_{Y_c}^{\text{TAB}}(Z, Z_0, Y_c, c_0) + \chi(Z, a)\frac{\partial^2 Y_c}{\partial Z^2} \tag{7.14}$$

where $\chi(Z, a)$ is the scalar dissipation rate, here modelled as follows :

$$\chi(Z, a) = a\ \mathcal{F}(Z) \tag{7.15}$$

where $\mathcal{F}(Z)$ is a function derived from the classical expression [69] adapted for counterflow diffusion flames where the fuel stream is at Z_{max}, not necessarily equal to unity, and the oxidiser stream is at Z_{min}, not necessarily equal to zero :

$$\mathcal{F}(Z) = \frac{(Z_{\text{max}} - Z_{\text{min}})^2}{2\pi}\text{exp}(-2[\text{erfc}^{-1}\left(2\,\frac{Z - Z_{\text{min}}}{Z_{\text{max}} - Z_{\text{min}}}\right)]^2) \tag{7.16}$$

Eq. (7.14) is resolved for various partially burnt gases mixture fractions Z_0, initial progress variables c_0 and strain rates a, using detailed chemistry in a tabulated form. A methodology for the definition of the initial state and boundary conditions of such a flamelet corresponding to non-zero values of Z_0 and c_0 and a given strain rate value is presented here. Flamelets with zero Z_0 and c_0 (diffusion flames between pure air and fuel streams) are covered in the standard version of the ADF model. For given values of Z_0 and c_0, a partially burnt gases composition is calculated in a homogeneous reactor with $Z = Z_0$, initially at $c = 0$, burning up to c_0, using the same kinetics mechanism used in the chemistry tabulation. This composition, whose species mass fractions are here denoted Y_k^0, is imposed initially on the partially burnt gases side of the flamelet. The initial fresh fuel side is computed according to the adiabatic mixing of these partially burnt gases with gaseous fresh fuel. Fuel mass fraction on the fuel side is equal to Z_{max}, depending on Z_0 and the saturation value of the mixture fraction under the studied conditions Z_{sat}, calculated as in Eq. (6.1). Mass fractions of the other species included in the kinetics mechanism are calculated as following :

$$Y_k = (1 - Z_{\text{max}})\ Y_k^0 \tag{7.17}$$

The initial composition stratification of the flamelet is considered linearly correlated with mixture fraction, varying from Z_0 to Z_{max}. This linear dependency allows to deduce the initial value of the progress variable $Y_c = Y_{\text{CO}} + Y_{\text{CO}_2}$ at any mixture fraction Z. Hence, Y_c initially varies linearly from Y_c^0 to $(1 - Z_{\text{max}})\ Y_c^0$, depending on Z_0 and c_0. A library of approximated flamelets is built for a range of values of Z_0, c_0 and a. This library gives access to the evolution of the equivalent progress variable $Y_c(Z, Z_0, c_0, a, t)$, allowing the estimation of the tabulated species mass fractions $Y_k(Z, Z_0, c_0, a, t) = Y_k^{\text{TAB}}(Z, Y_c(Z, Z_0, c_0, a, t))$.

Like in the original ADF model, once the approximate diffusion flames are calculated, integration is performed at each flamelet over PDFs of the mixture fraction Z. For this purpose, standardised β distributions are used, here defined by the mixture fraction mean $\widetilde{Z}$, variance $\widetilde{Z''^2}$, minimum Z_{min} and maximum Z_{max} values, as in Eq. (3.32). As will be explained later on, Z_{min} and Z_{max} depend on Z_0. Variance $\widetilde{Z''^2}$ is conveniently normalised by Z_{min} and Z_{max} to define unmixedness S_Z, as in Eq. (3.16). Mean mass fractions $\widetilde{Y_k}$ and mean reaction rates of the progress variable $\widetilde{\dot{\omega}}_{Y_c}$ are thus computed, taking into account both chemical and diffusive effects.

$$\widetilde{Y_k}(\widetilde{Z}, Sz, Z_0, c_0, a, t) = \int_{Z_{\text{min}}}^{Z_{\text{max}}} Y_k(Z, Z_0, c_0, a, t)\beta(Z)\,\mathrm{d}Z \tag{7.18}$$

$$\widetilde{\dot{\omega}}_{Y_c}(\widetilde{Z}, Sz, Z_0, c_0, a, t) = \int_{Z_{\text{min}}}^{Z_{\text{max}}} \frac{\partial Y_c}{\partial t}(Z, Z_0, c_0, a, t)\beta(Z)\,\mathrm{d}Z \tag{7.19}$$

These quantities are finally written as functions of $\widetilde{Z}, S_Z, Z_0, \widetilde{Y}_c, c_0$ and a using the bijective relation between time and mean progress variable and stored in a flamelet look-up table. Once the table has been generated, it can be read during the CFD calculation to obtain the tabulated values corresponding to the local values of $\widetilde{Z}, S_Z, Z_0, \widetilde{Y}_c, c_0$ and a. These local values are obtained by transport equations, as described hereafter.

As in the ECFM3Z model for multiple injection applications, markers are used in the CFD code to differentiate every injection event n from the $n-1$ injections preceding it. An averaged conservation equation is solved in every computational cell for the mean mixture fraction $\widetilde{Z}_n$ of every injection n :

$$\frac{\partial \overline{\rho}\widetilde{Z}_n}{\partial t} + \frac{\partial}{\partial x_i}\left(\overline{\rho}\widetilde{u_i}\widetilde{Z}_n\right) = \frac{\partial}{\partial x_i}\left(\overline{\rho}(\mathcal{D} + \mathcal{D}_t)\,\frac{\partial \widetilde{Z}_n}{\partial x_i}\right) + \overline{\rho}\dot{S}_{\widetilde{Z}_n} \tag{7.20}$$

The source terms $\dot{S}_{\widetilde{Z}_n}$, corresponding to the evaporation of the spray droplets of the respective injections, are estimated using the expressions proposed by Demoulin and Borghi [144]. Global mean mixture fraction $\widetilde{Z}$ is calculated as the sum of the separate injections' mixture fractions $\widetilde{Z}_n$:

$$\widetilde{Z} = \sum_{n=1}^{N} \widetilde{Z}_n \tag{7.21}$$

where N corresponds to the last injection having reached the computational cell ($Z_N \neq 0$). The partially burnt gases mixture fraction Z_0 is then evaluated as the sum of the mixture fractions of the previous $N-1$ injections.

$$Z_0 = \sum_{n=1}^{N-1} \widetilde{Z}_n \tag{7.22}$$

Local unmixedness S_Z values, needed to read in the flamelet look-up table, are computed based on the local $\widetilde{Z}$, $\widetilde{Z''^2}$, Z_{min} and Z_{max} (see Eq. (3.16)). The latter extremes depend on Z_0 ; Z_{min} is zero if only one injection has reached the computational cell, and Z_0 if more than one injection has reached the computational cell. Similarly, Z_{max} is either equal to the saturation value of the mixture fraction Z_{sat}, or calculated according to the adiabatic mixing of a fresh fuel gaseous stream with a partially burnt gases stream, as in Eq. (6.1). Variance $\widetilde{Z''^2}$ is obtained by the following conservation equation, considering that the separate injections behave similarly in terms of unmixedness.

$$\frac{\partial \overline{\rho}\widetilde{Z''^2}}{\partial t} + \frac{\partial}{\partial x_i}\left(\overline{\rho}\widetilde{u_i}\widetilde{Z''^2}\right) = \frac{\partial}{\partial x_i}\left(\overline{\rho}(\mathcal{D}+\mathcal{D}_t)\frac{\partial \widetilde{Z''^2}}{\partial x_i}\right) + 2\overline{\rho}\mathcal{D}_t\left(\frac{\partial \widetilde{Z}}{\partial x_i}\frac{\partial \widetilde{Z}}{\partial x_i}\right) - 2\overline{\rho}\widetilde{\chi} + \overline{\rho}\dot{S}_{\widetilde{Z''^2}} \tag{7.23}$$

where $\widetilde{\chi}$ is the mean scalar dissipation rate, classically estimated as :

$$\widetilde{\chi} = C_\chi \frac{\widetilde{Z''^2}}{k/\varepsilon} \tag{7.24}$$

with C_χ a constant chosen equal to 1. The source term $\dot{S}_{\widetilde{Z''^2}}$ of Eq. (7.23) is estimated using the expressions proposed by Demoulin and Borghi [144].

Strain rate a is a parameter with a strong influence on the flamelet structure and ignition [74]. Here, it is estimated according to the following :

$$a = \frac{\widetilde{\chi}}{\int_{Z_{\min}}^{Z_{\max}} \mathcal{F}(Z)\beta(Z)\,\mathrm{d}Z} \tag{7.25}$$

where $\mathcal{F}(Z)$ is the function of Eq. (7.16) derived from the classical expression of [69] for counterflow diffusion flames. The integral of Eq. (7.25) is tabulated and the strain rate can be deduced from $\widetilde{\chi}$.

Global mean normalised progress variable $\overline{c}$ is modelled as following :

$$\widetilde{Y}_c = 1 - \widetilde{Y}_{Fb} \tag{7.26}$$

where $\widetilde{Y}_{Fb}$ is the mean burnt fuel mass fraction. $\widetilde{Y}_{Fb}$ is calculated as the sum of the separate injections' burnt fuel mass fractions $\widetilde{Y}_{Fb}^n$:

$$\widetilde{Y}_{Fb} = \sum_{n=1}^{N} \widetilde{Y}_{Fb}^n \tag{7.27}$$

obtained by resolution of transport equations for $\widetilde{Y}_{Fb}^n$ of every injection n :

$$\frac{\partial \overline{\rho}\widetilde{Y}_{Fb}^n}{\partial t} + \frac{\partial}{\partial x_i}\left(\overline{\rho}\widetilde{u_i}\widetilde{Y}_{Fb}^n\right) = \frac{\partial}{\partial x_i}\left(\overline{\rho}(\mathcal{D}+\mathcal{D}_t)\,\frac{\partial \widetilde{Y}_{Fb}^n}{\partial x_i}\right) \tag{7.28}$$

The partially burnt gases normalised progress variable c_0 is then modelled as follows :

$$c_0 = 1 - \frac{Y_{Fb}^0}{Z_0} \tag{7.29}$$

where Y_{Fb}^0 is the burnt fuel mass fraction of the partially burnt gases, evaluated as the sum of the progress variables of the previous $N-1$ injections.

$$Y_{Fb}^0 = \sum_{n=1}^{N-1} \widetilde{Y}_{Fb}^n \tag{7.30}$$

The flamelet tabulation input parameters, that is mean mixture fraction $\widetilde{Z}$, unmixedness S_Z, partially burnt gases mixture fraction Z_0, mean progress variable $\widetilde{Y}_c$, partially burnt gases normalised progress variable c_0 and strain rate a, are hence gathered. The corresponding tabulated values (*e.g.* $\widetilde{\dot{\omega}}_{Y_c}(\widetilde{Z}, Sz, Z_0, \widetilde{Y}_c, c_0, a)$) are extracted from the flamelet look-up table for every computational cell and used in the CFD simulation at every time-step.

This novel modelling approach can now be implemented in a CFD code and used for the simulation of multiple injection Diesel cycles. It is expected to lead to more precise autoignition delay predictions and better estimations of heat release rate, compared to the turbulent combustion models currently used, resulting in an ameliorated cylinder pressure evolution that is closer to experimental data.

7.3 Conclusions

A novel modelling approach, adapted to the needs of modern multi-injection Diesel engine simulations, was presented. Its description was done in a generic way, so to cover the implementation of two turbulent combustion models based on tabulated chemistry : (1) the 3-zones Extended Coherent Flame Model (ECFM3Z) [113] and (2) the Approximated Diffusion Flame (ADF) [74] model. The focus was put in representing the effect of multiple injections in the chemistry tabulation. For this purpose, the addition of two dimensions, a mixture fraction Z_0 and a normalised progress variable c_0 was proposed, to account for the partially burnt gases of previous injections interacting with fresh fuel. A methodology to retrieve these two extra parameters in the CFD code was proposed for both turbulent combustion models.

Chapter 8

Conclusions and perspectives

In the framework of this Ph.D. thesis, self-ignited combustion of turbulent heterogeneous mixtures under multi-injection Diesel engine-relevant conditions was studied through DNS coupled with semi-detailed chemistry. Preliminary RANS simulations were conducted to obtain an estimation of the conditions inside the combustion chamber of an automotive Diesel engine. Turbulence characteristics, thermodynamic conditions, composition and temperature stratification were chosen following an extended physical analysis. A DNS configuration was established, consisting of a 2-D domain containing pockets of fuel randomly distributed within warm air or partially burnt gases, depending on the case. The medium is subjected to a turbulence field. The mixture autoignites after a certain period of time, depending on the combustion chemistry, the initial composition and temperature stratification and the mixing flow. The fuel segregation is limited to a small part in the center of the domain, so that the burnt gases expansion is negligible compared to the total volume of the domain, therefore allowing combustion under quasi-constant pressure.

A 2-D DNS database was generated and analysed, covering a range of single and split Diesel injection-relevant conditions. A parametric assessment was performed varying the progress of the pilot injection combustion c_0 and the velocity fluctuation level u' of the turbulence spectrum. The progress of combustion was found to present a multi-mode nature depending on c_0. Mixing partially burnt gases with fresh fuel potentially gives reactors that autoignite slower than equivalent fuel-air mixtures with same richness and total enthalpy. It can also result in mixtures presenting similar ignition delays with fuel-air mixtures that advance faster once initiated. Finally, it can give very reactive heterogeneous mixtures that burn almost instantly. An analysis of time and length scales of the DNS cases revealed that some of the studied cases (high c_0, low u', high Da) are more propitious for flamelet modelling than others (low c_0, high u', low Da).

Three different modelling approaches were tested *a priori* against the DNS data: (1) the Tabulated Homogeneous Reactor (THR), which is a direct exploitation of the chemistry tabulation ignoring any local mixture heterogeneity ; (2) the Presumed Conditional Moment (PCM)

model, which includes a separate statistical description for the mixture and the combustion progress ; (3) the Approximated Diffusion Flame (ADF) model, which considers the heterogeneous turbulent reactor as a diffusion flame. These modelling approaches are evaluated on the basis of an *a priori* comparison with the DNS database results. Since the same chemical kinetics mechanism is used for the generation of the chemistry tabulation, the study is entirely focused on the evaluation of different modelling assumptions.

Key observations are summarised as follows :

- The ranking of the models in terms of mean reaction rate prediction accuracy was generally the same, with ADF model giving the smallest discrepancies among the tested approaches, followed by PCM and THR models. Thus, ADF appeared as the main candidate amongst the evaluated approaches for modern multi-injection Diesel engine RANS simulation.
- Moving from lower to higher c_0 values, discrepancies were generally diminishing.
- The THR model gave more accurate results in the high than in the low turbulence intensity cases.
- The PCM model precision was generally indistinguishable between the low and high turbulence intensity u' cases.
- The assumption of statistical independence of mixture fraction Z and normalised progress variable c was found to be the main responsible for the discrepancies between averaged DNS and PCM results.
- The approximation of Z and/or c distributions by standardised β distributions can be imprecise, especially when kinetics include some stagnation of c (*e.g.* cool flame) or Z_0 (*e.g.* pilot injection), leading to significant additional errors in the PCM and ADF models.
- ADF model discrepancies, were found systematically higher in the high u' and low Da cases than in the low u' and higher Da cases, in agreement with the analysis of time and length scales of the DNS results.
- Taking into account the effects of multiple injections (c_0 and possibly Z_0) in the chemistry tabulation has proved to be an effective way of improving predictions of all the tested combustion models.

A novel modelling approach, adapted to the needs of modern multi-injection Diesel engine simulations, was finally proposed. Its description was done in a generic way, so to cover the implementation of two turbulent combustion models based on tabulated chemistry : (1) the 3-zones Extended Coherent Flame Model (ECFM3Z) [113] and (2) the Approximated Diffusion Flame (ADF) [74] model. The focus was put in representing the effect of multiple injections in the chemistry tabulation. For this purpose, the addition of two dimensions, a mixture fraction Z_0 and a normalised progress variable c_0 was presented, to account for the partially burnt gases of previous injections interacting with fresh fuel. A methodology to retrieve these two extra parameters in the CFD code was proposed for both turbulent combustion models.

This modelling approach, that can now be implemented in an industrial CFD code, is expected to lead to more precise autoignition delay predictions and better estimations of heat release rate, compared to the turbulent combustion models currently used, resulting to an ameliorated cylinder pressure evolution that is closer to experimental data. The main limitation in the application of the new approach for multi-injection Diesel engine simulation is expected to be the final table size, strongly impacting the precision of the simulation results. To overcome this problem, future work could be devoted to the use of neural networks or to the adaptation of the reduction techniques, as proposed in [86].

Bibliography

[1] J.B. Heywood. *Internal combustion engine fundamentals*. McGraw-Hill, 1988.

[2] S. Pischinger. Internal Combustion Engines. *VKA lecture notes, RWTH Aachen University*, 2013.

[3] How diesel engines work! (animation). Posted on YouTube by "Thomas Schwenke", `https://www.youtube.com/watch?v=s2WGFELXPNg`.

[4] Y. Shinohara, K. Takeuchi, O.E. Herrmann, and H.J. Laumen. 3000 bar common rail system. *MTZ worldwide eMagazine*, 72(1):489, 2011.

[5] L. Russier. *Lecture notes : Diesel combustion*. IFP Training (IFP School).

[6] C.Y. Choi and R.D. Reitz. An experimental study on the effects of oxygenated fuel blends and multiple injection strategies on DI Diesel engine emissions. *Fuel*, 78:1303–1317, 1999.

[7] Y. Yamaki, K. Mori, H. Kamikubo, S. Kohketsu, K. Mori, and T. Kato. Application of common rail fuel injection system to a heavy duty Diesel engine. *SAE Paper, 942294*, 1994.

[8] Y. Mingfa, W. Hu, Z. Zunqing, and Y. Yan. Experimental study of multiple injections and coupling effects of multi-injection and EGR in a HD Diesel engine. *SAE Paper, 2009-01-2807*, 2009.

[9] M. Badami, F. Mallamo, and F. Millo. Influence of multiple injection strategies on emissions, combustion noise and BSFC of a DI common rail Diesel engine. *SAE Paper, 2002-01-0503*, 2002.

[10] B. Mahr. Future and potential of Diesel injection systems. *Thermo-and Fluid Dynamic processes in Diesel Engines 2*, pages 3–17, 2004.

[11] Y. Liu and R.D. Reitz. Optimizing HSDI Diesel combustion and emissions using multiple injection strategies. *SAE Paper, 2005-01-0212*, 2005.

[12] Common rail Diesel. Posted on YouTube by "PF Jones", https://www.youtube.com/watch?v=K_c_iXBWYXg.

[13] G. Bruneaux and D. Maligne. Study of the mixing and combustion processes of consecutive short double Diesel injections. *SAE Paper, 2009-01-1352*, 2009.

[14] Z. Han, A. Uludogan, G.J. Hampson, and R.D. Reitz. Mechanism of soot and NOx emission reduction using multiple-injection in a Diesel engine. *SAE Paper, 960633*, 1996.

[15] T.C. Tow, A. Pierpont, and R.D. Reitz. Reducing particulate and NOx emissions by using multiple injections in a heavy duty DI Diesel engine. *SAE Paper, 940897*, 1994.

[16] D.A. Nehmer and R.D. Reitz. Measurement of the effect of injection rate and split injections on Diesel engine soot and NOx emissions. *SAE Paper, 940668*, 1994.

[17] N. Ishikawa, T. Uekusa, and T. Nakada. DI Diesel emission control by optimized fuel injection. *SAE Paper, 2004-01-0117*, 2004.

[18] C. Beatrice, P. Belardini, C. Bertoli, and N. Del Giocomo. Downsizing of common rail DI engines: influence of different injection strategies on combustion evolution. *SAE Paper, 2003-01-1784*, 2003.

[19] N. Dronniou, M. Lejeune, and I. Balloul. Combination of high EGR rates and multiple injection strategies to reduce pollutant emissions. *SAE Paper, 2005-01-3726*, 2005.

[20] M. Ikemoto, K. Omae, and K. Nishida. In-cylinder experimental analysis using piezo-driven Diesel injector equipped with needle-lift sensor. *JSAE Trans*, 41(6):1347–1352, 2010.

[21] J. Desantes, J. Arrègle, J. López, and A. García. A comprehensive study of Diesel combustion and emissions with post-injection. *SAE Paper, 2007-01-0915*, 2007.

[22] J. O'Connor and M. Musculus. In-cylinder mechanisms of soot reduction by close-coupled post-injections as revealed by imaging of soot luminosity and planar laser-induced soot incadescence in a Heavy-Duty Diesel engine. *SAE Int. J. Engines, 2014-01-1255*, 2014.

[23] N. Horibe, T. Komizo, T. Sumimoto, H. Wang, and T. Ishiyama. Smoke reduction effects by post injection for various injection parameters and combustion chamber shapes in a Diesel engine. *SAE Paper, 2014-01-2634*, 2014.

[24] N. Bordet, C. Caillol, and P. Higelin. A physical 0d combustion model using tabulated chemistry with presumed probability density function approach for multi-injection Diesel engines. *SAE Paper, 2010-01-1493*, 2010.

[25] T. Poinsot and D. Veynante. *Theoretical and Numerical Combustion, second edition*. Edwards, 2005.

[26] J.M. McDonough. *Introductory lectures on turbulence*. Departments of mechanical engineering and mathematics, University of Kentuky, 2007.

[27] D. Thévenin, O. Gicquel, J. de Charentenay, R. Hilbert, and D. Veynante. Two- versus three-dimensional direct simulations of turbulent methane flame kernels using realistic chemistry. *Proceedings of the Combustion Institute*, 29:2031–2039, 2002.

[28] H.K. Versteeg and W. Malalasekara. *An introduction to Computational Fluid Dynamics - the finite volume method*. Pearson Education, 2007.

[29] S. Chevillard, J.-B. Michel, C. Pera, and J. Reveillon. Evaluation of different turbulent combustion models based on tabulated chemistry using DNS of heterogeneous mixtures. *Combustion Theory and Modeling*, 21(3):440–465, 2017.

[30] J.-B. Michel and O. Colin. A tabulated diffusion flame model applied to Diesel engine simulations. *International journal of engine reseach*, 15(3):346–369, 2013.

[31] S. Chevillard. IFPEN internal report. 2015.

[32] R. Hessel, R.D. Reitz, M. Musculus, and J. O'Connor. A CFD study of post injection influences on soot formation and oxidation under Diesel-like operating conditions. *SAE Int. J. Engines*, 7(2):694–713, 2014.

[33] Y. Ra, P. Loeper, M. Andrie, R. Krieger, D. Foster, and R.D. Reitz. Gasoline DICI engine operation in the ltc regime using triple-pulse injection. *SAE Paper, 2012-01-1131*, 2012.

[34] R. Mobasheri and Z. Peng. Investigation of pilot and multiple injection parameters on mixture formation and combustion characteristics in a heavy duty DI Diesel engine. *SAE Paper, 2012-01-0142*, 2012.

[35] S.S. Pandurangi, N. Frapolli, M. Bolla, and K. Boulouchos. Influence of EGR on post-injection effectiveness in a heavy duty Diesel engine fuelled with n-heptane. *SAE Paper, 2014-01-2633*, 2014.

[36] L. Vervisch, R. Hauguel, P. Domingo, and M. Rullaud. Three facets of turbulent combustion modelling: DNS of premixed V-flame, LES of lifted nonpremixed flame and RANS of jet-flame. *Journal of Turbulence*, 5:1–36, 2004.

[37] B. Fiorina, R. Vicquelin, P. Auzillon, N. Darabiha, O. Gicquel, and D. Veynante. A filtered tabulated chemistry model for LES of premixed combustion. *Combustion and Flame*, 157(3):465–475, 2010.

[38] J. Galpin, C. Angelberger, A. Naudin, and L. Vervisch. Large-eddy simulation of H2-air auto-ignition using tabulated detailed chemistry. *Journal of Turbulence*, 9, 2008.

[39] J.-B. Michel, O. Colin, and D. Veynante. Comparison of differing formulations of the PCM model by their application to the simulation of an auto-igniting H2/air jet. *Flow Turbulence Combust.*, 83:33–60, 2009.

[40] J. Tillou, J.-B. Michel, C. Angelberger, and D. Veynante. Assessing les models based on tabulated chemistry for the simulation of Diesel spray combustion. *Combustion and Flame*, 161:525–540, 2014.

[41] L. Martinez, J.-B. Michel, S. Jay, and O. Colin. Evaluation of different tabulation techniques dedicated to the prediction of the combustion and pollutants emissions on a Diesel engine with 3D CFD. *SAE Paper, 2013-01-1093*, 2013.

[42] D. Aubagnac-Karkar, J.-B. Michel, O. Colin, P.E. Vervisch-Kljakic, and N. Darabiha. Sectional soot model coupled to tabulated chemistry for Diesel RANS simulations. *Combustion and Flame*, 162:3081–3099, 2015.

[43] A. Pires da Cruz and T.A. Baritaud. Self-ingnition and combustion modeling of initially nonpremixed turbulent systems. *Combustion and Flame*, pages 65–81, 2001.

[44] S. Chevillard, C. Pera, and J. Reveillon. Direct numerical simulation of turbubulent premixed flame to understand cyclic variability in spark-ignited engines. *Proccedings of the European Combustion Meeting*, pages 413–420, 2011.

[45] E. Mastorakos, T.A. Baritaud, and T.J. Poinsot. Numerical simulations of autoignition in turbulent mixing flows. *Combustion and Flame*, 109:198–223, 1997.

[46] A. Viggiano and V. Magi. A 2-D investigation of n-heptane autoignition by means of direct numerical simulation. *Combustion and Flame*, 137:432–443, 2004.

[47] S. Sreedhara and N. Lakshmisha. Autoignition in a non-premixed medium: DNS studies on the effects of three-dimensional turbulence. *Proceedings of the Combustion Institute*, 29:2051–2059, 2002.

[48] T. Echekki and J.H. Chen. Direct numerical simulation of autoignition in non homogeneous hydrogen-air mixtures. *Combustion and Flame*, 134:169–191, 2003.

[49] S. Mukhopadhyay and K. Abraham. Influence of compositional stratification on autoignition in n-heptane/air mixtures. *Combustion and Flame*, 158:1064–1075, 2012.

[50] S. Mukhopadhyay and K. Abraham. Influence of heat release and turbulence on scalar dissipation rate in autoigniting n-heptane/air mixtures. *Combustion and Flame*, 159:2883–2895, 2012.

[51] G. Bansal, A. Mascarenhas, and J.H. Chen. Direct numerical simulations of autoignition in stratified dimethyl-ether (DME)/air turbulent mixtures. *Combustion and Flame*, 162:688–702, 2015.

[52] M.B. Luong, G.H. Yu, T. Lu, S.H. Chung, and C.S. Yoo. Direct numerical simulations of ignition of a lean n-heptane/air mixture with temperature and composition inhomogeneities relevant to HCCI and SCCI combustion. *Combustion and Flame*, 162:4566–4585, 2015.

[53] A. Krisman, E.R. Hawkes, M. Talei, A. Bhagatwala, and J.H. Chen. Characterisation of two-stage ignition in Diesel engine-relevant thermochemical conditions using direct numerical simulation. *Combustion and Flame*, 172:326–341, 2016.

[54] A. Krisman, E.R. Hawkes, M. Talei, A. Bhagatwala, and J.H. Chen. A direct numerical simulation of cool-flame affected autoignition in Diesel engine-relevant conditions. *Proceedings of the Combustion Institute*, pages 1–9, 2016.

[55] T. Schoenfeld. *The AVBP handbook*. 2008.

[56] F.A. Williams. *Combustion theory, the fundamental theory of chemically reacting systems*. CRC Press, 2018.

[57] J.O. Hirschfelder, C.F. Curtiss, and R.B. Byrd. *Molecular theory of gases and liquids*, volume 26. Wiley New York, 1954.

[58] K.K. Kuo. *Principles of combustion*. Wiley New York, 1986.

[59] O. Colin and M. Rudgyard. Development of high-order Taylor-Galerkin schemes for LES. *Journal of Computational Physics*, 162(2):338–371, 2000.

[60] O. Cabrit and L. Artal. Direct numerical simulation of turbulent multispecies channel flow with wall ablation. *39th AIAA Thermophysics conference*, page 4401, June 2007.

[61] F. Cadieux, J.A. Domaradzki, T. Sayadi, S. Bose, and F. Duchaine. DNS and LES of separated flows at moderate Reynolds numbers. *Center for Turbulence research, NASA Ames/Stanford University, Proceedings of the summer program*, pages 77–89, June 2012.

[62] A. Velghe, J. Bohbot, and S. Jay. A high efficiency parallel architecture dedicated to internal combustion engine simulation coupled with chemical kinetic solver. *6th European Conference on Computational Fluid Dynamics*, 2014.

[63] B. Sportisse. An analysis of operator splitting techniques in the stiff case. *Journal of computational physics*, 161(1):140–168, 2000.

[64] Richard Courant, Kurt Friedrichs, and Hans Lewy. Über die partiellen differenzengleichungen der mathematischen physik. *Mathematische annalen*, 100(1):32–74, 1928.

[65] P.N. Brown, G.D. Byrne, and A.C. Hindmarsh. Vode: A variable-coefficient ode solver. *SIAM journal on scientific and statistical computing*, 10(5):1038–1051, 1989.

[66] A. Patel, S. Kong, and R.D. Reitz. Development and validation of a reduced reaction mechanism for HCCI engine simulations. *SAE Paper, 2004-01-0558*, 2004.

[67] H. Pitsch and N. Peters. A consistent flamelet formulation for non-premixed combustion considering differential diffusion effects. *Combustion and Flame*, 114:26–40, 1998.

[68] B. Fiorina, R. Baron, O. Gicquel, D. Thevenin, S. Carpentier, and N. Darabiha. Modelling non-adiabatic partially premixed flames using flame-prolongation of ildm. *Combustion Theory and Modelling*, 7:449–470, 2003.

[69] N. Peters. *Turbulent Combustion*. Cambridge University Press, 2000.

[70] D. Veynante and L. Vervisch. Turbulent combustion modeling. *Progress in Energy and Combustion Science*, 28:193–266, 2002.

[71] K.N.C. Bray. The chalenge of turbulent combustion. *26th Symposium (Int.) on Combustion, The Combustion Institute, Pittsburgh*, pages 1–26, 1996.

[72] H. Pitsch, Y. Wan, and N. Peters. Numerical investigation of soot formation and oxidation under Diesel engine conditions. *SAE paper, 952357*, 1995.

[73] C. Pierce and P. Moin. Progress-variable approach for large-eddy simulation of non-premixed turbulent combustion. *J. Fluid Mech.*, 504:73–97, 2004.

[74] J.-B. Michel, O. Colin, and D. Veynante. Modeling ignition and chemical structure of partially premixed turbulent flames using tabulated chemistry. *Combustion and Flame*, 152:80–99, 2008.

[75] P. Chassaing. *Turbulence en mécanique des fluides*. CEPADUES Editions, 2000.

[76] U. Maas and S. Pope. Simplifying chemical kinetics : Intrinsic low-dimensional manifolds in composition space. *Combustion and Flame*, 88:239 – 264, 1992.

[77] J. Nafe and U. Maas. Hierarchical generation of ILDMs of higher hydrocarbons. *Combustion and Flame*, 135:17–26, 2003.

[78] O. Gicquel, N. Darabiha, and D. Thevenin. Laminar premixed hydrogen/air counterflow flame simulations using flame prolongation of ildm with differential diffusion. *Proceedings of the Combustion Institute*, 28:2419–2425, 2000.

[79] Guillaume Lecocq, Stéphane Richard, Olivier Colin, and Luc Vervisch. Hybrid presumed pdf and flame surface density approaches for large-eddy simulation of premixed turbulent combustion: Part 1: Formalism and simulation of a quasi-steady burner. *Combustion and Flame*, 158(6):1201–1214, 2011.

[80] J.-B. Michel, O. Colin, C. Angelberger, and D. Veynante. Using the tabulated diffusion flamelet model ADF-PCM to simulate a lifted methane-air jet flame. *Combustion and Flame*, 156:1318–1331, 2009.

[81] J.A. Van Oijen, J. Lammers, and L. de Goey. Modeling of complex premixed burner systems by using flamelet-generated manifolds. *Combustion and Flame*, 127:2124–2134, 2001.

[82] J.A. Van Oijen and L. De Goey. Modelling of premixed counterflow flames using the flamelet-generated manifold method. *Combustion Theory and Modelling*, 6:463–478, 2002.

[83] J.A. Van Oijen and L. De Goey. A numerical study of confined triple flames using a flamelet-generated manifold. *Combustion Theory and Modelling*, 8:141–163, 2004.

[84] A. Vreman, B. Albrecht, J. Van Oijen, L. de Goey, and R. Bastiaans. Premixed and non-premixed generated manifolds in large-eddy simulation of Sandia flame D and F. *Combustion and Flame*, 153:394–416, 2008.

[85] S. Jay and O. Colin. A variable volume approach of tabulated detailed chemistry and its applications to multidimensional engine simulations. *Proceedings of the Combustion Institute*, 33:3065–3072, 2011.

[86] G. Ribert, O. Gicquel N. Darabiha, and D. Veynante. Tabulation of complex chemistry based on self-similar behavior of laminar premixed flames. *Combustion and Flame*, 146:649–664, 2006.

[87] G. Fiorina, O. Gicquel, and D. Veynante. Turbulent flame simulation taking advantage of tabulated chemistry self-similar properties. *Proceedings of the Combustion Institute*, 32:1687–1694, 2009.

[88] H. Wang, J. Warner, A. Oehlschlaeger, R. Bounaceur, J. Biet, P.-A. Glaude, and F. Battin-Leclerc. An experimental and kinetic modeling study of the autoignition of amethylnaphthalene/air and a-methylnaphthalene/n-decane/air mixtures at elevated pressures. *Combustion and Flame*, 157:1976–1988, 2010.

[89] G. Ribert, K. Wang, and L. Vervisch. A multi-zone self-similar chemistry tabulation with application to auto-ignition including cool-flames effects. *Fuel*, 91:87–92, 2012.

[90] S. Pope. Computationally efficient implementation of combustion chemistry using in situ adaptive tabulation. *Combustion Theory and Modelling*, 1:41–63, 1997.

[91] B. Yang and S.B. Pope. Treating chemistry in combustion with detailed mechanisms - in situ adaptive tabulation in principal directions - premixed combustion. *Combustion and Flame*, 112:85–112, 1998.

[92] P.K. Senecal, E. Pomraning, K.J. Richards - Convergent Thinking, LLC, T.E. Briggs, C.Y. Choi, R.M. McDavid, and M.A. Patterson - Caterpillar, Inc. Multi-dimensional modeling of direct-injection Diesel spray liquid length and flame lift-off length using CFD and parallel detailed chemistry. *SAE Paper*, 2003-01-1043, 2003.

[93] S. Singh, R.D. Reitz, and M. Musculus. Comparison of the characteristic time (CTC), representative interactive flamelet (RIF), and direct integration with detailed chemistry combustion models against optical diagnostic data for multi-mode combustion in a heavy-duty DI Diesel engine. *SAE Paper, 2006-01-0055*, 2006.

[94] S. Pope. Pdf methods for turbulent reactive flows. *Progress in Energy and Combustion Science*, 11:119–192, 1985.

[95] D. Haworth. Progress in probability density functions methods for turbulent reacting flows. *Progress in Energy and Combustion Science*, 36:168–259, 2010.

[96] R. Gordona, A. Masria, S. Pope, and G. Goldinc. Transport budgets in turbulent lifted flames of methane autoigniting in a vitiated co-flow. *Combustion and Flame*, 151:495–511, 2007.

[97] Y. Zhang, E. Kung, and D. Haworth. A PDF method for multidimensional modeling of HCCI engine combustion : effects of turbulence/chemistry interactions on ignition timing and emissions. *Proceedings of the Combustion Institute*, 30:2763–2771, 2005.

[98] M. Juddoo, A. Masri, and S. Pope. Turbulent piloted partially-premixed flames with varying levels of o-2/n-2 : stability limits and PDF calculations. *Combustion Theory and Modelling*, 15:773–793, 2011.

[99] A. Klimenko. Multicomponent diffusion of various admixtures in turbulent flow. *Fluid Dynamics*, 25:327–334, 1990.

[100] R. Bilger. Conditional moment closure for turbulent reacting flow. *Physics of Fluids*, 5:437–448, 1993.

[101] G. De Paola, E. Mastorakos, Y. Wright, and K. Boulouchos. Diesel engine simulations with multi-dimensional conditional moment closure. *Combustion Science and Technology*, 180:883–899, 2008.

[102] Y. Lee and K. Huh. Simulation of spray development and turbulent combustion processes in low and high speed Diesel engines by the CMC-ISR model. *Combustion Theory and Modelling*, 16:13–30, 2012.

[103] J. Seo, D. Lee, K. Huh, and J. Chung. Combustion simulation of a Diesel engine in the pHCCI mode with split injections by the spatially integrated CMC model. *Combustion Science and Technology*, 182:1241–1260, 2010.

[104] H. Pitsch, H. Barths, and N. Peters. Three-dimensional modeling of NOx and soot formation in DI-Diesel engines using detailed chemistry based on the interactive flamelet approach. *SAE paper, 962057*, 1996.

[105] N. Peters. Laminar diffusion flamelet models in non-premixed turbulent combustion. *Progress in Energy and Combustion Science*, 10:319–339, 1984.

[106] H. Barths, C. Antoni, and N. Peters. Three-dimensional simulation of pollutant formation in a DI Diesel engine using multiple interactive flamelets. *SAE paper, 982459*, 1998.

[107] H. Barths, H. Pitsch, and N. Peters. Three-dimensional simulation of DI Diesel combustion and pollutant formation using a two-component reference fuel. *Oil and Gas Science and Technology*, 54:233–244, 1999.

[108] H. Barths, C. Hasse, G. Bikas, and N. Peters. Simulation of combustion in direct injection Diesel engines using a Eulerian particle flamelet model. *Proceedings of the Combustion Institute*, 28:1161–1168, 2000.

[109] V. Mittal, D. Cook, and H. Pitsch. An extended multi-regime flamelet model for IC engines. *Combustion and Flame*, 159:2767–2776, 2012.

[110] C. Hasse and N. Peters. A two mixture fraction flamelet model applied to split injections in a DI Diesel engine. *Proceedings of the Combustion Institute*, 30:2755–2762, 2005.

[111] C. Felsch, M. Gauding, C. Hasse, S. Vogel, and N. Peters. An extended flamelet model for multiple injections in DI Diesel engines. *Proc. Combust. Inst.*, 32:2775–2783, 2009.

[112] O. Colin, A. Benkenida, and C. Angelberger. A 3D modeling of mixing, ignition and combustion phenomena in highly stratified gasoline engines. *Oil and Gas Science and Technology*, 58:47–62, 2003.

[113] O. Colin and A. Benkenida. The 3-zones extended coherent flame model (ecfm3z) for computing premixed/diffusion combustion. *Oil and Gas Science and Technology*, 59:593–609, 2004.

[114] A. Pires da Cruz, S. Jay, and O. Colin. Modélisation de la combustion essence. *IFP Technical Report, 57976*, 72(1):489, 2004.

[115] O. Colin, A. Pires da Cruz, and S. Jay. Detailed chemistry based auto-ignition model including low temperature phenomena applied to 3d engine calculations. *30th Symposium (Int.) on Combustion, The Combustion Institute, Pittsburgh*, pages 2649–2656, 2004.

[116] P. Beard, O. Colin, and M. Miche. Improved modelling of DI Diesel engines using subgrid descriptions of spray and combustion. *SAE Paper, 2003-01-0008*, 2003.

[117] M. Ihme, C.M. Cha, and H. Pitsch. Prediction of local extinction and re-ignition effects in non-premixed turbulent combustion using a flamelet/progress variable approach. *Proceedings of the Combustion Institute*, 30:793–800, 2005.

[118] M. Ihme and Y.C. See. Prediction of auto-ignition in a lifted methane/air flame using an unsteady flamelet/progress variable model. *Combustion and Flame*, 157:1850–1562, 2010.

[119] H. Lehtiniemi, F. Mauss, M. Balthasar, and I. Magnusson. Modeling diesel spray ignition using detailed chemistry and with a progress variable approach. *Combustion Science and Technology*, 178:1977–1997, 2006.

[120] L. Vervisch. *Prise en compte d'effets de cinetique chimique dans les flammes de diffusion turbulentes par l'approche fonction desité de probabilité*. PhD thesis, INSA de Rouen, 1991.

[121] J.-B. Michel. *Modélisation de la combustion turbulente d'un mélange hétérogène en vue de l'application à la silulation des modeurs Diesel*. PhD thesis, Ecole Centrale de Paris, 2008.

[122] J. Tillou. *Développement d'une modélisation basée sur la tabulation de schémas cinétiques complexes pour la simulation aux grandes échelles (LES) de l'autoinflammation et de la combustion turbulente non-prémélangée dans les moteurs à piston*. PhD thesis, Ecole Centrale de Paris, 2013.

[123] J. Galpin. *Modélisation LES de la combustion avec une prise en compte des effets de cinétique détaillée et en perspective d'application moteur*. PhD thesis, INSA de Rouen, 2007.

[124] D. Aubagnac-Karkar. *Sectional soot modeling for Diesel RANS simulations*. PhD thesis, Ecole Centrale de Paris, 2014.

[125] P. Domingo, L. Vervisch, and D. Veynante. Large-eddy simulation of a lifted methane jet flame in a vitiated coflow. *Combustion and Flame*, 152:415–432, 2008.

[126] H. Pitsch and P. Trisjono. Can combustion models be developed from DNS data? *19th Australasian Fluid Mechanics Conference*, page 350, December 2014.

[127] L.G. Clark, S. Kook, Q.N. Chan, and E.R. Hawkes. Effects of injection timing and spark timing on flame propagation in an optically accessible spark-ignition direct-injection (SIDI) engine. *19th Australasian Fluid Mechanics Conference*, pages 350–356, December 2014.

[128] J. Bohbot, N.Gillet, and A. Benkenida. IFP-C3D: an unstructured parallel solver for reactive compressible gas flow with spray. *Oil and Gas Science and Technology*, 64:309 – 336, 2009.

[129] J.H. Whitelaw, F.P. Arcoumanis, and J-M Desantes. *Thermo and fluid dynamic processes in Diesel engines*. Springer science and business media, 2013.

[130] T. Passot and A. Pouquet. Numerical simulation of homogeneous flows in the turbulent regime. *J Fluid Mechanics*, pages 181–441, 1987.

[131] D.L. Baulch, C.J. Cobos, R.A. Cox, C. Esser, and P. Frank. Evaluated kinetic data for combustion modelling. *J. Phys. Chem. Ref. Data*, 21:411–429, 1997.

[132] Z.K. Hong, D.F. Davidson, K.Y. Lam, and R.K. Hanson. A shock tube study of the rate constants of HO_2 and CH_3 reactions. *Combustion and Flame*, 159:3007–3013, 2012.

[133] J. Chen, E. Hawkes, R. Sankaran, S. Mason, and H. Im. Direct numerical simulation of ignition front propagation in a constant volume with temperature inhomogeneities I fundamental analysis and diagnostics. *Combustion and Flame*, 145:128–144, 2006.

[134] E. Hawkes, R. Sankaran, P. Pébay, and J. Chen. Direct numerical simulation of ignition front propagation in a constant volume with temperature inhomogeneities II parametric study. *Combustion and Flame*, 145:145–159, 2006.

[135] H. Pitsch and H. Steiner. Scalar mixing and dissipation rate in large-eddy simulations of non-premixed turbulent combustion. *Proceedings of the Combustion Institute*, 28(1):41–49, 2000.

[136] B. Galmiche, F. Halter, and F. Foucher. Effects of high pressure, high temperature and dilution on laminar burning velocities and markstein lengths of iso-octane/air mixtures. *Combustion and Flame*, 159:3286–3299, 2012.

[137] A. Klimenko and R. Bilger. Conditional moment closure for turbulent combustion. *Progress in Energy and Combustion Science*, 25:595–687, 1999.

[138] D. Thevenin and S. Candel. Effect of variable strain on the dynamics of diffusion flame ignition. *Combustion Science and Technology*, 91:73–94, 1993.

[139] S. Sreedhara and N. Lakshmisha. Direct numerical simulation of autoignition in a non-premixed, turbulent medium. *Proceedings of the Combustion Institute*, 28:25–34, 2000.

[140] R. Hilbert, F. Tap, D. Veynante, and D. Thévenin. A new modeling approach for the autoignition of a non-premixed turbulent flame using DNS. *Proceedings of the Combustion Institute*, 29:2079–2085, 2002.

[141] G. Borghesi, E. Mastorakos, and R.S. Cant. Complex chemistry dns of n-heptane spray autoignition at high pressure and intermediate temperature conditions. *Combustion and Flame*, 160:1254–1275, 2013.

[142] A. El Sayed, M. Mortensen, and J.Z. Wen. Assessment of the presumed mapping function approach for the stationary laminar flamelet modelling of reacting double scalar mixing layers. *Combustion Theory and Modelling*, 18(4-5):552–581, 2014.

[143] Z.Y. Han and R.D. Reitz. Turbulence modeling of internal combustion engines using RNG k-epsilon models. *Combustion Science and Technology*, 106:267–295, 1995.

[144] F.X. Demoulin and R. Borghi. Modeling of turbulent spray combustion with application to Diesel like experiment. *Combustion and Flame*, 129:281–293, 2002.

[145] J.-B. Michel, L. Martinez, and V. Knop. Advances in tabulation techniques for detailed prediction of Diesel engine emissions with 3D CFD. *SIA Diesel conference*, 2012.

Appendix I : Averaged DNS results

A total of 12 2-D DNSs were carried out for the purposes of this study. Their physical parameters summarised in Table 1.

Case	c_0	T^{init}	$\widetilde{S_Z}$	u'	l_t	η_k	τ_{AI}	τ_t	τ_c	Da
a_0	0.00	700 - 900	0.33	1.12	1.4	10	287	1052	1.7	621
a_1	0.05	701 - 942	0.39	1.12	1.4	10	323	947	1.7	549
a_2	0.10	702 - 967	0.41	1.12	1.6	11	418	1129	1.7	648
a_3	0.25	705 - 1034	0.44	1.12	1.8	13	333	1310	1.8	738
a_4	0.50	715 - 1158	0.51	1.12	2.2	15	49	1546	1.8	855
a_5	0.75	790 - 1350	0.53	1.12	2.7	19	-	1875	1.7	1102
a_6	1.00	818 - 1537	0.54	1.12	3.4	24	-	2419	1.5	1562
b_0	0.00	700 - 900	0.33	5.60	0.3	2	311	42	1.7	25
b_1	0.05	701 - 942	0.39	5.60	0.3	2	292	46	1.7	27
b_2	0.10	702 - 967	0.41	5.60	0.3	2	459	47	1.7	27
b_3	0.25	705 - 1034	0.44	5.60	0.4	3	335	52	1.8	30
b_4	0.50	715 - 1158	0.51	5.60	0.4	3	49	62	1.8	34
	[-]	[K]	[-]	[m/s]	[mm]	[µm]	[µs]	[µs]	[µs]	[-]

Table 1: Physical parameters of the different cases.

The evolutions of mean normalised progress variable $\overline{c}$, mean reaction rate of the progress variable $\widetilde{\dot{\omega}}_{Y_c}$ and average strain rate a of all DNS cases are regrouped here to provide an overview of the DNS database.

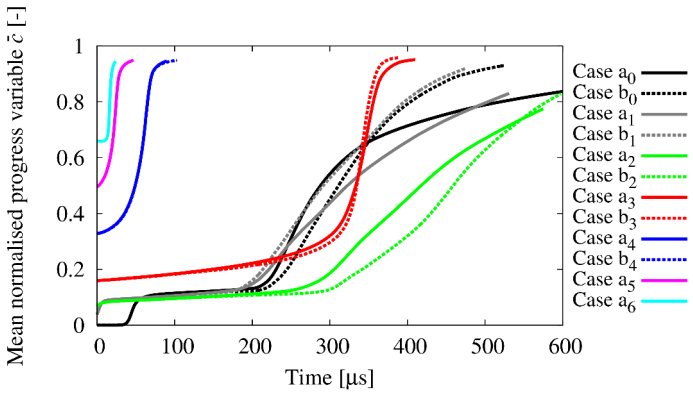

Figure 1: Temporal evolution of mean normalised progress variable $\bar{c}$ of all DNS cases.

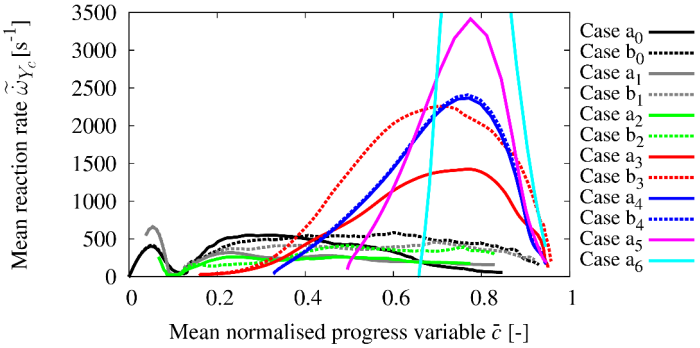

Figure 2: Evolution of mean reaction rate of the progress variable $\widetilde{\dot{\omega}}_{Y_c}$ with mean normalised progress variable $\bar{c}$ of all DNS cases.

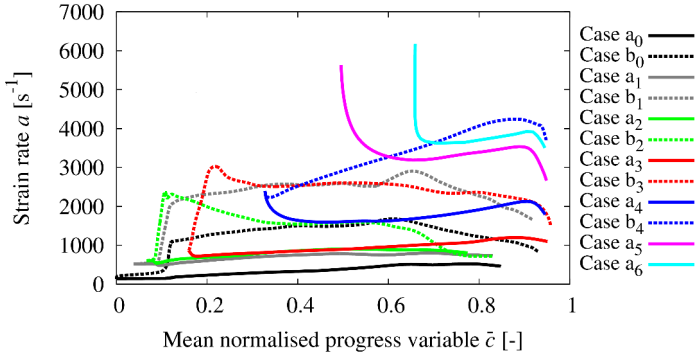

Figure 3: Average strain rate a of all DNS cases calculated as in Eq. (5.2).

Appendix II : DNS fields

The mixture fraction Z and normalised progress variable c fields of the DNS cases a_0 - a_4 and b_0 - b_4 are presented in the following figures. Five instants are chosen for every case: the initial state, an instant showing turbulent mixing before ignition, another illustrating the appearance of the first ignition spots, main ignition ($\overline{c} = 0.5$), and finally an image towards the end of the combustion process. In all of the cases the fields are expanding in the ambient environment due to the heat release of combustion, since there are no boundaries on the DNS domain (see Figure 4.7).

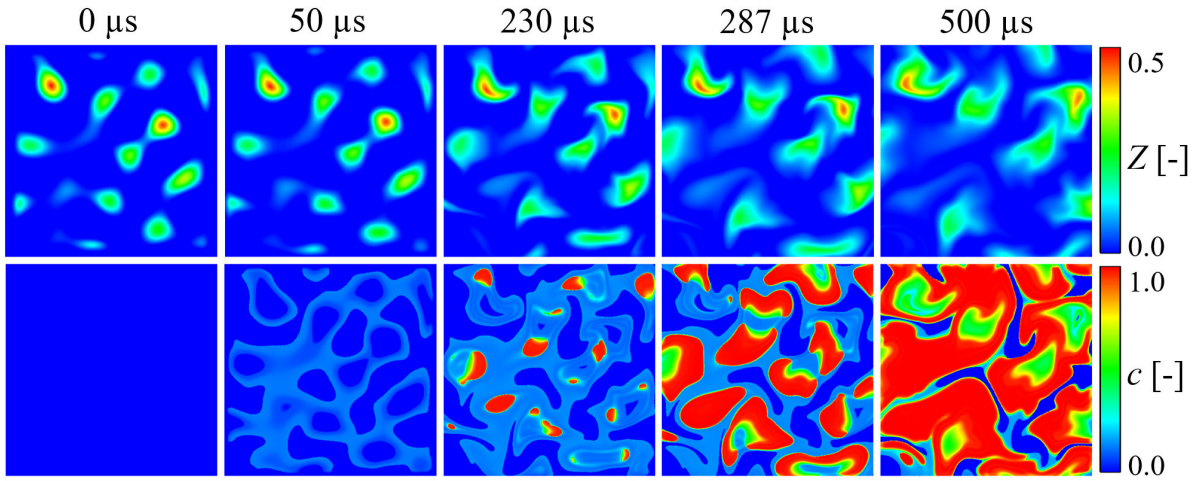

Figure 4: Instantaneous views for a sequence of times ; mixture fraction Z (first row) and normalised progress variable c (second row) fields of DNS case a_0.

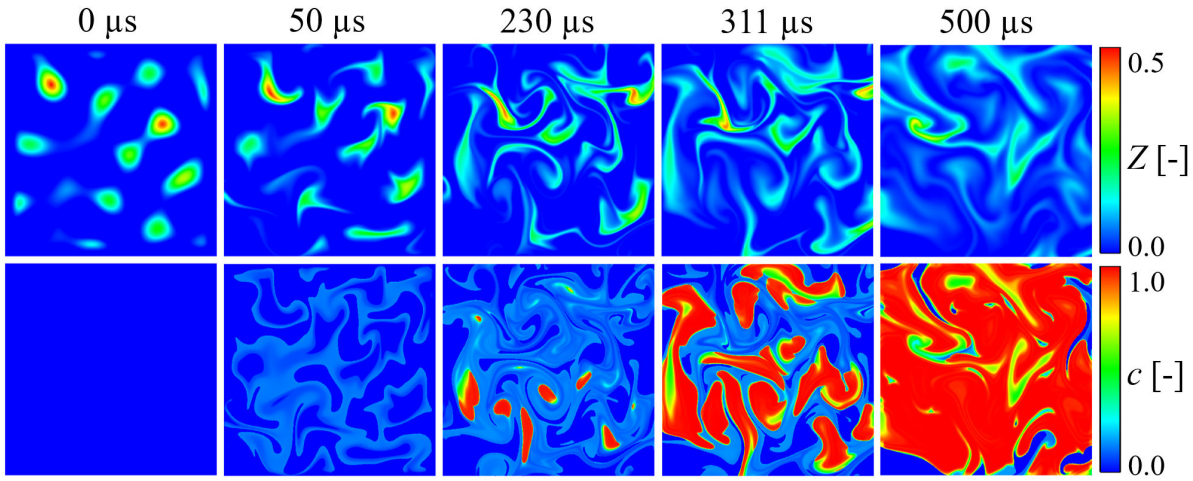

Figure 5: Instantaneous views for a sequence of times ; mixture fraction Z (first row) and normalised progress variable c (second row) fields of DNS case b_0.

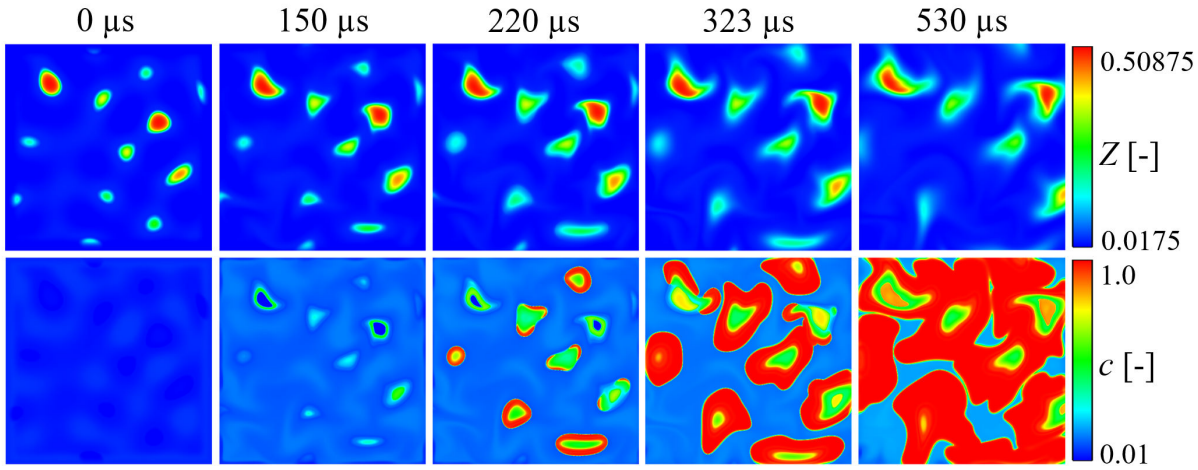

Figure 6: Instantaneous views for a sequence of times ; mixture fraction Z (first row) and normalised progress variable c (second row) fields of DNS case a_1.

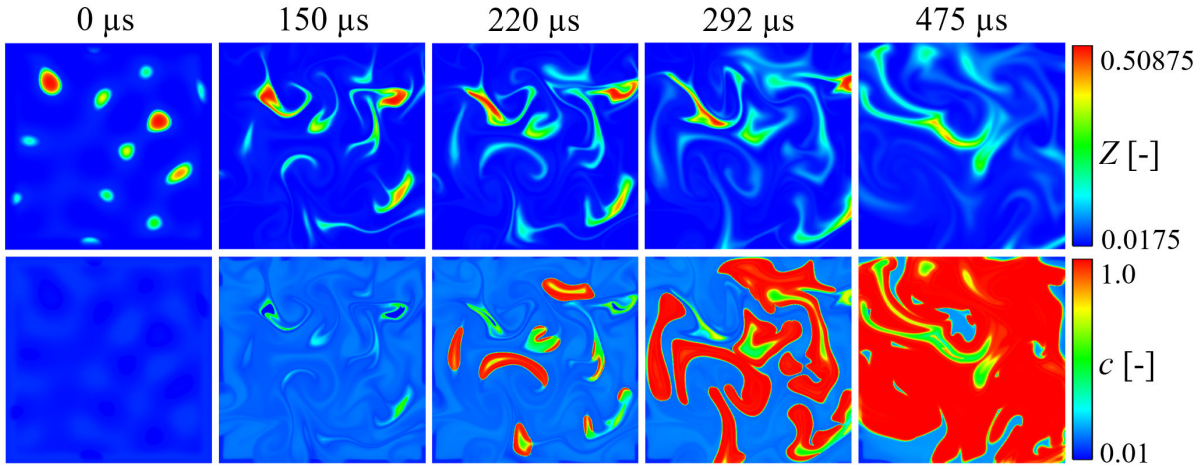

Figure 7: Instantaneous views for a sequence of times ; mixture fraction Z (first row) and normalised progress variable c (second row) fields of DNS case b_1.

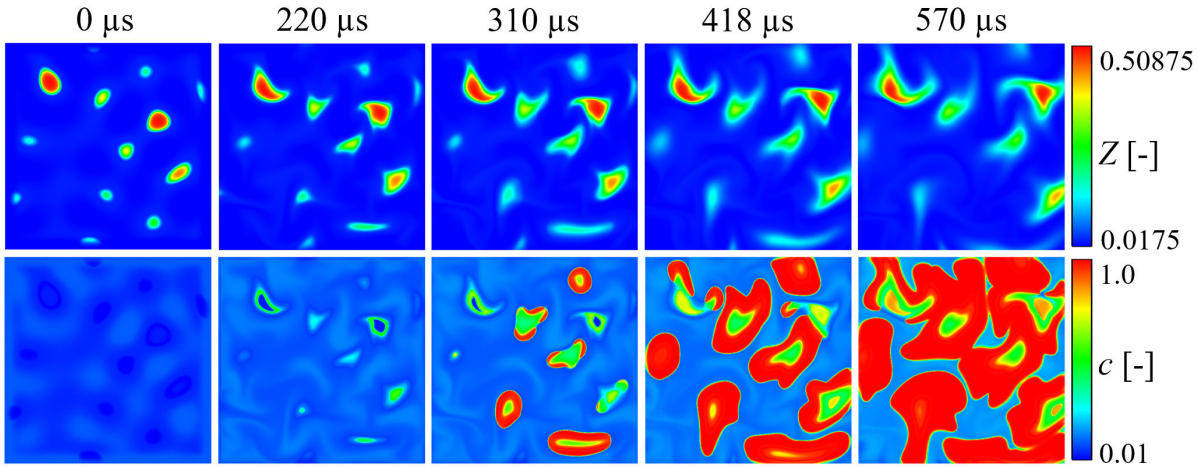

Figure 8: Instantaneous views for a sequence of times ; mixture fraction Z (first row) and normalised progress variable c (second row) fields of DNS case a_2.

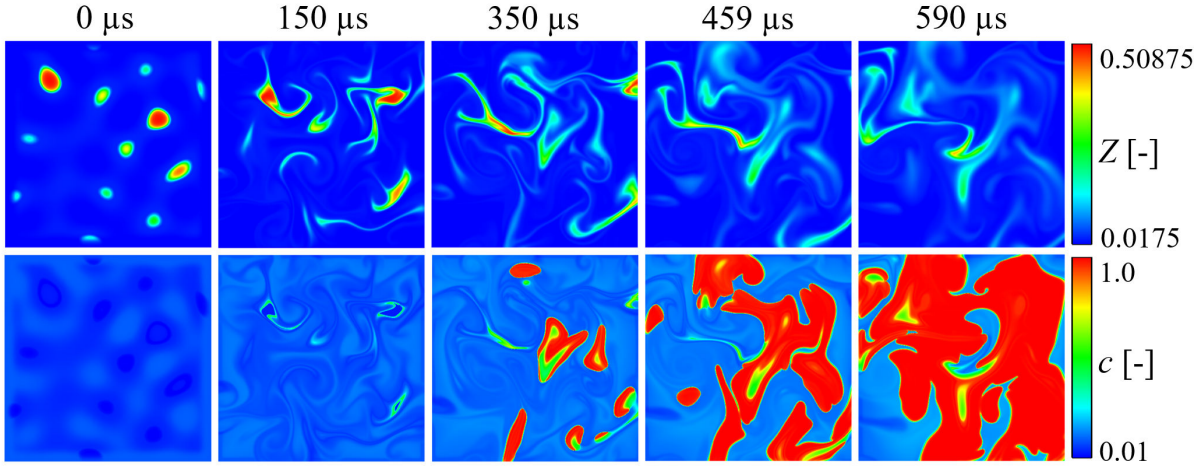

Figure 9: Instantaneous views for a sequence of times ; mixture fraction Z (first row) and normalised progress variable c (second row) fields of DNS case b_2.

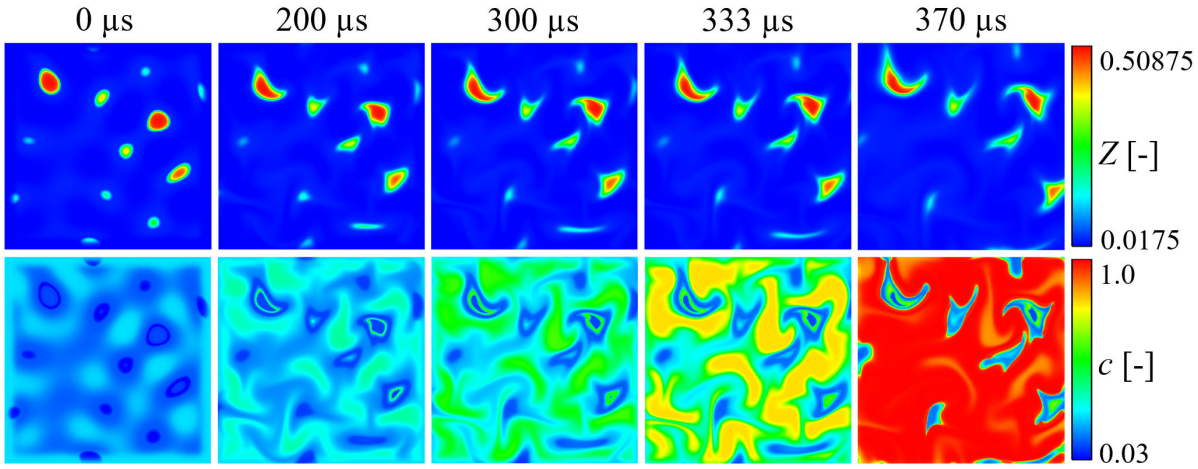

Figure 10: Instantaneous views for a sequence of times ; mixture fraction Z (first row) and normalised progress variable c (second row) fields of DNS case a_3.

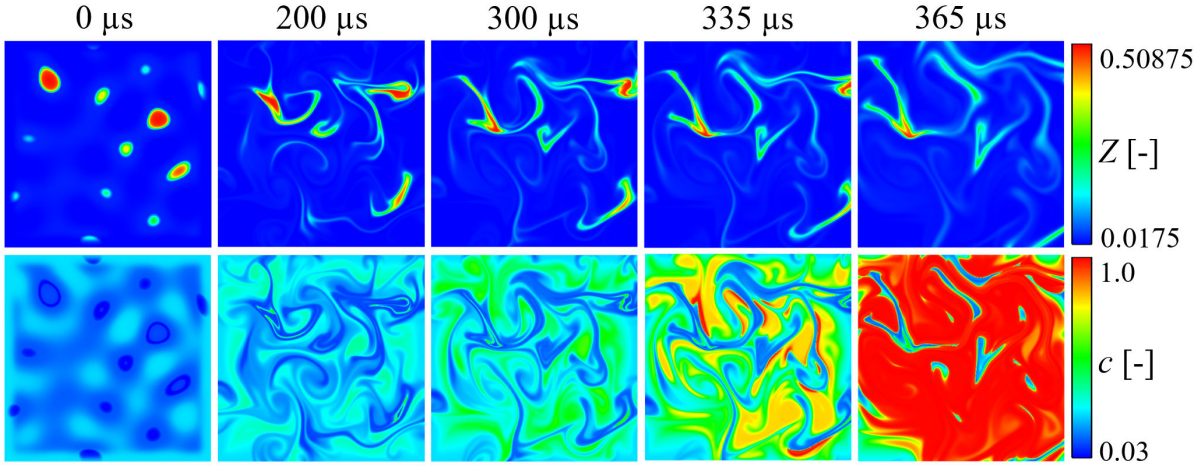

Figure 11: Instantaneous views for a sequence of times ; mixture fraction Z (first row) and normalised progress variable c (second row) fields of DNS case b_3.

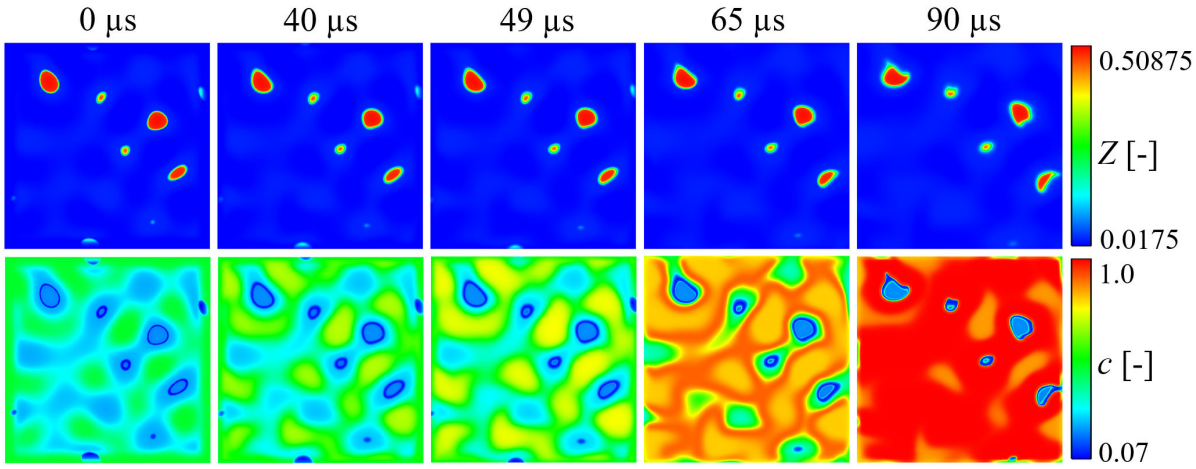

Figure 12: Instantaneous views for a sequence of times ; mixture fraction Z (first row) and normalised progress variable c (second row) fields of DNS case a_4.

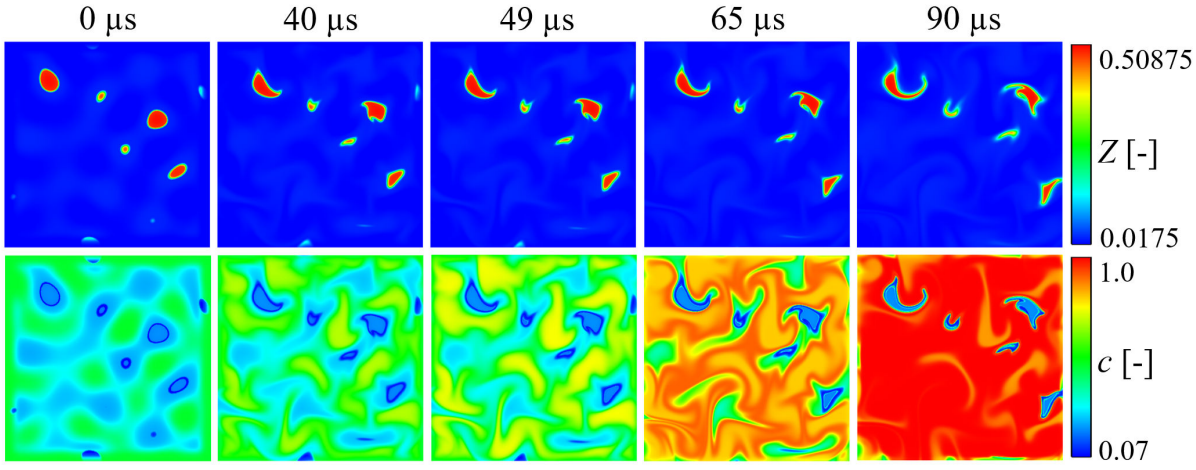

Figure 13: Instantaneous views for a sequence of times ; mixture fraction Z (first row) and normalised progress variable c (second row) fields of DNS case b_4.

Appendix III : Tabulations

This appendix regroups the various 0-D homogeneous reactor and 1-D unsteady strained laminar diffusion flame tabulations used for the purposes of this study.

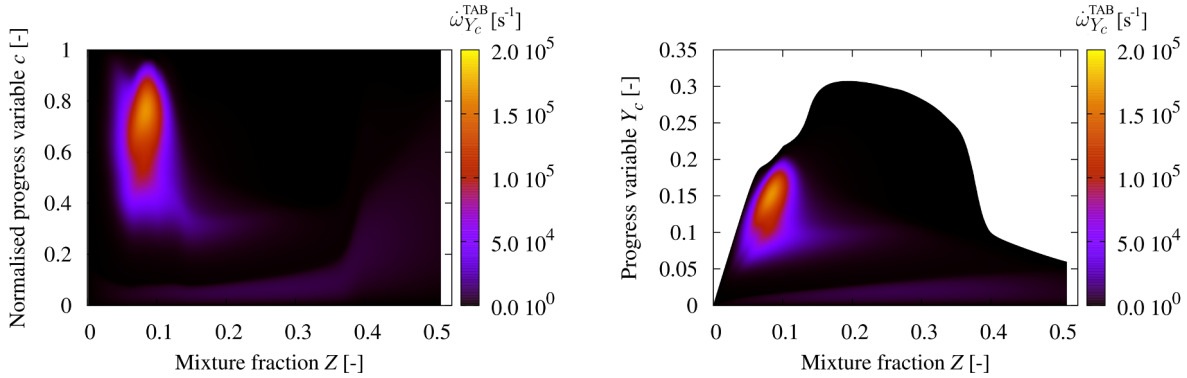

Figure 14: 0-D homogeneous reactor tabulation of reaction rate of the progress variable $\dot{\omega}_{Y_c}^{\text{TAB}}$ with mixture fraction Z and normalised progress variable c (left), and with mixture fraction Z and progress variable Y_c (right), using autoigniting fuel-air mixtures, adapted to single injection cases a_0 and b_0.

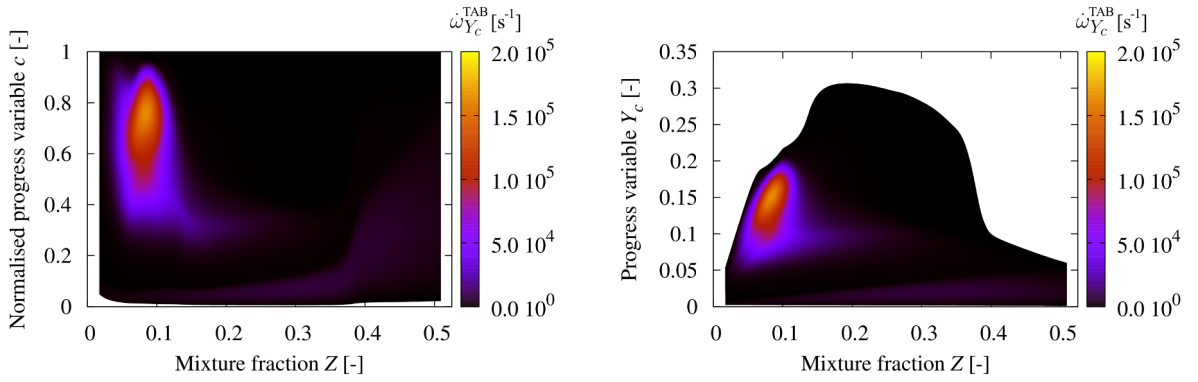

Figure 15: 0-D homogeneous reactor tabulation of reaction rate of the progress variable $\dot{\omega}_{Y_c}^{\mathrm{TAB}}$ with mixture fraction Z and normalised progress variable c (left), and with mixture fraction Z and progress variable Y_c (right), using autoigniting main injection fuel-pilot injection partially burnt gases mixtures, adapted to split injection cases a_1 and b_1 ($c_0 = 0.05$).

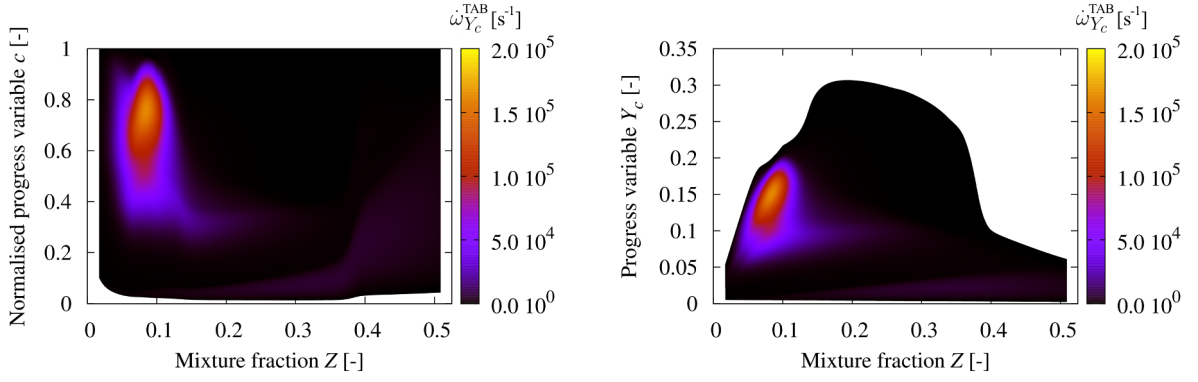

Figure 16: 0-D homogeneous reactor tabulation of reaction rate of the progress variable $\dot{\omega}_{Y_c}^{\mathrm{TAB}}$ with mixture fraction Z and normalised progress variable c (left), and with mixture fraction Z and progress variable Y_c (right), using autoigniting main injection fuel-pilot injection partially burnt gases mixtures, adapted to split injection cases a_2 and b_2 ($c_0 = 0.10$).

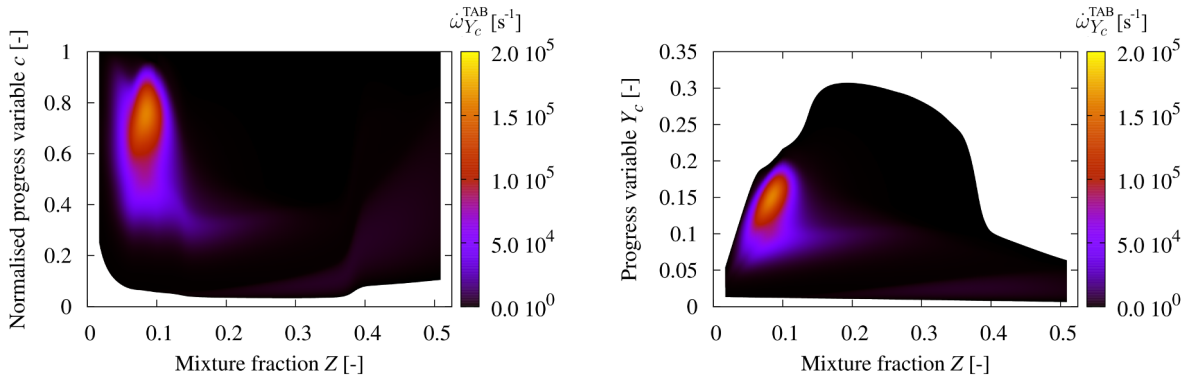

Figure 17: 0-D homogeneous reactor tabulation of reaction rate of the progress variable $\dot{\omega}_{Y_c}^{\mathrm{TAB}}$ with mixture fraction Z and normalised progress variable c (left), and with mixture fraction Z and progress variable Y_c (right), using autoigniting main injection fuel-pilot injection partially burnt gases mixtures, adapted to split injection cases a_3 and b_3 ($c_0 = 0.25$).

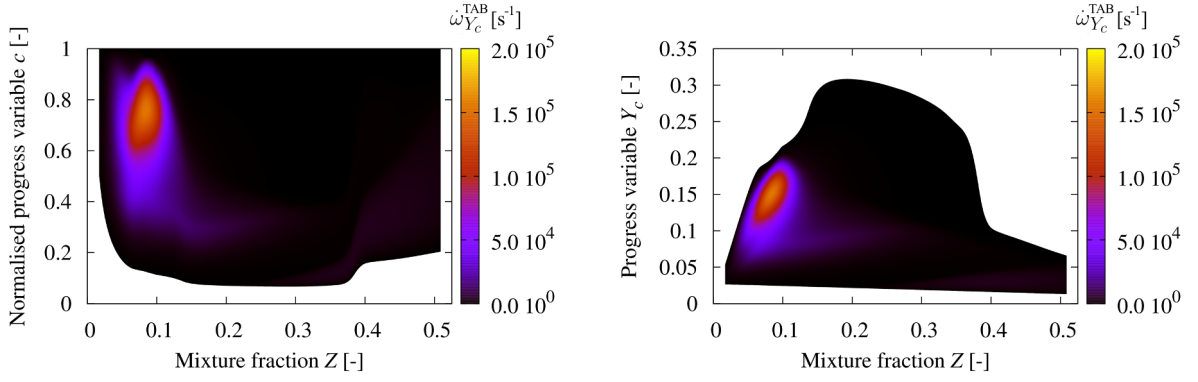

Figure 18: 0-D homogeneous reactor tabulation of reaction rate of the progress variable $\dot{\omega}_{Y_c}^{\mathrm{TAB}}$ with mixture fraction Z and normalised progress variable c (left), and with mixture fraction Z and progress variable Y_c (right), using autoigniting main injection fuel-pilot injection partially burnt gases mixtures, adapted to split injection cases a_4 and b_4 ($c_0 = 0.50$).

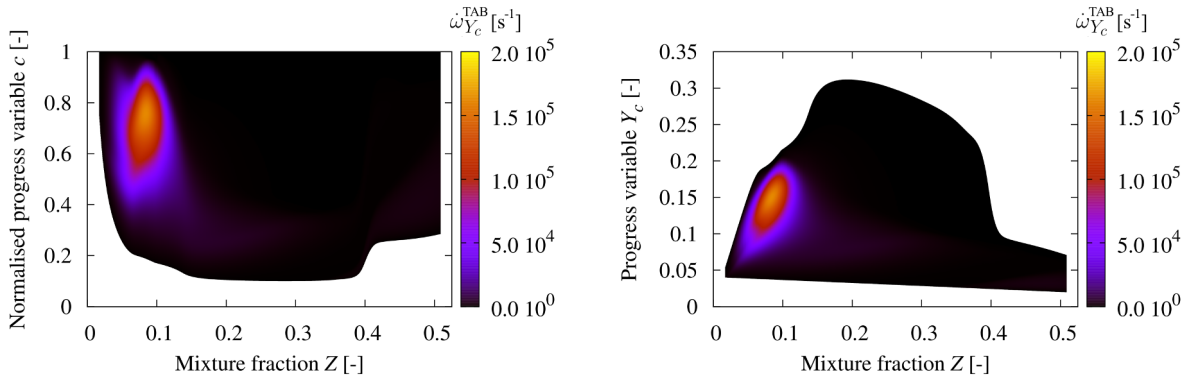

Figure 19: 0-D homogeneous reactor tabulation of reaction rate of the progress variable $\dot{\omega}_{Y_c}^{\mathrm{TAB}}$ with mixture fraction Z and normalised progress variable c (left), and with mixture fraction Z and progress variable Y_c (right), using autoigniting main injection fuel-pilot injection partially burnt gases mixtures, adapted to split injection case a_5 ($c_0 = 0.75$).

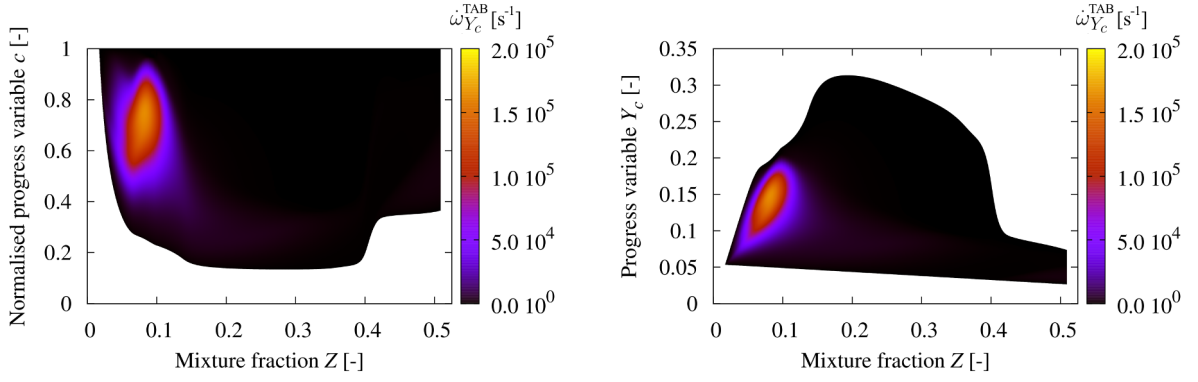

Figure 20: 0-D homogeneous reactor tabulation of reaction rate of the progress variable $\dot{\omega}_{Y_c}^{\mathrm{TAB}}$ with mixture fraction Z and normalised progress variable c (left), and with mixture fraction Z and progress variable Y_c (right), using autoigniting main injection fuel-pilot injection partially burnt gases mixtures, adapted to split injection case a_6 ($c_0 = 1.00$).

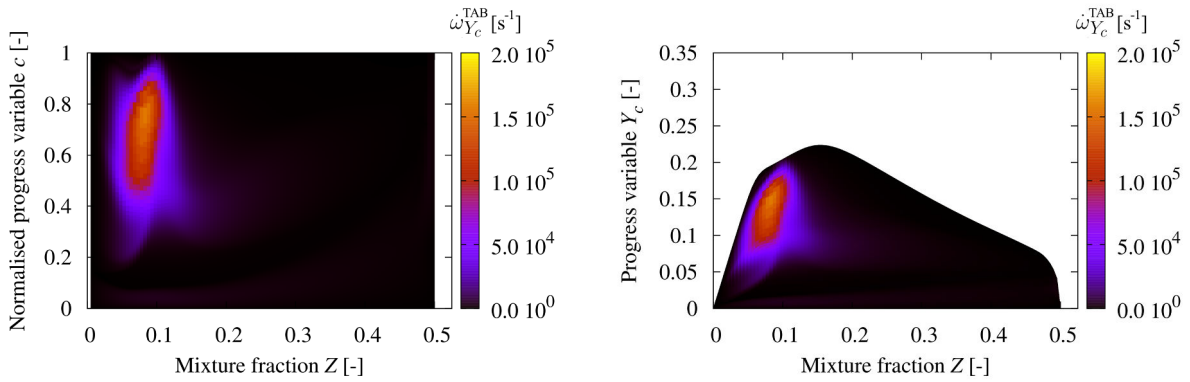

Figure 21: 1-D unsteady strained laminar diffusion flame tabulation of reaction rate of the progress variable $\dot{\omega}_{Y_c}^{\mathrm{TAB}}$ with mixture fraction Z and normalised progress variable c (left), and with mixture fraction Z and progress variable Y_c (right), adapted to single injection case a_0.

Appendix IV : ERC mechanism

	Reactions considered	A	β	Ea
1.	$nC_7H_{16}+H=C_7H_{15}\text{-}2+H_2$	4.38E+07	2.00	4760.0
2.	$nC_7H_{16}+OH=C_7H_{15}\text{-}2+H_2O$	9.70E+09	1.30	1690.0
3.	$nC_7H_{16}+HO_2=C_7H_{15}\text{-}2+H_2O_2$	1.65E+13	0.00	16950.0
4.	$nC_7H_{16}+O_2=C_7H_{15}\text{-}2+HO_2$	2.00E+15	0.00	47380.0
5.	$C_7H_{15}\text{-}2+O_2=C_7H_{15}O_2$	1.56E+12	0.00	0.0
6.	$C_7H_{15}O_2+O_2=C_7ket_{12}+OH$	4.50E+14	0.00	18232.7
7.	$C_7ket_{12}=C5H11CO+CH_2O+OH$	9.53E+14	0.00	41100.0
8.	$C5H11CO=C_2H_4+C_3H_7+CO$	9.84E+15	0.00	40200.0
9.	$C_7H_{15}\text{-}2=C_2H_5+C_2H_4+C_3H_6$	7.05E+14	0.00	34600.0
10.	$C_3H_7=C_2H_4+CH_3$	9.60E+13	0.00	30950.0
11.	$C_3H_7=C_3H_6+H$	1.25E+14	0.00	36900.0
12.	$C_3H_6+CH_3=C_3H_5+CH_4$	9.00E+12	0.00	8480.0
13.	$C_3H_5+O_2=C_3H_4+HO_2$	6.00E+11	0.00	10000.0
14.	$C_3H_4+OH=C_2H_3+CH_2O$	1.00E+12	0.00	0.0
15.	$C_3H_4+OH=C_2H_4+HCO$	1.00E+12	0.00	0.0
16.	$CH_3+HO_2=CH_3O+OH$	5.00E+13	0.00	0.0
17.	$CH_3+OH=CH_2+H_2O$	7.50E+06	2.00	5000.0
18.	$CH_2+OH=CH_2O+H$	2.50E+13	0.00	0.0
19.	$CH_2+O_2=HCO+OH$	4.30E+10	0.00	-500.0
20.	$CH_2+O_2=CO_2+H_2$	6.90E+11	0.00	500.0
21.	$CH_2+O_2=CO+H_2O$	2.00E+10	0.00	-1000.0
22.	$CH_2+O_2=CH_2O+O$	5.00E+13	0.00	9000.0

23.	$CH_2+O_2=CO_2+H+H$	1.60E+12	0.00	1000.0
24.	$CH_2+O_2=CO+OH+H$	8.60E+10	0.00	-500.0
25.	$CH_3O+CO=CH_3+CO_2$	1.57E+14	0.00	11800.0
26.	$CO+OH=CO_2+H$	8.99E+07	1.40	5232.9
27.	$O+OH=O_2+H$	4.00E+14	-0.50	0.0
28.	$H+HO_2=OH+OH$	1.70E+14	0.00	875.0
29.	$OH+OH=O+H_2O$	6.00E+08	1.30	0.0
30.	$H+O_2+M=HO_2+M$	3.60E+17	-0.70	0.0
31.	$H_2O_2+M=OH+OH+M$	1.00E+16	0.00	45500.0
32.	$H_2+OH=H_2O+H$	1.17E+09	1.30	3626.0
33.	$HO_2+HO_2=H_2O_2+O_2$	3.00E+12	0.00	0.0
34.	$CH_2O+OH=HCO+H_2O$	5.56E+10	1.10	-76.5
35.	$CH_2O+HO_2=HCO+H_2O_2$	3.00E+12	0.00	8000.0
36.	$HCO+O_2=HO_2+CO$	3.30E+13	-0.40	0.0
37.	$HCO+M=H+CO+M$	1.59E+18	0.90	56712.3
38.	$CH_3+CH_3O=CH_4+CH_2O$	4.30E+14	0.00	0.0
39.	$C_2H_4+OH=CH_2O+CH_3$	6.00E+13	0.00	960.0
40.	$C_2H_4+OH=C_2H_3+H_2O$	8.02E+13	0.00	5955.0
41.	$C_2H_3+O_2=CH_2O+HCO$	4.00E+12	0.00	-250.0
42.	$C_2H_3+HCO=C_2H_4+CO$	6.03E+13	0.00	0.0
43.	$C_2H_5+O_2=C_2H_4+HO_2$	2.00E+10	0.00	-2200.0
44.	$CH_4+O_2=CH_3+HO_2$	7.90E+13	0.00	56000.0
45.	$OH+HO_2=H_2O+O_2$	7.50E+12	0.00	0.0
46.	$CH_3+O_2=CH_2O+OH$	3.80E+11	0.00	9000.0
47.	$CH_4+H=CH_3+H_2$	6.60E+08	1.60	10840.0
48.	$CH_4+OH=CH_3+H_2O$	1.60E+06	2.10	2460.0
49.	$CH_4+O=CH_3+OH$	1.02E+09	1.50	8604.0
50.	$CH_4+HO_2=CH_3+H_2O_2$	9.00E+11	0.00	18700.0
51.	$CH_4+CH_2=CH_3+CH_3$	4.00E+12	0.00	-570.0
52.	$C_3H_6=C_2H_3+CH_3$	3.15E+15	0.00	85500.0

	Updated reactions	A	β	Ea
16.	$CH_3+HO_2=CH_3O+OH$	6.80E+12	0.00	0.0
34.	$CH_2O+OH=HCO+H_2O$	3.43E+09	1.18	-447.0

Note : A [mole-cm-sec-K], Ea [cal/mole]

université PARIS-SACLAY
ÉCOLE DOCTORALE
Sciences mécaniques et énergétiques, matériaux et géosciences (SMEMAG)

Titre : Simulation numérique directe pour la modélisation de la combustion Diesel dans des configurations d'injections multiples

Mots clés : DNS, modèles de combustion, injections multiples, Diesel

Résumé : Le moteur à allumage par compression est incontestablement une des solutions pour réduire les émissions de CO_2. L'utilisation de forts rapports de compression permet d'atteindre des rendements plus élevés que les moteurs à allumage commandé. Cependant, cette motorisation possède un certain nombre de défauts liés à l'inflammation du carburant et au contrôle du dégagement de chaleur. Ainsi, lorsque le moteur à allumage par compression est associé à un carburant Diesel et utilisant les systèmes d'injection traditionnels, les niveaux des émissions polluantes et du bruit de combustion peuvent devenir critiques. Une solution consiste à décomposer l'injection du carburant en plusieurs pulses (injections multiples) afin d'obtenir un contrôle optimal de la stratification du mélange air-carburant et du taux de dégagement de chaleur. Cette approche, rendue possible par le rail haute pression, est en train de devenir la règle dans les moteurs Diesel. Devant la complexité des phénomènes physico-chimiques rencontrés lors de de la combustion Diesel avec des injections multiples, la modélisation de celle-ci par des outils industriels telle que la modélisation 3D RANS (résolution des équations moyennes) reste un challenge. L'amélioration des modèles est donc essentielle afin de prédire le dégagement de chaleur et les émissions polluantes. Étant donné le manque de résultats expérimentaux précis, suffisamment détaillés et complets, l'amélioration substantielle des modèles reste problématique. La simulation numérique directe (DNS) est donc un outil permettant de générer des résultats détaillés et ainsi de développer et évaluer des modèles pour la simulation RANS. Dans cette thèse, différents modèles de combustion reposant sur une approche tabulée de la chimie ont été évalués afin de dégager leurs voies d'amélioration dans des configurations d'injections multiples, en ayant recours à des DNS de configurations représentatives d'injections multiples. Une base de données DNS représentative du problème a été construite, analysée et a servi ensuite de support à l'analyse approfondie des modèles étudiés. À la suite de cette analyse, certaines hypothèses sous-jacentes aux modèles ont été revisitées.

Title : DNS for RANS combustion modelling in multiple injection configurations

Keywords : DNS, combustion modelling, multiple injection, Diesel

Abstract : Compression-ignition engines are widely used, mainly due to their high thermal efficiency and consequent low CO_2 emissions compared to spark-ignition engines. However, this technology has some disadvantages related to the limited control over autoignition of the air-fuel mixtures and heat release rate. Hence, in compression-ignition engines at their most basic form, the level of combustion noise and emissions of nitrogen oxides and particulate matter can become critical. An effective strategy to tackle these problems is to decompose fuel injection into multiple injection pulses permitting an optimal control of the air-fuel mixture formation and, thus, of the autoignition delay and the heat release rate. Multiple injection strategies become more and more popular due to their advantages over conventional single injection cycles. The physical phenomena involved in such configurations, however, are complex and their modelling remains challenging, especially in the context of industrial 3D simulation using the Reynolds-averaged Navier-Stokes (RANS) formalism. The progress of compression-ignition applications depends to a great extent on the capacity of the physical models to predict heat release rate and pollutant emissions. The lack ofa experimental results at the scale of interest orientated this study towards the use of Direct Numerical Simulation (DNS) providing a model-free insight into the interaction between turbulent mixing and combustion chemistry. In the framework of this Ph.D. thesis, a DNS database was generated and analysed, covering a range of single and split Diesel injection-relevant conditions. Then, different turbulent combustion models based on tabulated chemistry were evaluated by comparison with the DNS results. Following this analysis, a new modelling approach adapted to multiple injection configurations was elaborated. Finally, a strategy for the application of the new modelling approach in 3D RANS was proposed for prospective multi-injection compression-ignition engine simulations with an improved accuracy.

Université Paris-Saclay
Espace Technologique / Immeuble Discovery
Route de l'Orme aux Merisiers RD 128 / 91190 Saint-Aubin, France